Unveiling the Sex-dependant Roles of Pannexin 1 in Skeletal Muscle and Its Influence in Duchenne Muscular Dystrophy

Emily Freeman

A thesis submitted to the University of Ottawa in partial fulfillment of the requirements for a Doctor of Philosophy

Department of Cellular and Molecular Medicine
Faculty of Medicine
University of Ottawa

Abstract

Skeletal muscle has a tremendous capacity to regenerate in healthy individuals. However, there is a dramatic impairment in regenerative potential in Duchenne muscular dystrophy (DMD) resulting in progressive muscle degeneration, weakness, and ultimately muscle wasting. Duchenne muscular dystrophy (DMD) is the most common lethal genetic disorder among children affecting every 1:3600-1:6000 male births. While it is known that DMD is caused by the loss of the structural protein dystrophin, the mechanisms that perpetuate the disease progression are poorly understood. Unfortunately, no cure exists for DMD and affected individuals succumb to the disease between the second and third decades of life, highlighting the importance of discovering new therapeutic strategies for DMD patients. Our laboratory has shown that expression of pannexin1 (Panx1 in rodent; PANX1 in human) is increased during myogenesis *in vitro* and muscle development and regeneration in *vivo*, while its levels are reduced in muscles from severely dystrophic mice. Here we demonstrated that loss of *Panx1* in male mice reduces progenitor number and fusion, decreases muscle fiber size, and significantly impairs muscle strength. Notably, these effects were more prominent in male than in female mice demonstrating a sex-dependant role for Panx1 in skeletal muscle. Using cell lines isolated from muscles of healthy donors and dystrophic patients, we found that PANX1 channel function is reduced in DMD myoblast cell lines. To investigate how Panx1 dysregulation contributes to DMD, a dystrophic (*mdx*) mouse model that lacks Panx1 (*Panx1*$^{-/-}$*/mdx*) was generated. *Panx1*$^{-/-}$*/mdx* mice have significantly reduced lifespan, impaired muscle strength, decreased muscle stem cell population, and increased signs of myofiber specific damage. Like myoblasts from healthy male mice, Panx1 channel inhibition reduced *mdx* myoblast fusion. Interestingly, overexpressing PANX1 in patient derived DMD myoblast cell

lines increased their differentiation and fusion, further suggesting that increased PANX1 protein levels may hold therapeutic benefits in dystrophic muscles. Overall, we demonstrate for the first time that Panx1 exerts sex-dependant roles in muscle maintenance regeneration, and strength. Furthermore, we found that absence of Panx1 exacerbates dystrophic features and significantly reduces the lifespan of dystrophic mice. Moreover, these findings suggest a potential therapeutic benefit of increasing Panx1 levels in the muscles of dystrophic patients.

Acknowledgements

First, I would like to thank Dr. Kyle Cowan and Dr. Stéphanie Langlois for providing me the opportunity to work on this project. I would like to acknowledge the members of my TAC for their guidance and expert advice throughout my entire degree, Dr. Bernard Jasmin, Dr. David Lohnes and Dr. Tommy Alain. I would also like to acknowledge all of my collaborators on this project whose work has been highlighted at the beginning of chapters 3 and 4 of this thesis.

It is important to note that this project would not have been successful without all the amazing people at CHEO and their never-ending support throughout these last 4 ½ years. Thank you to Keith Wilson and Bob for keeping the labs in tip-top shape and for our mini lab break conversations that always brightened my day (Go Leafs!!). Thanks to Lynn Kyte, Nathalie Earl, Martine St-Jean and Joycelyn Mmrah for tirelessly keeping the lab space safely running and for always being committed to making the CHEO experience a good one.

Of course, thank you to all my fellow colleagues at CHEO without their continual support I would have never finished this project. Especially for those who've been there from day one namely Dr. Xiao (mander) Xiang, Jared Lau, Stephen Holland, Kyle Malone, Nathan Baird, and Dr. Dung Hoang. Also thank you to those of you that have been a part of my CHEO experience for a shorter time, but we quickly became good friends, Dr. Marcos (Federico) Leyba, Marie-Eve St. Pierre, Dr. Nafisa Neault, Dr. Emily O'Connor, Anna Blinder, Ramone (Edwin) Caballero, Rebecca Hood, Daniel O'Neil, Kathryn Beaudry, Kelly Ho, Anu Varghese and Ally Welten.

To my family and friends who've always encouraged me throughout this process, you were my motivation when times got rough. To my late grandmother (grandma farm) I did it!!! I promised you I would be a scientist. And to my Uncle Ron; I hope the party is planned. Thank you to my parents, April Freeman and Steve Hagen and my sister Erika Adams who helped me get to this point in every way they could. And I can't forget my dog George Freeman for his never-ending comfort. Finally, to my adopted Ottawa family, my partner Colin Robillard, his brother Shayne and parents Debbie & Rob thank you immensely for all your help, I can't even scratch the surface for how thankful I am.

Table of Contents

List of Figures:

List of Tables

List of Abbreviations

AMPK – AMP-Activated protein kinase
AMP – Adenosine monophosphate
ARP - Actin related protein
AT1 - Angiotensin type 1 receptor
ATP - Adenosine triphosphate
Bio-ID – Biotin identification
bHLH - Basic helix-loop-helix
BMD - Becker's muscular dystrophy
Casp - Caspase
CBX – Carbenoxolone
CMV – Cytomegalovirus
Ctl - Control
Crmp2 - Collapsin response mediator 2
CSA - Cross-sectional area
DAGC - Dystrophin associated glycoprotein complex
DAPI - 4′,6-diamidino-2-phenylindole
DMD - Duchenne muscular dystrophy
DMEM - Dulbecco's Modified Eagles Medium
ECM - Extra-cellular matrix
EDL - Extensor digitorum longus
EGFR – Epidermal growth factor receptor
ETV4 - ETS variant transcription factor 4
FAPS – Fibro/adipogenic precursors
FBS - Fetal bovine serum
FGF-2 - Basic fibroblast growth factor (bFGF)
GA - Gastrocnemius
GO - Gene Ontology
hEGF - Human epithelial growth factor
H&E - Hematoxylin and Eosin
HSMM - Humans skeletal muscle myoblasts
LTBP4 - Latent transforming binding growth factor 4
MAPK – Mitogen activated protein kinase
Mark1 – Microtubule affinity regulating kinase 1
MyoG - Myogenin
MHC - Myosin heavy chain
Myh3 - Myosin heavy chain 3
MRF4 - Myogenic regulatory factor 4
MRF - Myogenic regulator factor
Myf5 - Myogenic factor 5

NFAT - Nuclear of activated T cells
nNOS - Nitric oxide synthase
NSAID - Non-steroidal anti-inflammatory drug
PGC-1α - Peroxisome proliferator activated receptor alpha
Panx1 - Pannexin 1 in reference to mouse
PANX1 - Pannexin1 in reference to human
Panx1 KO - Pannexin 1 knockout
Pard3 – Partitioning defective 3
Pax – Paired box transcription factor
PFA -Paraformaldehyde
PBS - Phosphate buffered saline
PBN - Probenecid
PBST - Phosphate buffered saline solution supplemented with Tween-20
PV curve - Pressure-volume curve
Quads - Quadriceps
ROS - Reactive oxygen species
SCs - Satellite Cells
sd - Standard Deviation
sem – Standard error of the mean
Sol – Soleus
SR – Spectrin repeats
TA - Tibialis anterior
TGF-β - Transforming Growth Factor Beta
UTRN - Utrophin
WT – Wild-type

Chapter 1 : General Introduction

1.1 Skeletal Muscle Development and Regeneration

1.1.1 Development of Skeletal Muscle and Satellite Cell Specification

Skeletal muscle is one of the largest organs in the body as it accounts for approximately 40% of total body weight (Frontera and Ochala 2015). Skeletal muscle contributes to a vast number of bodily functions through the conversion of chemical energy into mechanical force. Most known are its functions in posture and movement however, skeletal muscle is also critical for metabolism and maintenance of body temperature (Frontera and Ochala 2015). Skeletal muscle is comprised of long multinucleated cylindrical cells known as muscle fibers. These fibers bundle together and are interlaced with a complex network of blood vessels, nerves and the extracellular matrix (ECM) which typically consists of fibrous proteins (collagen, laminin, and proteoglycans) (Frontera and Ochala 2015; Dumont, Bentzinger, et al. 2015).

During embryonic development, three germ layers are formed namely the endoderm, ectoderm, and mesoderm (Dumont, Bentzinger, et al. 2015; Anne-Gaëlle Borycki et al. 1999). All skeletal muscle originates from the mesoderm which is subdivided into the lateral, intermediate, and paraxial mesoderm. Somites are bilateral divisions that form from the paraxial mesoderm along the anterior-posterior axis. It is the dorsal-ventral region of the somite, termed the dermomyotome, that gives rise to the majority of skeletal muscle (Tajbakhsh et al. 1998; Dumont, Bentzinger, et al. 2015; Buckingham 2001). Limb muscle develops in the hypaxial part of the dermomyotome from which myogenic precursors migrate, proliferate, and differentiate.

During development, myogenic precursors express the Paired-box transcription factor Pax3 and eventually express the Paired-box transcription factor Pax7. While Pax3 is indispensable for embryonic myogenesis, Pax7 is more important during late fetal and post-natal muscle

development. This is demonstrated in *Pax3*-null embryos which display segmentation defects in the somites and loss of the dermomyotome (Tajbakhsh et al. 1998; Tremblay et al. 1998). In consequence, Pax3 mutant embryos exhibit muscle abnormalities specifically failure to form limb muscles (Goulding, Lumsden, and Paquette 1994). Conversely, *Pax7*-null mice fully develop skeletal muscle and appear normal but die within 2-3 weeks after birth. However, lethality in the Pax7 mutant mouse was associated with neural crest defects rather than muscular defects (Mansouri et al. 1996).

In the majority of myogenic precursors, Pax3 activates myogenic factor 5 (Myf5) which leads to the downregulation of Pax3 and initiation of differentiation (Goulding, Lumsden, and Paquette 1994; Tremblay et al. 1998). As myogenesis progresses, a small subset of Pax3-positive progenitors turn on Pax7giving rise to the eventual pool of adult muscle stem cells termed satellite cells (Seale et al. 2000; Zammit et al. 2006). In adult muscle tissue, a subset of Pax3 positive cells remain however the full extend to how Pax3 influences adult tissue is unknown. Interestingly, Pax3 binds to only 6.4% of Pax7 targets, indicating independent roles for Pax3 and Pax7 (Soleimani et al. 2012). In adult SCs, Pax3 has been associated with activation of the myogenic lineage and SC survival however the role of Pax7 in adult tissue has been further elucidated. (Der Vartanian et al. 2019; Relaix et al. 2006).

1.1.2 Skeletal Muscle Regeneration

Skeletal muscle has remarkable regenerative capacity as it can repair itself within a few weeks following injury (Dumont, Bentzinger, et al. 2015; Hernandez-Hernandez et al. 2017; Collins et al. 2005). The process of muscle regeneration relies on satellite cells (SCs), which are named after their location between the sarcolemma membrane and basal lamina of muscle fibers.

SCs are identified by their ubiquitous expression of Pax7 (Seale et al. 2000; Seale, Polesskaya, and Rudnicki 2003). While not required for embryonal myogenesis, Pax7-positive SCs are the primary cell population required for adult muscle regeneration. Several studies have demonstrated that inducible knockout of Pax7 in adult mice impairs muscle regeneration following cardiotoxin injury (Von Maltzahn 2013; Kuang et al. 2007). Conversely, Pax7 overexpression in myogenic precursors prevents differentiation and maintains cells in a stem cell state (Zammit et al. 2006; Olguin et al. 2007).

In healthy tissue, Pax7 expressing SCs exist in a quiescent state which is maintained via active Notch signaling however, following injury they become activated and proliferate. During the proliferation stages SCs can divide either symmetrically to give rise to two identical daughter cells or asymmetrically giving rise to one $Myf5^{+}$ committed progenitor and one $Myf5^{-}$ stem cell which repopulates the SC pool (Kuang et al. 2007; Dumont, Wang, et al. 2015). This ability to both self-renew giving rise to additional SCs and to differentiate to repair muscle was best shown in 2008 when Sacco and colleagues transplanted a single Pax7-positive SC cell into SC-deficient mice (Sacco et al. 2008). Luciferase based tracing of the single SC revealed its ability to establish a new SC pool and to give rise to new fully differentiated myofibers (Sacco et al. 2008).

Committed progenitors initiate a series of sequential transcription factor activations allowing for the differentiation and maturation of muscle. This involves the family of basic helix-loop-helix (bHLH) transcription factors referred to as the myogenic regulatory factors (MRFs). The MRFs include Myf5, MyoD, myogenin (MyoG), and myogenic regulatory factor 4 (MRF4) (Hernandez-Hernandez et al. 2017; Dumont, Bentzinger, et al. 2015; Zammit et al. 2006). Pax7 positive quiescent SCs become activated in part by switching off Notch signaling. Canonical Notch targets, specifically the Hes/Hey family of proteins. inhibit expression of the later MRFs MyoD

and MyoG (Wen et al. 2012; Buas, Kabak, and Kadesch 2010). In the absence of Notch signaling in the activated SCs, Pax7 initiates the expression of Myf5 and/or MyoD which signal in part for proliferation. It is this proliferative stage in which the progenitors are referred to as myoblasts (Figure 1). Eventually, Myf5/MyoD triggers the expression of MyoG which down regulates Pax7, marking a point of no return for SCs as prior to MyoG expression they may return to a SC state (Füchtbauer and Westphal 1992; Hernandez-Hernandez et al. 2017). Upon MyoG activation, progenitors exit the cell cycle, and eventually express MRF4. These MyoG/MRF4 expressing progenitors are referred to as myocytes (Figure 1). Additionally, outside of its role in myogenic differentiation MRF 4 (also known as Myf6) has recently been identified to be involved in myokine production (Lazure et al. 2020). One myokine under regulation of MRF4 is EGF (epidermal growth factor), which has known roles in promoting SC expansion (Lazure et al. 2020). Therefore, it is likely that MRF4 also regulates earlier stages of myogenesis via regulation of myokine secretion.

Myocytes will fuse together to form new myofibers or fuse into existing myofibers (Proulx, Merrifield, and Naus 1997). This process of fusion requires the presence of fusogen proteins two of which have been discovered to date, myomaker and myomerger (Quinn et al. 2017; Millay et al. 2013). Expression of these fusogens is specific to the myoblast/myocyte stage as they are no longer detected after formation of myofibers/myotubes. This stringent expression is critical for the maintenance of muscle tissue as their membrane remodelling abilities are thermodynamically unfavourable (Leikina et al. 2018). Indeed, forced expression of either myomaker or myomerger outside of this window is associated with muscle damage and atrophy (Witcher, Sun, and Millay 2023). These proteins have roles independent from that of each other as myomerger has identified roles in fusion pore formation and myomaker is suspected to be involved in hemifusion of the

membranes. However, loss of either myomaker or myomerger significantly prevents myoblast fusion thus impeding differentiation (Quinn et al. 2017; Millay et al. 2013; Leikina et al. 2018).

Following fusion, these now multi-nucleated cells can be identified by the presence of centrally located nuclei. These myofibers eventually mature with the nuclei migrating to the periphery of the fiber. Further maturation allow myofibers to take on either a fast or slow twitch phenotype by expressing the respective isoforms of myosin heavy chain (MHC) (Schiaffino et al. 2015). Naïve myofibers typically express MHC3 or MHC4 which will eventually be downregulated and replaced by Type II (Fast twitch) MHC isoforms. In order of slowest to fastest, the fast-twitch isoforms include MHC type IIa, IIx, and IIb (not expressed in humans). Slow twitch or type I fibers will continue to mature and later turn on MHC type I (Schiaffino et al. 2015). While each muscle is comprised of multiple MHC isoforms, the percentage at which they express slow and fast twitch MHC isoforms will determine the twitch type of the muscle (Schiaffino et al. 2015).

As evident by this complex series of events, muscle regeneration is a tightly regulated process. Indeed, failed muscle regeneration is associated with a variety of diseases, further emphasising the importance of this process and associated MRFs. Failed cell cycle exit of myoblasts is speculated to give rise to myogenic sarcomas such as rhabdomyosarcoma (Fu et al. 2014; Keller and Guttridge 2013). While incomplete differentiation and exhaustion of the SC pool has been linked to muscular dystrophy (Dumont and Rudnicki 2016; Hernandez-Hernandez et al. 2017; Kuang et al. 2007). In all, adult muscle regeneration is a complex series of events, and its tight regulation is critical for the maintenance of muscle health.

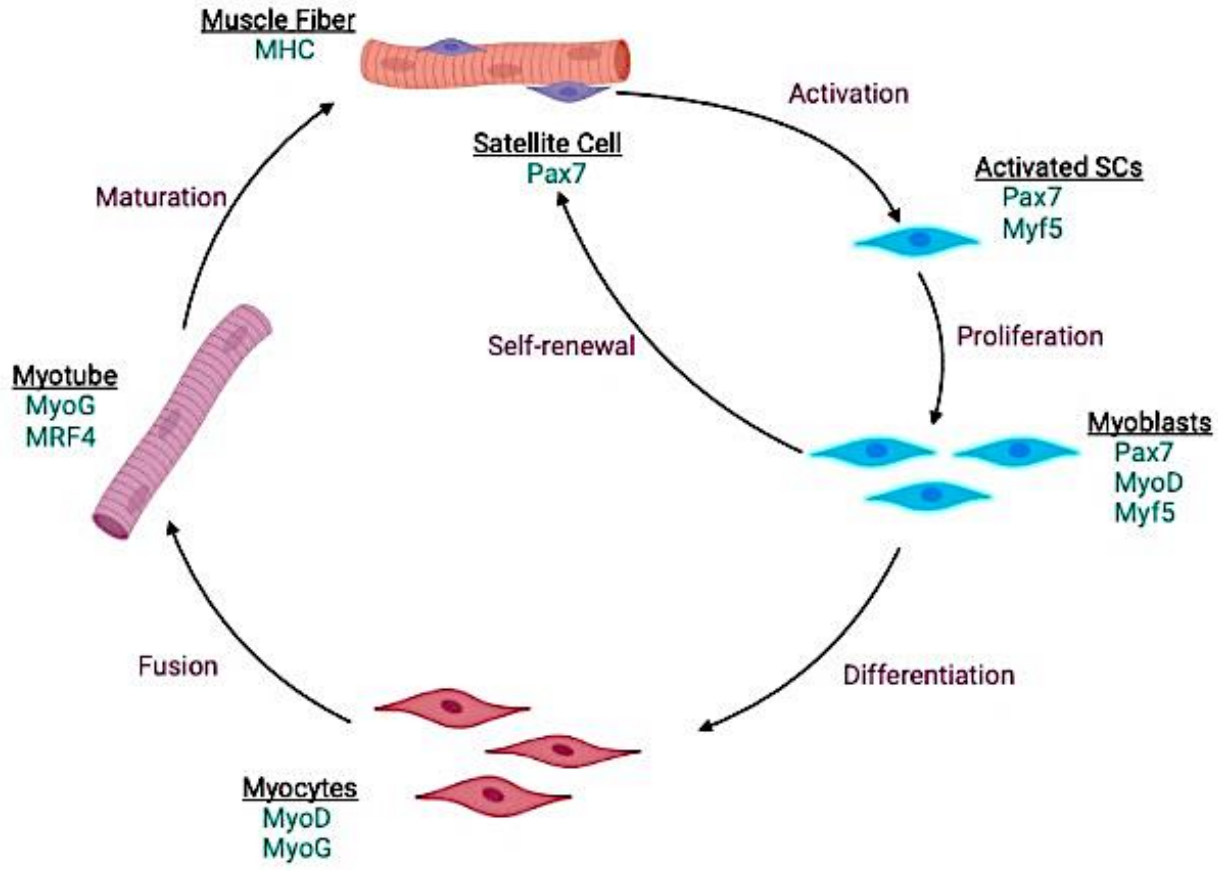

Figure 1.1: Myogenic Lineage.

Muscle regeneration relies on a population of adult muscle stem cells termed satellite cells (SC), which are identified by their ubiquitous expression of Pax7. Following injury, activated SCs express Myf5 and proliferate to generate Myf5/ MyoD positive myoblasts. These progenitors may either return to a SC state in a process known as self-renewal or differentiate by exiting the cell cycle, down-regulating Pax7, and turning on myogenin (MyoG). Differentiated progenitors or myocytes fuse together to form new myotubes which express MRF4 and eventually mature to express various isoforms of myosin heavy chain (MHC). Figure was generated in BioRender.

1.2. Duchenne Muscular Dystrophy

1.2.1 Duchenne Muscular Dystrophy Discovery and Cause

Duchenne muscular dystrophy (DMD) is the most common lethal genetic disorder affecting every 1:3600-1:6000 male births (Bushby et al. 2016; Baxter 2010; Dumont and Rudnicki 2016). DMD was first documented in the 1860's by the French neurologist Guillaume

Duchenne. At that time, DMD was known only by its early symptoms of delayed motor milestones during toddler ages such as standing and walking. As the disease advances, there is progressive muscle wasting displayed by the loss of ambulation before or within the teenage years. This is accompanied by respiratory and cardiac complications that worsen into adulthood (Bushby et al. 2016; Baxter 2010). Life expectancy of affected individuals lies between the second and third decade of life. The milder allelic form of DMD, Becker's muscular dystrophy (BMD), usually has improved outcomes and delayed disease milestones which vary from patient to patient based on disease severity and response to clinical interventions (Baxter 2010).

It wasn't until the 1980's that the underlying cause of DMD was discovered and identified to be an X-linked loss of function mutation in the *dmd* gene which encodes for the structural protein dystrophin (Baxter 2010; Bushby et al. 2016; Campbell and Kahl 1989). The *dmd* gene is the largest gene in the genome comprising of 2.4Mb (Annemieke Aartsma-Rus, Ieke B Ginjaar, and Kate Bushby 2016; Campbell and Kahl 1989). As evident from its large size, the *dmd* gene is subject to a spectrum of mutations. While the majority of mutations are exon deletions (~68 %) or insertions (11 %), small base-pair mutations have also been reported in ~20 % of patients (Annemieke Aartsma-Rus, Ieke B Ginjaar, and Kate Bushby 2016). These mutations may occur anywhere in the gene however a mutation hot spot exists between exons 45-55 for deletions and between exons 2-10 for insertions. DMD is associated with the complete loss of dystrophin whereas in BMD, a partially functional version of the dystrophin protein remains. Commonly, BMD is associated with mutations which preserve the reading frame of *dmd* resulting in the production of a truncated or malformed dystrophin protein (Bushby et al. 2016; Annemieke Aartsma-Rus, Ieke B Ginjaar, and Kate Bushby 2016; Duan 2019).

Nonetheless, complete or partial loss of dystrophin results in failure to form the dystrophin associated glycoprotein complex (DAGC) (Gumerson J. 2011). In healthy muscle, the DAGC acts as a structural support system by connecting the actin cytoskeleton of myofibers to the lower part of the ECM known as the basal lamina. This structure is thought to aid muscle by absorbing force during muscle contractions and thus preventing contraction-induced myofiber damage (Gumerson J. 2011). Loss of the DACG leaves muscle susceptible to repetitive rounds of damage leading to the accumulation of inflammation, fibrosis, and fat deposits within the muscle (Klingler et al. 2012; Campbell and Kahl 1989; Gumerson J. 2011).

1.2.2 Cellular Implications of Dystrophin Absence

Aside from its structural role, many cell signaling pathways use the DAGC as a foundation. For instance, syntrophin, a DAGC protein, has been shown to bind to nitric oxide synthase (nNOS) and to regulate the production of nitric oxide in myofibers (Garbincius and Michele 2015; Dumont and Rudnicki 2016). Nitric oxide has been demonstrated to directly affect SC proliferation and differentiation through non-canonical Wnt signaling (Buono et al. 2012). While mutations in syntrophin itself have not been linked to any dystrophies, dystrophin-deficient myofibers have substantially reduced levels of nNOS which may contribute to disease progression (Rando 2001). The loss of nNOS is just one example of how the DAGC is required for proper cell signalling as the AMP-activated protein kinase (AMPK), Notch, mitogen-activated protein kinase (MAPK) and several G-protein signaling pathways also rely on the DAGC for efficient signaling (Constantin 2014; Rando 2001; Dumont and Rudnicki 2016).

The notion that dystrophin acts as a center for cell signaling is reflected in its structure and evolutionary conservation. Dystrophin has been detected in evolutionarily early appearing species

such as sponges which have evolved prior to the appearance of skeletal muscle (Mirouse 2023) . Indeed, the presence of dystrophin is not restricted to skeletal muscle and many alternatively spliced dystrophin variants have been identified in other tissues (Mirouse 2023; Constantin 2014). Dystrophin in its full form contains an N-terminal actin binding domain followed by a rod domain comprised of 24 spectrin repeats (SR) (Mirouse 2023; Blake, Tinsley, and Davies 1996). Specific SRs have been identified to bind to several cell signaling components including phospholipids (SR1-3), Mark2/Par1b (SR8-9), actin (SR11-14/17) nitric oxide synthase (SR 16-17) and microtubules (SR 20-22)(Mirouse 2023). Dystrophin further connects to DAGC components via a WW and Zinc finger domains which are responsible for dystroglycan binding and the C-terminal domain which is required for attachment to syntrophin and dystobrevin (Mirouse 2023; Blake, Tinsley, and Davies 1996). As is evident by the multiple points of attachment to signaling molecules, partial or full loss of dystrophin largely disrupts cell signaling.

One study of interest demonstrated that dystrophin affects SC function as well. Dumont and colleagues demonstrated that dystrophin is required for the establishment of cell polarity during asymmetric SC division (Dumont, Wang, et al. 2015). In this role, dystrophin established SC polarity by sequestering the microtubule affinity regulating kinase (Mark2; also known as Par1b) allowing for the partitioning defective 3 (Pard3) protein to polarize to the opposite side of the cell. Absence of dystrophin lead to a loss of polarity, impaired mitotic spindle organization, and significantly reduced the number of successful asymmetric divisions (Dumont, Wang, et al. 2015). Furthermore, the DAGC has been shown to indirectly influence Pax7 activity. In healthy SCs, the activation of Myf5 via Pax7 is dependent on the methylation of Pax7 by the arginine methyltransferase Carm1 (Chang et al. 2018). However, phosphorylation of Carm1 via P38γ prevents its translocation into the nucleus and subsequently prevents methylation of Pax7. The

DAGC has been shown to sequester P38γ to the myofiber membrane allowing for the eventual activation of Myf5. In the absence of the DAGC, P38γ was free to phosphorylate Carm1 preventing Pax7 methylation and Myf5 activation (Chang et al. 2018). Both this study and the one by Dumont et al. (2015) linked DAGC disruption in SCs to the loss of committed progenitors which subsequently impaired differentiation. These mechanisms are thought to in part contribute to the reduced regenerative capacity of dystrophic muscle.

In all, dystrophin and the DAGC are critical for protecting myofibers from damage and in regulating various pathways of myogenic cell signaling controlling processes such as proliferation and differentiation to maintain overall muscle homeostasis. This panoply and breadth of roles dystrophin holds is maintained in both mature skeletal muscle and myogenic precursors and highlights the multi-factorial pathogenesis of DMD. It is this multi-factorial role of dystrophin that leaves the exact mechanisms that perpetuate the disease progression poorly understood and emphasizes the need for new clinical interventions to improve the quality of life for patients with dystrophies.

1.2.3 Current and Exploratory Therapies for DMD

Current clinical interventions for DMD are centered around the use of the corticosteroids prednisone and deflazacort (Baxter 2010). Long-term and early (2-6 years of age) administration of corticosteroids improves limb strength and postpones cardiac decline in dystrophic patients. However, the mechanism of action of these drugs are still poorly understood and adverse effects including bone weakness, obesity, and hypertension often outweigh many of the benefits (Sienkiewicz et al. 2015; Baxter 2010). With the adverse effects of current treatments and the poor

outcome DMD patients have despite treatment, it is of upmost importance for current research to discover new therapeutic avenues for DMD.

Ongoing clinical trials for DMD cover a vast range of approaches including gene/translation therapy, cell therapy, and pharmacological interventions. Typically, gene therapies focus on either repairing or replacing dystrophin. While the large *dmd* gene does not incorporate well into genetic vectors, many genetic approaches are focused on delivering truncated micro-dystrophin to mimic the less severe Becker's muscular dystrophy (Okada and Takeda 2013; Duan 2019). Translational therapies utilize exon-skipping technology such as oligonucleotides or morpholinos to omit the mutated exon (Dunckley et al. 1993; Okada and Takeda 2013; McGreevy et al. 2015). However, these therapies require the knowledge of exactly where in the *dmd* gene the mutation occurred. Consequently, translation targeted therapies require a large degree of optimization and exclude patients in which large deletions or insertions are the cause of dystrophin absence (McGreevy et al. 2015).

On the other hand, cell therapies usually involve the use of stem cells to deliver dystrophin-containing muscle precursors to dystrophic muscles. In fact, early SC transplant pre-clinical trials have been encouraging with transplanted cells successfully giving rise to mature dystrophin-positive myofibers (Skuk, Goulet, and Tremblay 2006). Despite this, challenges including getting clinically relevant levels of dystrophin expression, having transplanted cells reaching all muscles especially those of the respiratory system, and reducing the risk of uncontrolled proliferation leading to sarcoma formation all contribute to their lack of success in clinical trials (Miller et al. 2018; Sienkiewicz et al. 2015).

In addition to those targeting exon-skipping, pharmacological interventions have many potential targets with the majority centered around either SC differentiation or muscle protection

through the improvement of altered processes such as fibrosis, inflammation, Ca^{2+} homeostasis, and muscle atrophy(Dumont and Rudnicki 2016; Sienkiewicz et al. 2015; Yao et al. 2021). Some approaches have focused on repairing the comprised function of SCs. Indeed, Wang and colleagues (2019) have demonstrated that stimulation of epidermal growth factor receptor (EGFR) promoted *in vivo* asymmetric division and improved muscle strength of *mdx* mice (Y. X. Wang et al. 2019). Another potential target is transforming growth factor beta (TGF-β), which is involved in the regulation of fibrotic tissue (Yao et al. 2021; Allen et al. 2013). One clinical study has shown that blocking the TGF-β activator, angiotensin type 1 receptor (AT1), with Losartan or targeting its production using the angiotensin converting enzyme inhibitor lisinopril, significantly improved cardiac function in dystrophic patients but had minimal effects on skeletal muscle fibrosis (Allen et al. 2013).

Another potential therapeutic approach to DMD is upregulation of the dystrophin homologue, utrophin (UTRN). While dystrophin acts as a structural foundation throughout the myofiber sarcolemma, utrophin has a similar role in the myotendinous and neuromuscular junctions. However, during embryonic myogenesis and in some myopathies including DMD, UTRN can be localized throughout the sarcolemma (Blake, Tinsley, and Davies 1996; Gramolini and Jasmin 1999). It is thought that this increase or re-distribution of UTRN found in myopathies may indicate a potential compensatory role for the protein. Indeed, dystrophic patients with higher levels of UTRN tend to have less aggressive disease pathology leading to the notion that increasing UTRN levels may be a promising therapeutic avenue for DMD (Duan 2019; Blake, Tinsley, and Davies 1996; Perkins and Davies 2002). In C2C12 cells, metformin has been demonstrated to increase utrophin levels via AMPK signalling (Ljubicic and Jasmin 2015). Additionally, metformin treatment in dystrophic patients has been associated with improved insulin sensitivity

and subsequently decreased adipose tissue (Ljubicic and Jasmin 2015). Furthermore Celecoxib, an FDA approved NSAID (Non-steroidal anti-inflammatory drug) currently used for rheumatoid arthritis, increases grip strength, decreases inflammation, and promotes a fast to slow fiber type transition in the *mdx* mouse model of DMD (Péladeau, Adam, and Jasmin 2018). These effects are thought to be linked to increased UTRN levels following celecoxib treatment (Péladeau, Adam, and Jasmin 2018).

1.3 Pannexins

Pannexins (Panx in rodents; PANX in humans) are a relatively new discovery as they were first reported in 2000 by Panchin and colleagues (Panchin et al. 2000). This small family of proteins consists of three members (Panx1-3) and were discovered by their sequence homology (25-33%) to innexins, invertebrate gap junction proteins (Panchin et al. 2000; Penuela, Gehi, and Laird 2013). Despite their similarities, there is no *in vivo* evidence of pannexins forming gap junctions. Instead, they form functional single transmembrane channels permeable to small molecules <1 kDa in size (Penuela, Gehi, and Laird 2013; Medina et al. 2020). Pannexins are best characterized in mouse and humans where pannexins share over 94 % conserved homology between the two species (Penuela, Gehi, and Laird 2013). Pannexin 1 (Panx1) is the most highly studied pannexin and it is ubiquitously expressed throughout the body. Panx2 was thought to be restricted to the central nervous system but, more recently Panx2 has been detected in murine skin where it promoted UVB-induced keratinocyte apoptosis highlighting that Panx2 may have more undiscovered roles in tissues outside the nervous system (Sanchez-Pupo et al. 2022). The least studied pannexin is Panx3, likely due to difficulty detecting it at both the transcript and protein levels. Despite this, Panx3 has been found in select tissues including skin, bone, cartilage, skeletal

muscle, liver, kidney, and spleen (Penuela, Gehi, and Laird 2013; Bruzzone et al. 2003; Baranova et al. 2004, 3; Ambrosi et al. 2010). Commonly, Panx3 has roles similar to Panx1 and may even compensate for the absence of Panx1 under certain conditions (Whyte-Fagundes et al. 2018; Abitbol et al. 2019). This may be linked to the homology in structure Panx1 and Panx3 share, whereas Panx2 shares the least amount of structural homology with the other pannexins (Baranova et al. 2004; Penuela, Gehi, and Laird 2013).

1.3.1 Pannexin 1 Channel Structure and Expression

Recent cryo-electron microscopy revealed that PANX1 channels are comprised of seven monomers (Michalski et al. 2020; Z. Deng et al. 2020). Pannexin monomers consist of four-pass transmembrane domains with one intracellular loop, as well as an intracellular amino (N-) and carboxy (C-) termini. This generates two-extracellular loops which contain glycosylation sites. Panx1 glycosylation creates three distinct species with different molecular weights. The unglycosylated Gly-0 species which typically localizes to endoplasmic reticulum, the moderately glycosylated Gly-2 species which associates with a few organelles including the golgi and mitochondria, and the heavily glycosylated Gly-3 species most commonly found at the plasma membrane (Ruan et al. 2020; Boassa et al. 2007; Gehi, Shao, and Laird 2011). These extracellular loops are also the suspected binding sites of most channel inhibitors. The C-terminus of Panx1 is longer than the N-terminus and thought to be the site with the most Panx1-protein interactions. Additionally, the C-terminus likely forms a plug in the channel pore allowing for these protein interactions to govern channel function (Ruan et al. 2020; Jin et al. 2020; Michalski et al. 2020). Conversely, the shorter N-terminus is thought to also play a role in channel permeability (Ruan et al. 2020; Gehi, Shao, and Laird 2011).

Pannexin channels are activated by various stimuli including mechanical stretch, high extracellular K^+ concentrations, low intracellular Ca^{2+} levels, receptor-induced signaling pathways, and proteolytic cleavage of the C-terminus (Penuela, Gehi, and Laird 2013; Silverman et al. 2009; Ruan et al. 2020). Similarly, changes in Ca^{2+}, K^+, and extracellular adenosine triphosphate (ATP) concentrations can prevent channel opening. Aside from the cellular environment, there are several Panx1 inhibiting compounds that prevent channel activity. Commonly used inhibitors include probenecid (PBN), 18α glycyrrhetinic acid, spironolactone, and carbenoxolone (CBX). CBX is of particular interest as it has been shown to bind to and block the extracellular pore of Panx1, however like all these inhibitors it may also bind to other channels such as connexins (Ruan et al. 2020; Penuela, Gehi, and Laird 2013). With regards to Panx1 there is one commonly used specific inhibitor, the mimetic peptide ^{10}Panx1.

Panx1 channel function is also governed by several post-translational modifications including phosphorylation of intracellular located tyrosine residues via SRC non-receptor kinase, serine phosphorylation via serine/threonine kinases, and S-nitrosylation of cystine residues (DeLalio et al. 2019; Langlois et al. 2023; Lohman et al. 2012). Interestingly, these modifications may either promote or inhibit channel opening depending on their location on the protein and what other modifications are present at that time. Finally, Panx1 channels are also modified by ubiquitination, which is thought to mark the channel for degradation allowing for Panx1 turnover (Boyce et al. 2018).

Pannexin channels have a large array of functions, which are reflected by the diverse locations of their expression. Panx1 can be found in cell membranes ubiquitously throughout the body. Panx1 has many reported roles including those in inflammasome activation (Silverman et al. 2009), apoptosis (Chekeni et al. 2010), carcinogenesis (Jiang and Penuela 2016), and cellular

proliferation and differentiation (Wicki-Stordeur and Swayne 2013). Interestingly, Panx1 channel function differs between cell types. For instance, in ectopically expressed Panx1 significantly impairs differentiation of rat epidermal keratinocytes and encourages structural changes promoting their differentiation (Penuela et al. 2014; Celetti et al. 2010). Conversely, inhibition of Panx1 channels reduces the malignant properties of neuroblastoma, a neural precursor originated cancer by inhibiting the proliferation and promoting differentiation of neural precursors (Langlois et al. 2023; Wicki-Stordeur and Swayne 2013; Wicki-Stordeur et al. 2012).

1.3.2 Pannexin1 in Cell Signaling

Pannexins have primarily been studied as ATP-release channels, suggesting that signaling affected by pannexin channel activity is typically indirect and in a paracrine fashion. As the field of pannexin research grows, more evidence linking pannexin channels directly to cell signaling has become available. Roles for PANX1/Panx1 have now been identified in purinergic, TNF-α, and Wnt/β-catenin pathways, to name a few (H. Liu et al. 2019; Seref-Ferlengez et al. 2019; Celetti et al. 2010).

One of the most common signaling pathways Panx1 channels have been shown to work through is purinergic signaling, which relies on P2 receptors. Purinergic (P2) receptors are split into two families: 1) the ligand gated P2X (ionotropic) receptors, and 2) the G-protein coupled P2Y receptors (Burnstock 2018; Burnstock, Arnett, and Orriss 2013). Several groups have demonstrated an interaction between pannexin 1 and various P2 receptors (Buvinic et al. 2009; Riquelme et al. 2013; 2015; Arias-Calderón et al. 2016). In almost all cases, Panx1-mediated ATP release stimulates the opening of the associated P2 receptor allowing for an influx of Ca^{2+} into the cell. For example, in $CD4^{+}$ cells ATP release via Panx1 was shown to activate P2Y2 receptors,

which in turn led to kinase activation, membrane depolarization, and increased susceptibility to HIV-1 viral entry (Séror et al. 2011). Panx1 activation of P2 receptors has been involved in many additional processes including vasodilation/vasoconstriction (Locovei, Bao, and Dahl 2006), cardiac muscle function (Ju et al. 2003), and apoptosis (Chekeni et al. 2010).

In addition to the P2 receptors, PANX1/Panx1 has been shown to interact with a large variety of proteins. For example, in the mouse neuro-crest derived N2a cell line, *in silico* cross-analysis revealed that Panx1 interacts with cytoskeletal proteins, mitogen-activated protein kinases (MAPK), heat shock proteins, and components of the mitochondrial electron transport system (Frederiksen et al. 2019). In rhabdomyosarcoma, a sarcoma thought to originate from skeletal muscle, our laboratory has identified AHNAK, UTRN, and myosin heavy chain 9 as some of the most highly enriched protein interactors by both Bio-ID and co-immunoprecipitation approaches (Xiang et al. 2021). While there were some overlapping hits between these two studies, the variance in the top hits were attributed to differences in cell types highlighting how the PANX1 interactome and subsequently Panx1/PANX1 based signaling would differ between cells and tissues, as well as in the context of health versus diseases. Interestingly, our group also shown that, similar to wild-type PANX1, channel-defective PANX1 mutants are also able to elicit tumour suppressive effects in rhabdomyosarcoma (Xiang et al. 2018), suggesting that Panx1 can regulate cellular processes through mechanisms that are independent from its canonical channel functions. This further implies a role for Panx1 interacting proteins in the regulation of Panx1 downstream signaling and functions.

1.3.3 Pannexin1 in the Skeletal Muscle

Panx1/PANX1 is expressed at the protein level in both satellite cells and skeletal muscle myofibers at the sarcolemma membrane and in t-tubules (Langlois et al. 2014, Pham et al 2018).

During murine myogenesis, Panx1 can be detected as early as E14.5 and continues to increase until its highest levels are reached around 4 weeks of age and are then maintained until at least 12 weeks (Pham et al. 2018). Similarly, Panx1 levels also increase during muscle regeneration following acute muscle injury induced by cardiotoxin *in vivo* (Pham et al. 2018). In adult muscle differentiation, Panx1 protein is detected early in SC and myoblasts, however it is most highly expressed in mature muscle tissue (Langlois et al. 2014). Our laboratory has reported that overexpression of PANX1 in human primary myoblasts promote their differentiation and fusion while pharmacological inhibition of PANX1 impaired these processes (Langlois et al. 2014; Pham et al. 2018). Additionally, Panx1 channel inhibition in the C2C12 murine myoblast cell line prevented the increase of MyoD expression and subsequently the myogenic commitment of reserve cells, which typically remain in a progenitor state following the induction of differentiation (Riquelme et al. 2015). Moreover, a recent report suggested that Panx1 promotes cytoskeletal changes that allows for bleb-based myoblast migration and fusion (Suarez-Berumen et al. 2021).

While the exact mechanism by which Panx1 may influence muscle health is not yet known, it is postulated that Panx1 mediates ATP release from skeletal muscle fibers functioning as a signaling molecule. Findings from Buvinic and colleagues (2019) demonstrated that ATP release following electrical stimulation of myofibers was blocked following the addition of the ^{10}Panx1 peptide, thus implicating this response was mediated through Panx1 channels (Buvinic et al. 2009). Furthermore, they demonstrated that ATP release from the myofibers was reciprocated by changes in mRNA levels of interleukin-6 and the c-fos transcription factor, both genes implicated in myoblast proliferation and differentiation (Buvinic et al. 2009). The ability of Panx1 mediated ATP release to induce transcriptional changes has also been reported in fast to slow fiber type transitions. Specifically, in response to electrical stimuli, caveolin-1 activates Panx1 in the t-tubule

system of myofibers initiating an influx of Ca^{2+} into the t-tubule network via Panx1 mediated activation of P2Y channels. This series of events was associated with increased transcription of slow twitch isoforms of troponin, a protein involved in muscle contraction (Jorquera et al. 2013).

When activated, P2X receptors allow for an influx of calcium (Ca^{2+}) into the myofiber where Ca^{2+} has the ability to regulate myogenic proliferation, differentiation, and fiber-type specification (Tu et al. 2016; Morishima and Nakanishi 2015). Interestingly, this relationship between Panx1 and P2 receptors has also been implicated in contraction potentiation of skeletal muscle. Repetitive electrical stimulation of skeletal muscle typically leads to enhanced contractile force caused by increased ATP release and a flux of intracellular Ca^{2+} (Riquelme et al. 2013). Importantly, blockade of either Panx1 or P2 receptors, impaired this process further implicating a cell signaling mechanism involving both Panx1 channels and P2 receptors (Riquelme et al. 2013). Similarly, this Panx1-P2 receptor relationship has been reported to regulate inflammation in the diabetic model of high-fat diet fed mice. Here, the skeletal muscle of mice on a high-fat diet had increased Panx1 mediated activation of P2 receptors resulting in the overstimulation of the NF-kB pathway and subsequently increased inflammation and insulin sensitivity when compared to mice on a regular diet (Jorquera et al. 2021). Together these findings demonstrate that the influence of Panx1 in muscle occurs likely through P2 receptor signaling and the associated outcomes differ depending upon where in the muscle these events are occurring and the specific stimuli initiating this sequence.

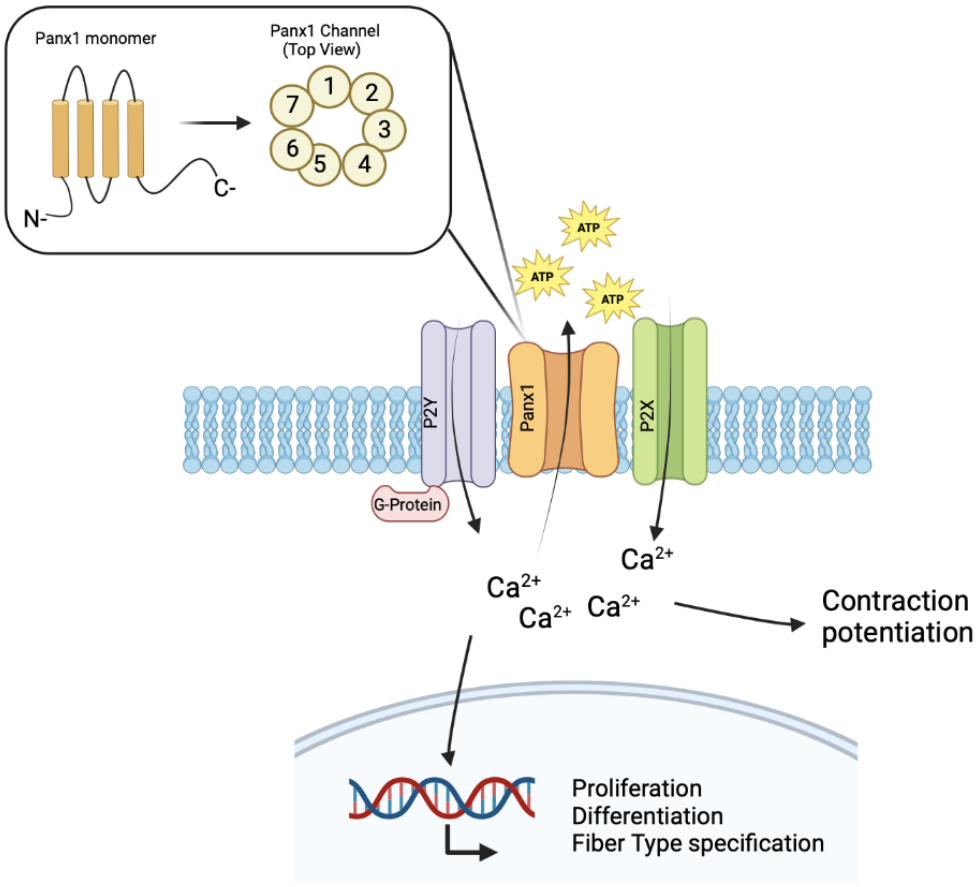

Figure 1.2: Panx1 signaling in skeletal muscle.

Panx1 channels are comprised of seven monomers which are four pass transmembrane proteins containing an intracellular amino (N-) and carboxy (C-) termini. ATP release via Panx1 channels activates the P2X and G-protein coupled- P2Y receptors leading to Ca2+ influx and accumulation. Ca2+ accumulation is involved in several signaling pathways leading to transcriptional changes that regulate progenitor proliferation and differentiation, alongside fiber-type specification. Additionally, Ca2+ accumulation via the Panx1-P2 pathway is required for contraction potentiation. Figure generated in BioRender.

1.3.3 A Potential role for Panx1 in DMD pathogenesis

With the emerging roles of Panx1 in skeletal muscle, Panx1 may play a role in muscular diseases such as DMD. A previous report from our laboratory showed that Panx1 protein levels

decreased in the severely dystrophic *utrophin*$^{-/-}$*/dystrophin*$^{-/-}$ mouse model, but not in the mildly dystrophic *C57Bl/10-mdx* (*mdx*) mouse model leading to the impression that Panx1 protein levels may correlate with disease severity (Pham et al. 2018). Indeed, Panx1 has been implicated in many processes that are altered in DMD including inflammation (Jorquera et al. 2021; Silverman et al. 2009), fibrosis (Crespo Yanguas et al. 2018), apoptosis (Chekeni et al. 2010), progenitor fusion and differentiation (Langlois et al. 2014; Suarez-Berumen et al. 2021). Panx1 has also been suggested to be the primary route of ATP release in myofibers isolated from *mdx* mice (Valladares et al. 2013). Interestingly, in normal skeletal muscle, Panx1 resides with dystrophin in a multi-protein complex indicating that Panx1 channel formation and/or function may be altered following loss of dystrophin (Arias-Calderón et al. 2016). These findings implicate that Panx1 may be dysregulated in DMD and that loss of Panx1 channel function may have deleterious effects in dystrophic muscle. However, before Panx1 can be considered as a therapeutic target for DMD the exact role of Panx1 in healthy and dystrophic muscle must be determined.

1.4 Rationale and Hypothesis

Despite several studies demonstrating that Panx1 levels are upregulated during muscle differentiation *in vitro* and during *in vivo* muscle development and regeneration, the specific role of Panx1 in skeletal muscle has yet to be investigated. Taking into consideration its proposed role in skeletal muscle and evidence supporting an interaction with dystrophin, it is possible that Panx1 signaling in the absence of dystrophin may be impaired contributing to the pathogenesis of DMD. Notably, our laboratory has previously reported that Panx1 protein levels are decreased in severely dystrophic mice further suggesting that Panx1 is dysregulated in DMD. Together, with evidence supporting a functional role for Panx1 in myogenesis, muscle contraction, and fast-to-slow muscle

fiber transition, these data suggest that the down-regulation of Panx1 levels seen in DMD muscles may contribute to disease progression by facilitating processes such as muscle damage, degeneration, and weakness. Therefore, I hypothesized:

1) Panx1 plays a significant physiological function in skeletal muscle maintenance and regeneration by regulating myogenic differentiation and SC function.

2) Loss of Panx1 function in dystrophic muscles exasperates dystrophic symptoms, worsening disease progression of Duchenne muscular dystrophy.

1.5 Objectives

1) To assess the effect of *Panx1* loss on skeletal muscle maintenance regeneration, and SC function using female and male global *Panx1* knockout mice compared to wild-type animals.

Results from this objective will establish the role of Panx1 in skeletal muscle maintenance and regeneration, as well as in myoblast differentiation and SC function, and identify any potential sex-differences.

2) Evaluate the dystrophic hallmarks of a novel dystrophic (*mdx*) mouse model that lacks Panx1 (*Panx1*$^{-/-}$*/mdx*) compared to those of *mdx* mice and use clinical specimens and cells derived from DMD patients to assess PANX1 levels and function.

This objective will determine the role of Panx1 in the pathogenesis of DMD.

Chapter 2 : General Materials and Methods

2.1 Experimental Animals

As described in Freeman et al 2022 (Freeman et al. 2022) *Panx1* knockout (KO; *Panx1*$^{-/-}$) mice and their wild-type (WT) controls were generated from *Panx1*$^{+/-}$ breeding pairs generously provided by Dr. Leigh-Anne Swayne (University of Victoria). Original *Panx1* KO mice were generated by Dr. Valery Shestopalov (Dvoriantchikova et al. 2012) and were backcrossed a minimum of six times prior to our use (Sanchez-Arias et al. 2019). To generate *mdx* mice lacking *Panx1*, male *Panx1*$^{-/-}$ mice were crossed with female *mdx* (*DMD*$^{mdx/mdx}$) mice to generate *Panx1*$^{+/-}$*/DMD*$^{mdx/Y}$ male mice. Male *Panx1*$^{+/-}$*/DMD*$^{mdx/Y}$ mice were then crossed with female *mdx* mice. Resulting *Panx1*$^{+/-}$*/DMD*$^{mdx/Y}$ male mice and *Panx1*$^{+/-}$*/DMD*$^{mdx/mdx}$ female mice were crossed to generate the experimental male *Panx1*$^{-/-}$*/mdx* (*Panx1*$^{-/-}$*/ DMD*$^{mdx/Y}$) mice and their control *Panx1*$^{+/+}$*/mdx* (*Panx1*$^{+/+}$*/ DMD*$^{mdx/Y}$) mice. The *mdx* (C57BL/10ScSn-Dmd^{mdx}/J) mice were purchased from The Jackson Laboratory (strain #001801). Mice were genotyped as described by Sanchez-Arias et al 2019 (Sanchez-Arias et al. 2019) and for the nonsense mutation in exon 23 of the *dystrophin* gene as described by Shin et al., (2011) (Shin et al. 2011). Mice were housed under a 12h light/dark cycle with food and water ad libitum. All experiments were conducted in accordance with the University of Ottawa Animal Care Guidelines and the Canadian Council of Animal Care Guidelines. Body weights were recorded and for the *Panx1*$^{-/-}$ */mdx* mice survival was also tracked. All measurements and assessments were done in a blinded fashion.

2.2 Tissue Specimens and Patient-derived Cell Lines

After institutional ethics board approval (CHEO Research Ethics Board, protocol CHEOREB# 19/49X), archived frozen pediatric muscle samples were obtained, as secondary use of clinical samples, from the Department of Pathology and Laboratory Medicine, Children's Hospital of Eastern Ontario (CHEO), Ottawa, Ontario, Canada. Experiments were carried out in accordance with the CHEO Ethics Board guidelines and regulations.

All healthy (Ctl) and dystrophic (DMD) HSMM cell lines were kindly generated by the Dr. Chazaud laboratory (Universitié de Lyon) and were isolated as previously described (Massenet et al. 2020). HSMM cells were culture in were cultured in Ham's F14 media supplemented with 30 % FBS, 10 µm/ml of insulin (16634, Sigma-Aldrich, St. Louis MO, USA), 25 ng/ml FGF-2 (SRP4037, Sigma-Aldrich), 10 ng/ml hEGF (E9644, Sigma-Aldrich), 2 µg/ml amphotericin B (A2942, Sigma-Aldrich), and 1 % penicillin/streptomycin.

2.3 Tissue Specimens and Processing

For murine samples, male and female mice (12-week-old) were euthanized and the *tibialis anterior* (TA), *extensor digitorum longus* (EDL), *soleus* (Sol), *gastrocnemius* (Gastroc) and *quadriceps* (Quad) were harvested, weighed and either flash frozen in liquid nitrogen for homogenization or embedded in Tissue-TeK OCT compound (Fisher Health Care, Rockford IL, USA) and frozen in isopentane pre-cooled in liquid nitrogen. Samples were stored at -80 ºC until use. Cross-sectional area (CSA), fiber number, and central nuclei analysis were completed in frozen muscle sections stained with Hematoxylin and Eosin while Masson trichrome staining was done on paraffin embedded sections. Paraffin embedding, tissue processing, and staining of

paraffin-embedded tissue were performed at the Louise Pelletier Histology Core Facility at the University of Ottawa.

For degeneration/regeneration experiments, 25 µl of 10^{-5} M cardiotoxin (Millipore) was injected into the TA muscle of 6-week-old *Panx1* KO or WT male and female mice to induce muscle degeneration and regeneration as previously described (Pham et al. 2018; Condrea 1974; Clow and Jasmin 2010; Ravel-Chapuis et al. 2014). At different time points after injection, mice were euthanized, TA muscles were harvested, embedded in Tissue-Tek OCT compound. Samples were stored at -80 ºC until use.

2.4 Forelimb Grip Strength, Kondziella's Inverted Screen Test, EchoMRI and Pole Test

Forelimb grip strength measurements of 12-week-old mice were completed using the Chatillon DFE II digital meter (Columbus Instruments, Columbus, USA), as we have previously described (Freeman et al. 2022). Following acclimatization to the workspace, each mouse was allowed to grip the grid firmly and then gently pulled horizontally relative to the grid until release. The maximum peak force value was recorded. This was repeated for a total of five times for each mouse with 10–15 seconds intervals between trials.

Kondziella's inverted screen test was performed on 12-week-old mice (Bonetto, Andersson, and Waning 2015) Following acclimatization to the work area, mice were placed on a flat wire-mesh screen, which was then inverted such that mice use all four limbs to hang on the screen. Time to fall, an indicator of overall strength and endurance (Graber et al. 2013) was recorded with a maximum hanging time of 600 seconds. Each mouse had three trials and rested for 10 minutes between each trial. Data are presented as the average latency to fall of the three trials.

EchoMRI was performed by a technician at the Animal Behavior Core Facility at the University of Ottawa on the EchoMRI-700 body composition analyzer and associated software (Houston, TX, USA). For the pole descending test, 12-week-old mice were placed near the top of a textured metal pole (diameter: ~8 mm; height: ~55 cm) with their nose facing upwards. The time taken to turn completely around (time to turn) and to climb down the pole face down were recorded (time to descend). If the animal fell from the pole, the maximum value of 120 seconds was given. Mice were tested in 5 consecutive trials. (Giraldo et al. 2018). All tests were performed at the Animal Behavior Core Facility at the University of Ottawa.

2.5 Maximum Force and Force Frequency Curve

Control solution contained (in mM): 118.5 NaCl, 4.7 KCl, 2.4 $CaCl_2$, 3.1 $MgCl_2$, 25 $NaHCO_3$, 2 NaH_2PO_4, and 5.5 d-glucose. Solutions were continuously bubbled with 95 % O_2–5 % CO_2 to maintain a pH of 7.4. Experiments were performed at room temperature. Total flow of solutions in the muscle chamber was 15 ml/minute being split just above and below the muscle to prevent any buildup of reactive oxygen species.

Mice (12-week-old) were euthanized, and their soleus and diaphragm were then dissected out. For force measurements, 5–7 mm wide diaphragm strips were used. Muscle length was adjusted to give maximal tetanic force. Muscles were positioned horizontally in a Plexiglas chamber. One end of the muscle was fixed to a stationary hook, whereas the other end was attached to a force transducer (model400A; Aurora Scientific Canada). Similarly to methods described in Ammar et al (2015) the transducer was connected to a data acquisition system (KCP13104; Keithley), and data were recorded at 5 kHz (Ammar et al. 2015). Electrical stimulations were applied across two platinum wires (4 mm apart) located on opposite sides of the fibers. They were

connected to a Grass S88 stimulator and a Grass SIU5 isolation unit (Grass Technologies, Cheshire UK). Tetanic contractions were elicited with 200-ms trains of 0.3-ms, 10-V (supramaximal voltage) pulses. Stimulation frequencies were set to give maximum tetanic force: 140 Hz for soleus and 200 Hz for diaphragm during maximization and equilibrium stages. The force–frequency relationship was measured after a 30 min equilibrium period over a range from 1- 200 Hz for both soleus and diaphragm. Twitch and tetanic force, defined as the force developed following a single stimulation pulse or a train of pulses, respectively, was calculated as the difference between the maximum force during a contraction and the force measured 5 ms before the contraction was elicited. Forces are presented in N/cm^2.

2.6 Lung Function Analysis

Prior to lung function analysis 12-week-old mice were euthanized with an intraperitoneal injection of Dorminal (Pentobarbital Sodium Injection, BP, Rafter & Products, AB, Canada). The pressure-volume (PV) curve was performed 10-15min following euthanasia via a small animal ventilator (FlexiVent, Scireq). As described in Kang et al 2020, an 18-gauge cannula attached to the flexiVent was secured to the trachea in a supine position (M. H. Kang et al. 2020). At regular intervals the lungs were inflated to a maximum pressure of 30 mm H_2O then deflated with regular intervals thus generating the PV curve. The PV curve represents that of the entire chest cavity and was normalized to total body weight of the animal. The residual volume (RV), and compliance were then calculated from the PV curve.

2.7 Hematoxylin & Eosin and Masson Trichrome Staining

Muscles cross sections (12 μm) were stained with Hematoxylin and Eosin (Sigma-Aldrich, ST. Louis, MO, USA) dehydrated though ethanol washes (70 %, 95 %, 100 %), cleared with xylene, and mounted with Fluoromount G (Thermo Fisher Scientific, Carlsbad CA, USA). The Masson trichrome staining was done according to manufacturer's protocols at the Louise Pelletier Histology Core Facility. Entire tissue sections were scanned using the EVOS FL Auto (Thermo Fisher Scientific, Ontario, CA) under 10X magnification. CSA was measured from randomly selected fibers (100-250 fibers for the Sol and 200-500 for the TA). Fiber number counts were performed on the entire section and represented as fibers per mm^2. Central nuclei counts were performed on entire muscle scans and data represents the average of three serial sections. For the Masson trichrome staining, data represents the percentage of muscle section stained in blue (collagen) (Van De Vlekkert, Machado, and d'Azzo 2020). All measurements were calculated using the ImageJ (FIJI) software.

2.8 Rhodamine Phalloidin stain

Snap frozen TA and Sol sections were first stained for laminin following the Immunofluorescence protocol listed in the "Immunofluorescence" section of this chapter. One modification to this protocol was the blocking buffer which was replaced with 1 % bovine serum albumin diluted in PBS. Before mounting, samples were incubated 30-60 minutes with rhodamine phalloidin (R415, Invitrogen Whitby ON, CA) prepared in DMSO following manufacturer's

guidelines. Slides were mounted with DAPI-fluoromount as described in the "Immunofluorescence" section of this chapter.

Slides were imaged with the Olympus Fluoview FV1000 confocal microscope under the 40X objective. As many fields of views possible for each muscle where imaged (any signs of freezing damage or tissue tears were excluded as this would interfere with cytoskeletal measurements). All imaging parameters were kept consistent between each tissue. Image analysis was performed following the methods described by Romanelli et al 2020 (Romanelli, Varela, and Benech 2020). Percentage of area stained with rhodamine phalloidin, laminin and DAPI were assessed using ImageJ maintaining the same threshold settings for all images. F-actin occupied area was calculated as the area in each section stained with rhodamine phalloidin minus the area labeled for laminin and for DAPI, as F-actin does not typically occupy these areas. Final numbers for each animal were the average of all considered field of views.

2.9 *Ex Vivo* Single Myofibers Isolation and Culture

EDL myofibers were dissected from 8-week-old mice as previously described Brun, Wang, & Rudnicki (2018) (Brun, Wang, and Rudnicki 2018; Freeman et al. 2022). Isolated EDLs were incubated in filtered 0.2 % collagenase type I (Worthington, Lakewood NJ, USA) dissolved in Delbecco's modified eagle's medium (DMEM) (supplemented with 1 % penicillin/streptomycin and 110 mg/L sodium pyruvate) (Cytiva Logan, UT, USA) supplemented with 1 % penicillin/streptomycin, at 37 °C for 1 hour. Myofibers were released from the tendons by gently titrating the EDLs in a 10 cm dish containing DMEM with a wide bore glass pasture pipette coated in fetal bovine serum (FBS) (Sigma, St. Louis, MO, USA). Fibers were then washed 3 times by transferring into a new 35 mm dish with 4 ml of DMEM. A 5-10 min recovery period at 37 °C was

allocated between each wash with a final recovery period of 1 hour prior to placement into culture. All dishes were coated with FBS and allowed to dry to prevent attachment of myofibers. Myofibers were cultured in 1 % Chick embryo extract (MP biomedicals, Solon, OH, USA) and 20 % FBS in DMEM (supplemented with 1 g/L glucose, L-glutamine, and 110 mg/ml sodium pyruvate). Myofibers were cultured at 37 °C, in 5 % CO_2.

2.10 Myoblasts Isolation and Culture

Primary myoblasts were isolated from 8-week old all hindlimb muscles following a protocol adapted from Yoshioka et al 2020 (Yoshioka et al. 2020). Muscles were minced and digested for 2 hours in 0.2 % Type I collagenase (LS004194, Worthington, Lakewood, NJ, USA) dissolved in DMEM supplemented with 1% penicillin/ streptomycin. Homogenates were diluted in PBS and filtered through a 100 µm nylon mesh strainer (Thermo Fisher Scientific). The flow-through was centrifuged at 1200 RPM for 5 minutes and the resulting cell pellet was resuspended in growth medium (DMEM supplemented with 30 % FBS, 1% Chick embryo extract (2850145, MP biomedicals, Solon, OH, USA), 2.5 ng/ml of basic fibroblast growth factor (bFGF/FGF-2) (SRP4037, Sigma-Aldrich) and 1 % penicillin/streptomycin). Fibroblasts and remaining debris were removed by pre-plating 3-5 times for 2 hours each on non-coated dishes. Cells were then cultured on dishes coated in 100 µg/ml of collagen (354236, Corning, Bedford, MA, USA) diluted in PBS. The purity of each cell line generated was assessed by immunostaining for Pax7. Only cell preparations with >85 % of nuclei being Pax7 positive were utilized. In addition, only cells below passage number 7 were used in effort to reduce fibroblast contamination and to ensure minimal phenotypic shifts due to cell age.

2.11 Differentiation Assays

For the differentiation assays, primary myoblasts (50 000 cells/well) were seeded in collagen coated IBIDI 8-well chamber slides. When confluence reached at least 80 %, cells were serum-starved to induce differentiation by switching to differentiation media (DMEM supplemented with 5 % horse serum, 1 % penicillin/streptomycin) which marked day 0 of the time course. Myoblasts were treated with either PBS (Ctl) or 25 µg/ml of carbenoxolone (CBX; Sigma-Aldrich, C4790) starting upon the switch to differentiation conditions (day 0) and refreshed every 24 hours.

HSMM (70 000 cells/well) were seeded in 24-well dishes containing one collagen coated glass cover slip. Cells were transduced with a lentivector containing either GFP or PANX1 (Xiang et al. 2018) one day prior to induction of differentiation as stated above. Cells were fixed in 3.7 % PFA every day for 3 days for primary myoblasts and on day 5 of differentiation for HSMM. Cells were stained for myosin heavy chain (MHC) and either mounted with Fluoromount-DAPI (Southern Biotech, Birmingham, AL, USA) or stained with Hoechst-33342 (10 µg/ml) (Invitrogen). Cells were imaged with the EVOS FL Auto fluorescent microscope (Thermo Fisher Scientific) under 20X magnification. The differentiation index (number of MHC positive cells/ total number of nuclei) and fusion index (number of nuclei in myotubes/total number of nuclei) were analyzed from days 3-5.

2.12 Dye Uptake Assays

The low [K^+] solution (145 mM NaCl, 5 mM KCl, 1.4 mM $CaCl_2$, 1 mM $MgCl_2$, 10 mM HEPES diluted in ddH_2O) and high [K^+] solution (60 mM NaCl, 50 mM KCl, 1.4 mM $CaCl_2$, 1

mM $MgCl_2$, 10 mM HEPES diluted in ddH_2O) were prepared as described by Silverman et *al* 2009 (Silverman et al. 2009). Cells were washed twice with 1 ml of either the low [K^+] or high [K^+] solution, then incubated in a fresh 1 ml of the low [K^+] or high [K^+] solution for 5 minutes at 37 °C, in 5% CO_2. Next, cells were incubated with 4 mg/ml of sulforhodamine B dye (S1307, Invitrogen, Waltham MA, USA) dissolved in low [K^+] or high [K^+] solution for 15 minutes at 37 °C, in 5% CO_2, washed, and imaged immediately with the EVOS FL Auto fluorescent microscope (Thermo Fisher Scientific) under 10X magnification. Ten random fields of view were imaged per slide. Images were counted for the incidence of dye uptake defined as the percentage of cells that up took the dye.

2.13 Transfection

Human skeletal muscle myoblasts (HSMM) on collagen-coated 35mm dishes were transfected with 5 nM of Silencer® Select siRNA targeting *PANX1* (5' CGAUCAGUUUCAGUGCAAAtt 3') or 5 nM of the Silencer® Select Negative Control No. 1 (ambion 4390843, Thermo Fisher Scientific, Carlsbad CA, USA) using Lipofectamine 2000 (Thermo Fisher Scientific) as per the manufacturer's protocol. Dye uptake assays were performed 48 hours post-transfection. Once completed, cell lysates were collected to confirm successful knockdown via western blotting.

2.14 Immunofluorescence

Tissue, myofibers, and myoblasts were fixed in 3.7 % PFA diluted in PBS for 20 minutes and permeabilized in 0.1 M glycine and 0.1 % Triton X-100 in PBS for 10-15 minutes. Non-

specific labeling was blocked for 1 hour in 5 % horse serum, 2 % BSA and 0.1 % Triton X-100 in PBS. Samples were incubated with antibodies against their desired target at either room temperature for 1 hour or 4 °C overnight for myofibers (See Table #1 For complete list of primary antibodies). Incubation with anti-mouse Alexa Fluor 488 or anti-rabbit Alexa Fluor 594 (1:1000, Cat# A11017 and Cat# A11012, Life technologies, Eugene, OR, USA) secondary antibodies were then incubated temperature for 1 hour. Slides were mounted with Fluoromount-DAPI (Southern Biotech, Birmingham, AL, USA). Myoblasts seeded in IBIDI Chambers were instead co-stained with Hoechst-33342 (10 µg/ml) (Invitrogen). Samples were visualized with either the EVOS FL Auto (ThermoScientific) under 20X magnification or with the Olympus Fluoview FV1000 confocal microscope under 20X, 60X or 100X magnification.

2.15 Western Blotting

Tissue samples were homogenized in 1 % SDS using the Omni Bead Ruptor (Omni International, Kennesaw GA) as previously described (Pham et al. 2018). Cell Lysates were lysed in 150 mM NaCl, 10 mM Tris, 1 mM EDTA, 1 mM EGTA, 1 % Triton, 0.5 % NP-40, and proteinases and phosphatase inhibitors (Cell Signaling ON. CA) for 1 hour. All samples centrifuged at 12 000 rpm to remove cell debris. Equal amounts of protein were separated by SDS-PAGE, transferred to PVDF membranes, and non-specific binding was blocked with 5 % bovine serum albumin in PBS + 0.05 % Tween 20. Membranes were incubated with their primary antibody of interest overnight at 4 °C (See Table #1 For complete list of primary antibodies). Secondary antibodies Alexa 680- (1:5000, Cat#A21009, Thermo Fisher Scientific, Carlsbad CA, USA) or Infrared fluorescent-labeled secondary antibodies IRDye800 (cat#925-32210, Li-COR Biosciences, Lincoln, NE, USA) were used at 1:5000 – 1:10 000. Immunoblots were processed

with the Odyssey infrared-imaging system (LI-COR biosciences) and quantified using the ImageJ software.

2.16 Statistical Analysis

The data were analyzed using unpaired or paired two-tailed student's *t*-tests, one-way ANOVA followed by Tukey's *post hoc* tests, and two-way ANOVA followed by Sidak's *post hoc* tests. The level of significance was set at $*P \leq 0.05$, $**P \leq 0.01$, $***P \leq 0.001$. All data are represented as mean ± s.d. The number of animals and specific statistical tests used for each experiment are indicated in the figure legends. All tests and/or counts were performed blinded to the observer. The individual data (each animal) points are also displayed on the graphs. Graphs and associated statistical tests were generated in the Prism 8 (GraphPad) software.

Table 1: Complete List of Primary Antibodies

Antibody target/ name	Company	Catalogue number	Western Dilution	IF Dilution
Alpha tubulin (TU-02)	Santa Cruz (CA, USA)	SC-8035	1:1000	N/A
Cleaved Caspase-3 D175	Cell Signaling (MA, USA)	9661s	1:1000	N/A
GAPDH 14C10	Cell Signaling (MA, USA)	2118	1:1000-1:5000	N/A
GAPDH 6C5	Advanced immunochemicals (CA USA)	2-RGM2	1:5000	N/A
Laminin	Abcam (Cambridge UK)	ab11575	N/A	1:500
MHC MF20	R&D Biosystems	MAB4470	1:5000-1:10 000	1:500
Mouse Panx1 D9M1C	Cell Signaling (MA, USA)	91137	1:200	N/A
Myh3 F1652	Santa Cruz (CA, USA)	sc-53091	N/A	1:250
MyoD	Novus (CO, USA)	NBP1-54153SS	1:500	1:250
MyoG F5D	Santa Cruz (CA, USA)		1:500	1:250
PANX1 (Human)	Sigma Aldrich (MO, USA)	HPA016930	1:1000	1:200
Pax 7 hybridoma cell supernatant	DSHB, (IA, USA)	N/A	1:10	1:2
P2Y1 (E-1)	Santa Cruz (CA, USA)	Sc-377324	1:100	N/A

Chapter 3 : Results Part 1; Sex-Dependent Role of Pannexin 1 in Regulating Skeletal Muscle and Satellite Cell Function

Authors: Emily Freeman, Stéphanie Langlois, Kaylee Scott, Aymeric Ravel-Chapuis, Bernard J. Jasmin, Kyle N. Cowan

Status: Data from this chapter has been published in *The Journal of Cell Physiology* July 2022. DOI: 10.1002/jcp.30850

3.1 Author Contributions and Acknowledgements

I would like to acknowledge Dr. Stéphanie Langlois for her assistance with the maintenance of the mouse colony, assistance with the P2Y1 western blots (Figure 3.4), performing the inverted screen test (Figures 3.1J and 3.1I) and the genotyping shown in Figure 3.6A, and for her critical review of this chapter. Our previous CO-OP student Kaylee Scott (BSc) helped immensely with troubleshooting western blots for this aim and contributed to Figures 3.1A and 3.2A. Dr. Aymeric Ravel-Chapuis of the Dr. Bernard Jasmin laboratory performed the cardiotoxin injections and collected the affiliated samples. Dr. Kyle Cowan aided with the study design and project supervision. Special thanks to Dr. Leigh Anne Swayne and Dr. Valery Shestopalov for providing us with *Panx1*$^{+/-}$ breeders, Alexandra Welten (MSc) for technical assistance during dissections and the University of Ottawa Animal Behaviour Core facility for their training in the grip strength and wire hang measures. This study was funded in part by the Department of Surgery at the Children's Hospital of Eastern Ontario, the Children's Hospital of Eastern Ontario Research Institute and Queen Elizabeth II Graduate Scholarship in Science and Technology (QEII-GSST).

3.2 Background and Rationale

It has been previously demonstrated that Panx1 levels increase during myoblast differentiation *in vitro* and during *in vivo* regeneration (Langlois et al. 2014; Pham et al. 2018; Suarez-Berumen et al. 2021). Overexpression of Panx1 protein promotes differentiation of human skeletal muscle myoblasts (HSMM) while its inhibition in both human and murine models impedes differentiation (Langlois et al. 2014; Riquelme et al. 2015; Suarez-Berumen et al. 2021). Additionally, Panx1 protein levels increase during murine embryonic development implicating it

in the development of post-natal skeletal muscle (Pham et al. 2018). Panx1 signaling via P2 receptors has been suggested to play key roles in contraction-potentiation (Buvinic et al. 2009; Riquelme et al. 2013) and excitation-transcription coupling leading to changes in muscle plasticity (Jorquera et al. 2013). Despite this accumulating evidence indicating a role for Panx1 in skeletal muscle health and development, this had yet to be investigated in detail. Furthermore, with sex playing a well-known role in the development, differentiation, and maintenance of skeletal muscle, it had yet to be Investigated as to whether Panx1 plays sex-specific roles in this context.

3.3 Results

3.3.1 Genetic Ablation of Panx1 Affects Male Muscle Fiber Size and Strength

Prior to characterizing the *Panx1* knockout mice, Panx1 protein levels in the *Tibialis anterior* (TA), *Extensor digitorum longus* (EDL), *Soleus* (Sol), *Gastrocnemius* (Gastroc), and *Quadriceps* (Quad) muscles in 12-week-old male wild-type (WT) mice were analyzed through western blot analysis. In agreement with our previous observation (Pham et al. 2018), higher Panx1 levels were found in the Sol of male mice while the TA, EDL, Gastroc, and Quad showed weaker Panx1 expression (Figure 3.1A). The specificity of the Panx1 antibody is shown by the absence of signal in the TA from male global *Panx1* knockout (*Panx1* KO) mice compared to their WT littermates (Figure 3.1B). In accordance with previous reports, the total body weight of male *Panx1* KO mice was equivalent to that of WT littermates (Sanchez-Arias et al. 2019; Lee et al. 2018) (Figure 3.1C). Male *Panx1* KO mice had comparable wet muscle weight to that of WT controls in all muscles (TA, EDL, Sol, Gastroc, and Quad) collected (Figure 3.1D), implying that loss of *Panx1* does not result in any large-scale muscle wasting or hypertrophy in male mice.

To examine whether *Panx1* loss affects fiber size, the fiber cross sectional area (CSA) was assessed in cross-sections from one fast- and one slow-twitch muscle that express higher levels of Panx1, namely the TA and Sol, respectively. This was also done in 12-week-old animals as myofiber size is stabilized by that age (Bachman et al. 2018). In male TA muscles, the fiber size distribution shows that *Panx1* KO mice have an increased number of smaller fibers (1001-2000 μm^2) than their WT counterparts (Figure 3.1E). This was complemented by a ~40 % decrease in the mean fiber size of the TA (Figure 3.1F). The Sol muscle from male *Panx1* KO mice also showed a higher frequency of smaller fibers (Figure 3.1G) and had a ~25 % reduction in the mean fiber size (Figure 3.1H).

To determine whether this reduction in fiber CSA correlates with diminished muscle strength, the forelimb grip strength of male *Panx1* KO was measured. In line with our CSA data, male *Panx1* KO mice had significantly reduced forelimb grip strength (Figure 3.1I). We additionally tested muscle function with the Kondziell''s inverted wire hang test in which *Panx1* KO males had a significantly reduced latency to fall, further indicating a loss of muscle strength in male *Panx*1 KO mice.

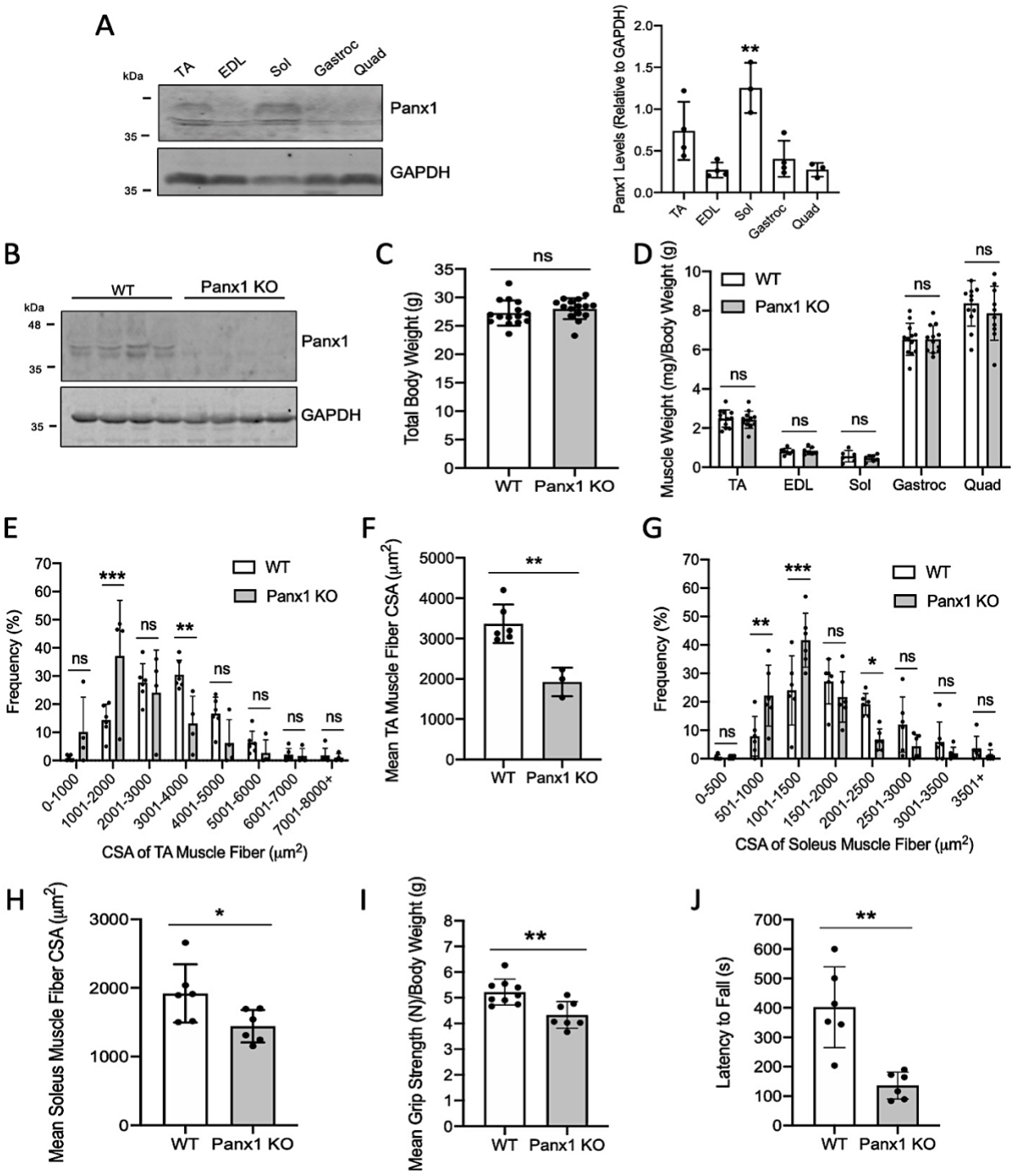

Figure 3.1: Loss of *Panx1* reduces male muscle size and strength.

A) Representative Western blot showing Panx1 and GAPDH levels in select hindlimb muscles isolated from male WT mice (LEFT). Quantification of Panx1 protein levels normalized to GAPDH (RIGHT) (n=3; One-way ANOVA followed by Tukey's post hoc). **B)** The specificity of the Panx1 antibody was verified by the presence of bands in TA muscle from WT (n=4) and the

absence of signal in TA muscle from Panx1 KO (n=4). **C)** The total body weight (g) of 12-week-old male WT (n=15) and Panx1 KO (n=15; unpaired two-tailed student's t-test) mice. **D)** The wet muscle weight of the Tibialis anterior (TA), Extensor digitorum longus (EDL), Soleus (Sol), Gastrocnemius (Gastroc), and Quadriceps (Quad) muscles in 12-week-old male Panx1 KO ($n \geq 6$; Two-way ANOVA followed by Sidak's post hoc) compared to that of WT mice ($n \geq 6$;One-way ANOVA followed by Sidak's post hoc). Male TA muscles from WT and Panx1 KO mice were measured for fiber cross-sectional area (CSA) and the **E)** distribution of CSAs (n=3-6; Two-way ANOVA followed by Sidak's post hoc) and the **F)** mean CSA were plotted (n=3-6; unpaired two-tailed student's t-test). Male Sol muscles were measured for the **G)** distribution of fiber sizes (n=6: Two-way ANOVA followed by Sidak's post hoc) **H)** mean CSA (n=6; two-tailed, unpaired student's t-test). **I)** Mean forelimb grip strength normalized to body weight (g) in adult male WT and Panx1 KO mice (n=7-9; unpaired two-tailed student's t-test). **J)** Mean wire hang fall latency (seconds) of male WT and Panx1 KO mice (n=6; unpaired two-tailed student's t-test). Data are represented as mean ± s.d. *P<0.05, **P<0.01, ***P<0.001, n.s: non-significant.

We next assessed overall Panx1 protein levels in TA, EDL, Sol, Gastroc and Quad of adult (12-week-old) female WT mice. Similar to the male WT muscles and in agreement with our previous data (Pham et al. 2018), Panx1 protein was detected in all isolated muscles with the highest levels being in the Sol (Figure 3.2A). In accordance with previous reports, the total body weight of female *Panx1* KO mice was comparable to that of their WT counterparts (Figure 3.2B) (Sanchez-Arias et al. 2019; Lee et al. 2018). The wet muscle weight of all isolated muscles also did not differ between female *Panx1* KO and WT mice (Figure 3.2C).

Unlike their male littermates, female *Panx1* KO mice showed no changes in the fiber size distribution or mean fiber size of the TA (Figure 3.2 D-E) or Sol muscles (Figure 3.2 F-G). In line with these findings, female WT and *Panx1* KO mice had comparable mean forelimb grip strength and latency to fall during the wire hang test (Figure 3.2 H-I). These findings suggest that, while Panx1 is necessary for proper male muscle function, it may be dispensable in female muscle.

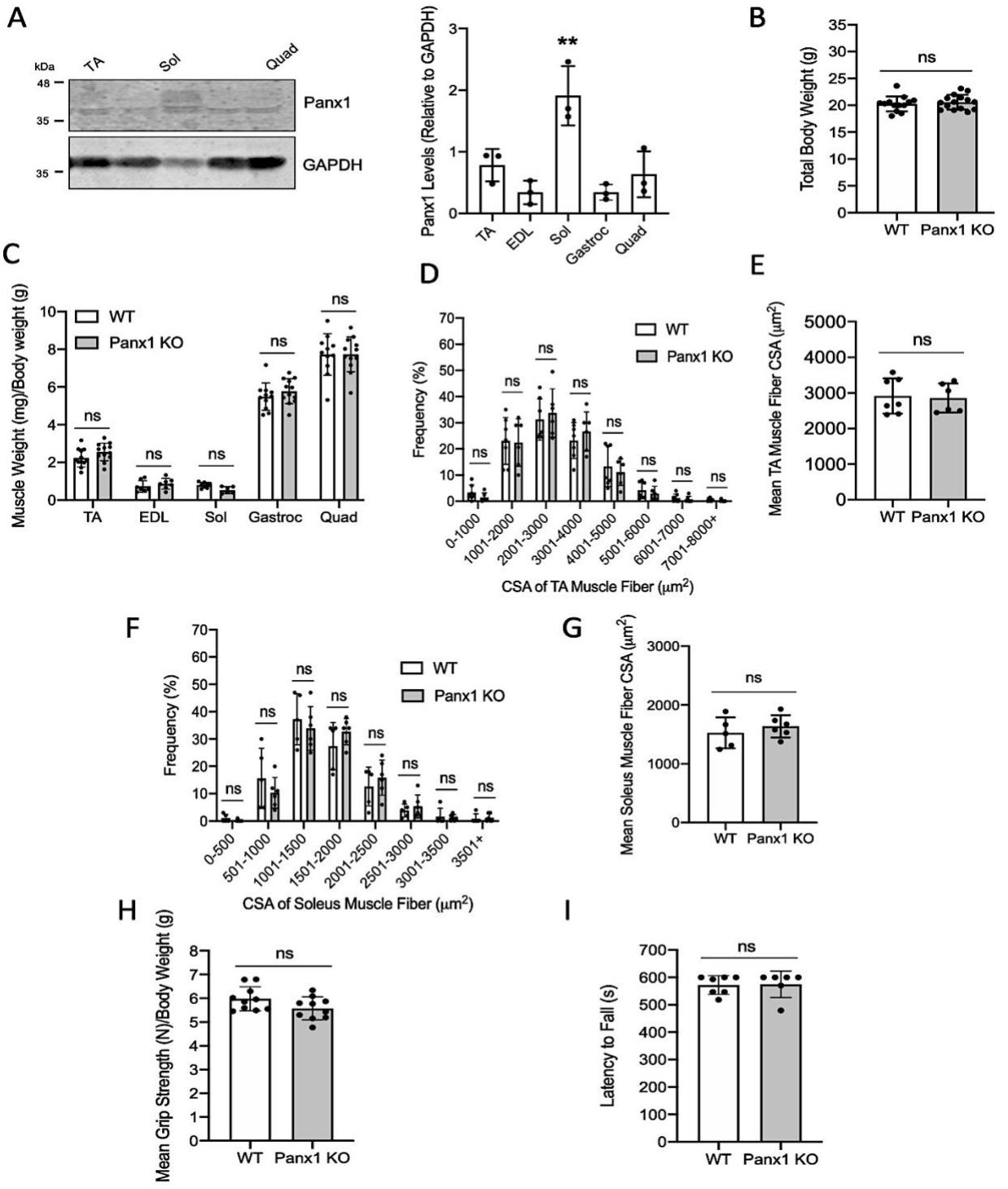

Figure 3.2 :Loss of *Panx1* does not affect female muscle size and strength.

A) Representative Western blot showing Panx1 and GAPDH levels in select hindlimb muscles isolated from female WT mice (left). Quantification of Panx1 protein levels normalized to GAPDH (right) (n=3; One-way ANOVA followed by Tukey's post hoc). **B)** The total body weight (g) of 12-week-old female WT (n=13; unpaired two-tailed student's *t*-test) and Panx1 KO (n=15) mice.

C) The wet muscle weight of the *Tibialis anterior* (TA), *Extensor digitorum longus* (EDL), *Soleus* (Sol), *Gastrocnemius* (Gastroc), and *Quadriceps* (Quad) muscles in 12-week-old female *Panx1* KO (n≥6) compared to that of WT mice (n≥6; Two-way ANOVA followed by Sidak's post hoc). Female TA muscles were measured for fiber cross-sectional area (CSA) and the **D)** distribution of CSAs (n≥6; Two-way ANOVA followed by Sidak's post hoc) and the **E)** mean CSA were plotted (n≥6; unpaired two-tailed student's t-test). Female WT and *Panx1* KO Sol muscles were measured for the **F)** distribution of fiber sizes (n≥5; Two-way ANOVA followed by Sidak's post hoc) **G)** mean CSA (n≥ 5; unpaired two-tailed student's t-test). **H)** Mean forelimb grip strength normalized to body weight (g) of adult female WT and *Panx1* KO mice (n=10; unpaired two-tailed student's *t*-test). **I)** Latency to fall (seconds (s)) during wire hang (n=≥6; unpaired two-tailed student's *t*-test). Data are represented as mean ± s.d. ***P*<0.01, n.s: non-significant.

3.3.2 Panx1 is Required in Males for Efficient Myoblast Fusion

To examine whether the sex-specific reduction of fiber size in male *Panx1* KO mice may be due to defects in progenitor differentiation and/or fusion, primary myoblasts were isolated from the hindlimbs of female and male WT and *Panx1* KO mice and induced to differentiate via serum starvation for 3 days. Myoblasts were stained for the late differentiation marker myosin heavy chain (MHC) (Figure 3.3A), and the differentiation and fusion indices were determined. Neither the differentiation index nor the fusion index was significantly altered in myoblasts from female *Panx1* KO mice compared to that of WT myoblasts (Figure 3.3 B-C). While primary myoblasts from male *Panx1* KO mice had a comparable differentiation index to that of WT myoblasts at all timepoints, the fusion index of *Panx1* KO myoblasts was significantly decreased on days 2 and 3 (Figure 3.3 D-E).

We next quantified MHC levels in the TA and Sol muscles of *Panx1* KO and WT mice, as well as in the Gastroc since it represents a significant proportion of the muscles from which primary myoblasts were isolated for the differentiation and fusion assays (Figure 3.3 F-M). In female mice, similar MHC levels were detected between the two genotypes in all selected muscles (Figure 3.3 F-I). The male TA and Sol muscles also had comparable levels of MHC between Panx1

KO and WT littermates. Notably, the Gastroc muscles of male *Panx1* KO mice had significantly less MHC than that of WT mice (Figure 3.3 J-M). Together, these data indicate that genetic ablation of *Panx1* significantly impedes myoblast fusion, as well as gastrocnemius muscle maturation in male mice.

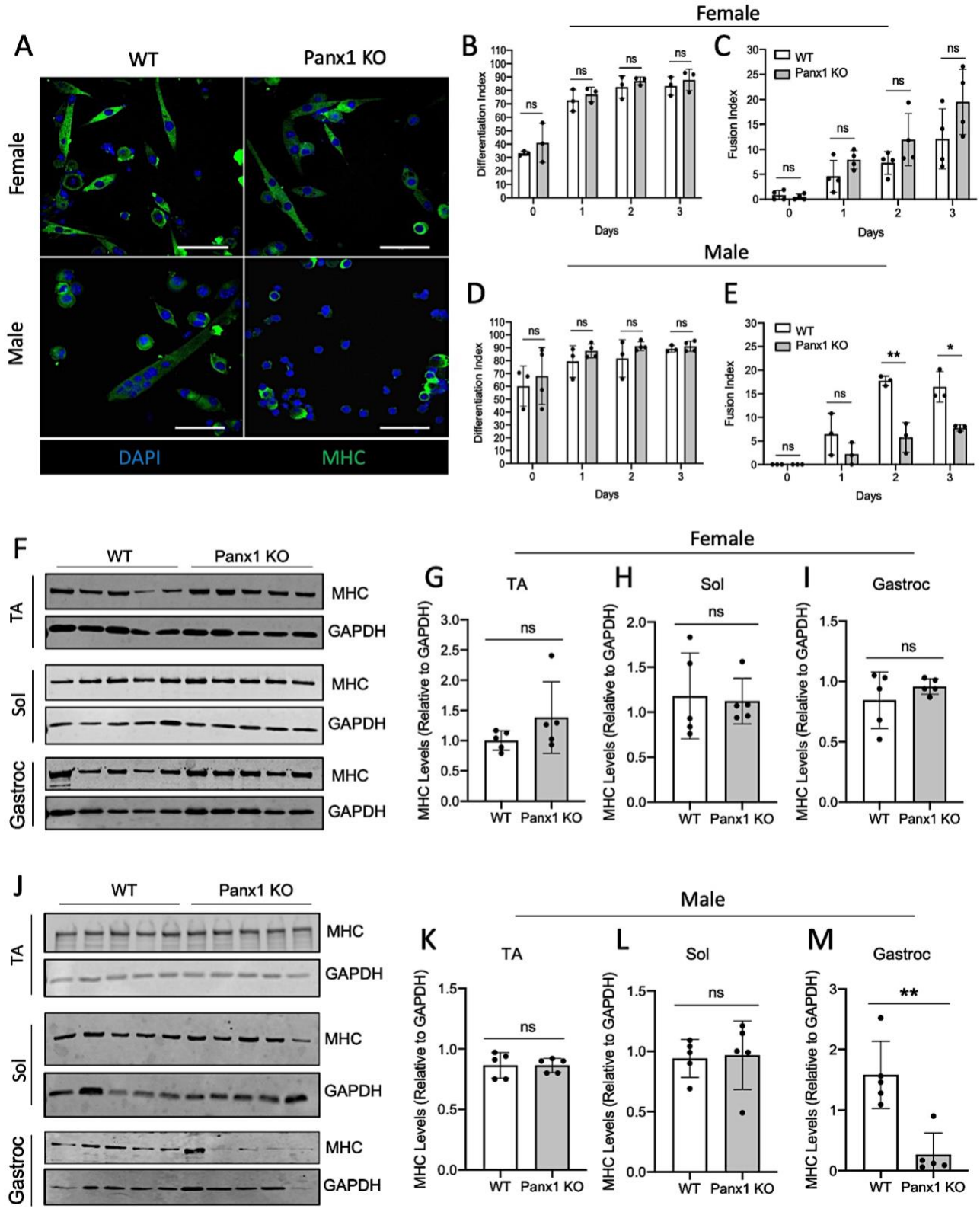

**** Figure caption on next page**

Figure 3.3: Male *Panx1* KO primary myoblasts have reduced fusion and the gastrocnemius muscle from these mice express less MHC.

A) Primary myoblasts were allowed to differentiate for 3 days to produce myotubes. Myotubes were stained with MHC (green) and DAPI (blue). Representative images of day 3 are shown. Scale bar = 50 µm. Myotubes from female mice were analyzed daily for differentiation by the **B)** differentiation index (proportion of MHC positive nuclei/total nuclei) and the **C)** fusion index (number of nuclei in myotubes/total nuclei) (n=4; Two-way ANOVA followed by Sidak's post hoc). **D)** Differentiation and **E)** fusion indices were similarly calculated for myoblasts from male mice (n=3; Two-way ANOVA followed by Sidak's post hoc). **F)** Western blots of MHC and GAPDH levels and quantification in female **G)** TA, **H)** Sol and **I)** Gastroc (n=5; unpaired two-tailed students *t*-test). **J)** Western blots of MHC and GAPDH levels and quantification in female **K)** TA, **L)** Sol and **M)** Gastroc (n=5; unpaired two-tailed students *t*-test). Data are represented as mean ± s.d. **P*<0.05, ***P*<0.01, n.s.: non-significant.

3.3.3 Difference in P2Y1 Receptor Expression does not Account for the Sex-Dependent Effect of the Loss of *Panx1*

It has been shown that Panx1 channels mediate the acquisition of myogenic commitment and increase MyoD levels in C_2C_{12} reserve cells via a process that involves P2Y1 receptors (Riquelme et al., 2015). Additionally, it has been reported that Panx1 facilitates muscle contraction potentiation by activating P2Y1 receptors (Riquelme et al. 2013). Thus, to establish if differences in P2Y1 expression could potentially account for the sex-dependent effect seen in the *Panx1* KO mice, we assessed P2Y1 levels in myoblasts derived from female and male WT and *Panx1* KO mice (Figure 3.4 A-D). The protein levels of P2Y1 were comparable between WT and *Panx1* KO mice in both males and females (Figure 3.4A-D), suggesting that the effects seen here are not due to a sex specific alteration of P2Y1 levels in the KO mice.

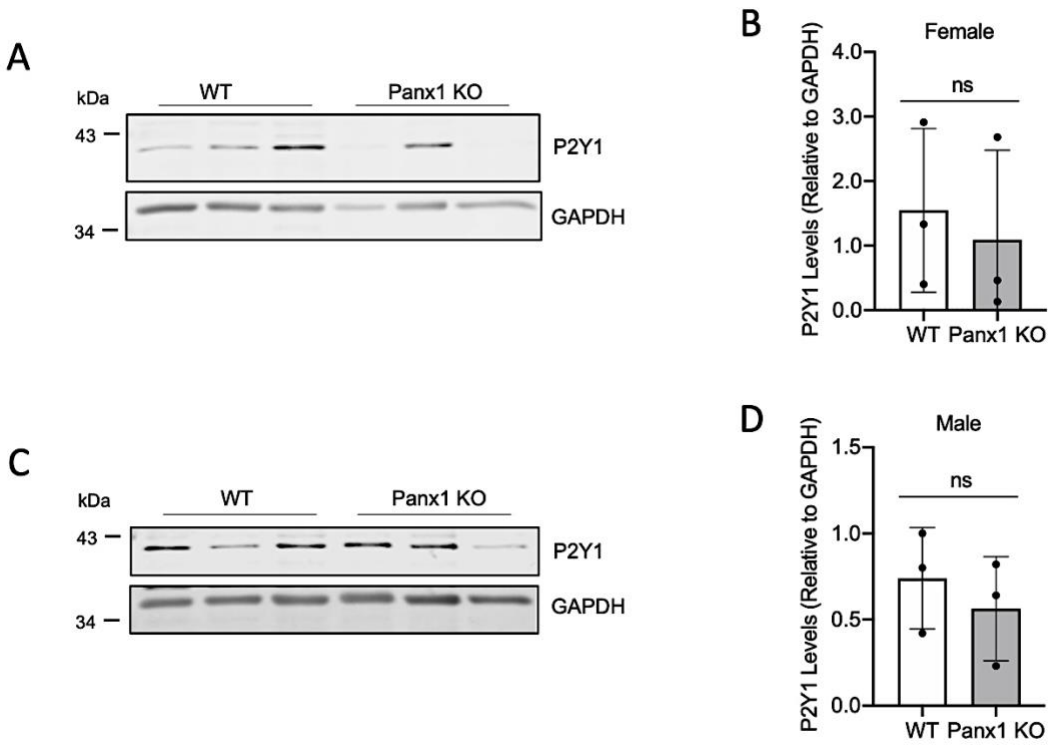

Figure 3.4:P2Y1 levels are not altered following loss of *Panx1*.

A) Western blot of P2Y1 and GAPDH levels in female WT and *Panx1* KO myoblasts and the **B)** quantification of P2Y1 levels normalized to GAPDH (n=3; unpaired two-tailed student's *t*-test). **C)** Western blot of P2Y1 levels in male WT and *Panx1* KO myoblasts and **D)** quantification of P2Y1 levels normalized to GAPDH (n=3; unpaired two-tailed student's *t*-test). Data represents mean ± s.d. **P*<0.05; ** *P*<0.01; ns, non-significant.

3.3.4 Loss of *Panx1* Reduces Satellite Cell Number and Delays Early Satellite Cell Differentiation in Myofibers from Male Mice

To elucidate whether Panx1 regulates SC number and their progression through proliferation and differentiation *ex vivo*, cultured single-fiber SCs isolated from the EDL of female and male WT and *Panx1* KO mice were used. This culture model has the advantage of preserving the myofibers attachment to SCs which endogenously express Panx1 (Figure 3.5A), enabling their native activation, proliferation, and differentiation on myofibers (Brun, Wang, and Rudnicki 2018). In this model, SCs initially only express Pax7, then activate MyoD, and enter the cell cycle. Proliferating cells then either down-regulate Pax7 to differentiate, or down-regulate MyoD and self-renew (Hernandez-Hernandez et al. 2017; Zammit et al. 2004; Collins et al. 2005). WT and *Panx1* KO myofibers were first examined for the number of SCs immediately (0 hours) after isolation by Pax7 immunostaining (Figure 3.5B). As previously observed (Neal, Boldrin, and Morgan 2012), SC number was lower in WT female mice compared to WT male mice (Figure 3.5C,D). Female *Panx1* KO mice had comparable SC numbers to that of WT mice (Figure 3.5C). Conversely, male *Panx1* KO mice had significantly less SCs per fiber than WT mice indicating that loss of *Panx1* interferes with development of the SC pool in male muscle (Figure 3.5D).

After 48 hours in culture, cells were then stained for Pax7 and MyoD to determine the percentage of self-renewing ($Pax7^+/MyoD^-$), proliferating ($Pax7^+/MyoD^+$), and differentiating ($Pax7^-/MyoD^+$) cells from each genotype (Figure 3.5E). Of all the populations assessed after 48 h of culture there was no significant difference between female WT and *Panx1* KO mice (Figure 3.5F-H). However, in male mice the proportion of self-renewing ($Pax7^+/MyoD^-$) cells was increased in male *Panx1* KO myofibers (Figure 3.5I). While the proportion of

proliferating ($Pax7^+/MyoD^+$) cells was not affected (Figure 3.5J), the proportion of differentiating ($Pax7^-/MyoD^+$) cells was significantly decreased in myofibers from male *Panx1* KO mice (Figure 3.5K).

To assess terminal differentiation, myofibers were fixed after 72 hours of culture, labelled for the differentiation marker Myogenin (MyoG) (Figure 3.5L) (Hernandez-Hernandez et al. 2017; Zammit et al. 2006). Interestingly, the percentage of MyoG positive cells was comparable between WT and *Panx1* KO myofibers isolated from both female and male mice (Figure 3.5M-N). These data are in line with our findings from primary myoblasts showing terminal differentiation is not altered by genetic ablation of *Panx1*. Collectively these data indicate that male, but not female, muscles require Panx1 for the development of the SC pool and this likely causes defects in early differentiation.

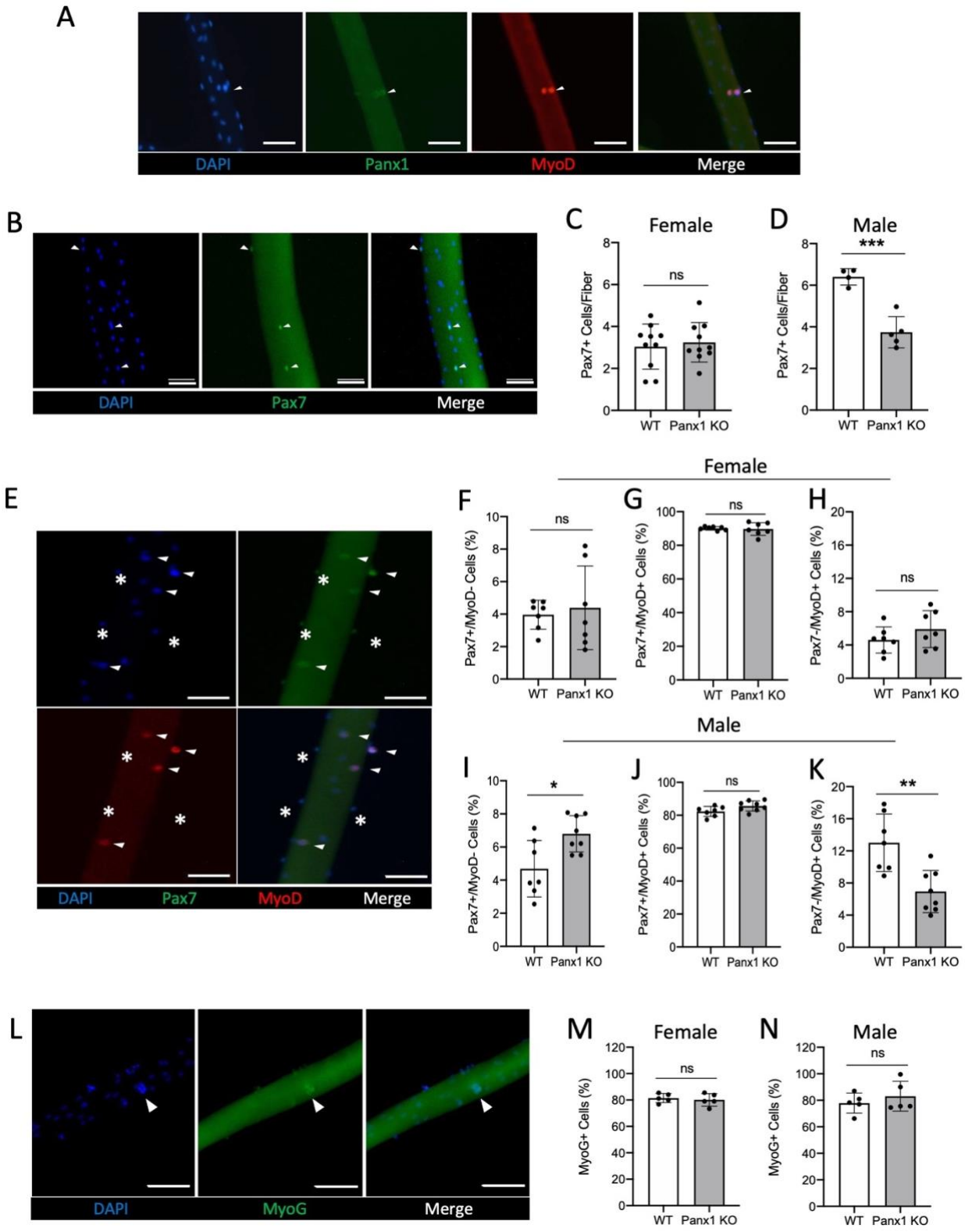

****Figure caption on next page**

Figure 3.5: Genetic ablation of *Panx1* reduces satellite cell numbers in males but not females.

A) Myofibers were isolated from the EDL of WT mice and stained for DAPI (blue), Panx1 (green), and MyoD (red). Arrows depict fiber-bound muscle progenitors. Scale bar = 50 µm. **B)** Representative images of 0 h myofibers stained for DAPI (blue) and Pax7 (green). Scale bar = 50 µm. Myofibers isolated from **C)** female (n=10; unpaired two-tailed student's *t*-test) and **D)** male (n=4-5; unpaired two-tailed student's *t*-test) mice were fixed immediately after isolation and assessed for number of Pax7 positive cells per fiber. **E)** Representative images of myofibers stained following 48 h of culture for DAPI (blue), Pax7 (green), and MyoD (red). Scale bar = 50 µm. Female myofibers were fixed at 48h post isolation and assessed for the percentage of **F)** self-renewing ($Pax7^+/MyoD^-$), **G)** proliferating ($Pax7^+/MyoD^+$), and **H)** differentiating ($Pax7^-/MyoD^+$) cells (n=7; unpaired two-tailed student's *t*-test). Male myofibers were also fixed at 48h and the percentage of **I)** self-renewing ($Pax7^+/MyoD^-$), **J)** proliferating ($Pax7^+/MyoD^+$), and **K)** differentiating ($Pax7^-/MyoD^+$) cells was counted (n=7-8; unpaired two-tailed student's *t*-test). **L)** Representative images of myofibers fixed after 72h of culture and stained for DAPI (blue) and MyoG (green). At 72 h post isolation, myofibers from **M)** female (n=5; unpaired two-tailed student's *t*-test) and **N)** male (n=5; unpaired two-tailed student's *t*-test) EDL muscle and the percentage of MyoG positive cells was counted. Data are represented as mean ± s.d. **P*<0.05, ****P*<0.01, ****P*<0.001, n.s.: non-significant.

3.3.5 Impairment of fusion in myoblasts from male *Panx1* KO mice is due to loss of *Panx1* and not the *Casp11^{mut}*

A previous report highlighted that Panx1 KO mice contain a passenger mutation resulting in the deletion of *caspase 11* (*Casp11^{mut}*). Genotyping confirmed the presence of this mutation in our *Panx1* KO mice, but not in their WT littermates (Figure 3.6A). To ensure that this *Casp11^{mut}* was not contributing to our findings, myofibers isolated from 8-week-old C57Bl/6J mice were treated with Panx1 pharmacological inhibitors carbenoxolone (CBX) (25 µM) and probenecid (PBN) (1 mM). Since male myofibers were the only ones to show differences, only myofibers from male mice were considered for this experiment. Myofibers treated with either CBX or PBN were fixed at 48 hours and assessed for the population of self-renewing, proliferating and differentiation progenitor as described in section 3.4.4. However, neither CBX nor PBN altered any of the populations assessed (Figure 3.6 B-D). These data infer that the loss of self-renewing cells observed in male *Panx1* KO myofibers (Figure 3.5 I)

is likely due to the loss of the SC pool observed in these mice and not an effect on SC activation nor proliferation.

Female and male WT myoblasts were next treated with CBX (25 μM) to confirm the role of Panx1 in progenitor fusion described above (Figure 3.3D) (Figure 3.6E). CBX treatment did not significantly affect the differentiation index (MHC positive cells/total nuclei) nor fusion index (number of nuclei in myotubes/ total nuclei) in female WT myoblasts (Figure 3.6 F-G). While differentiation was not greatly altered, CBX treatment in male WT myoblasts significantly decreased the fusion index (Figure 3.6 H-I). These data recapitulate my previous findings from *Panx1* KO myoblasts and that the impairment of fusion in myoblasts from male *Panx1* KO mice is due to loss of *Panx1* and not the $Casp11^{mut}$. These data further indicate that loss of Panx1 channel function significantly impairs male, but not female, myoblast fusion.

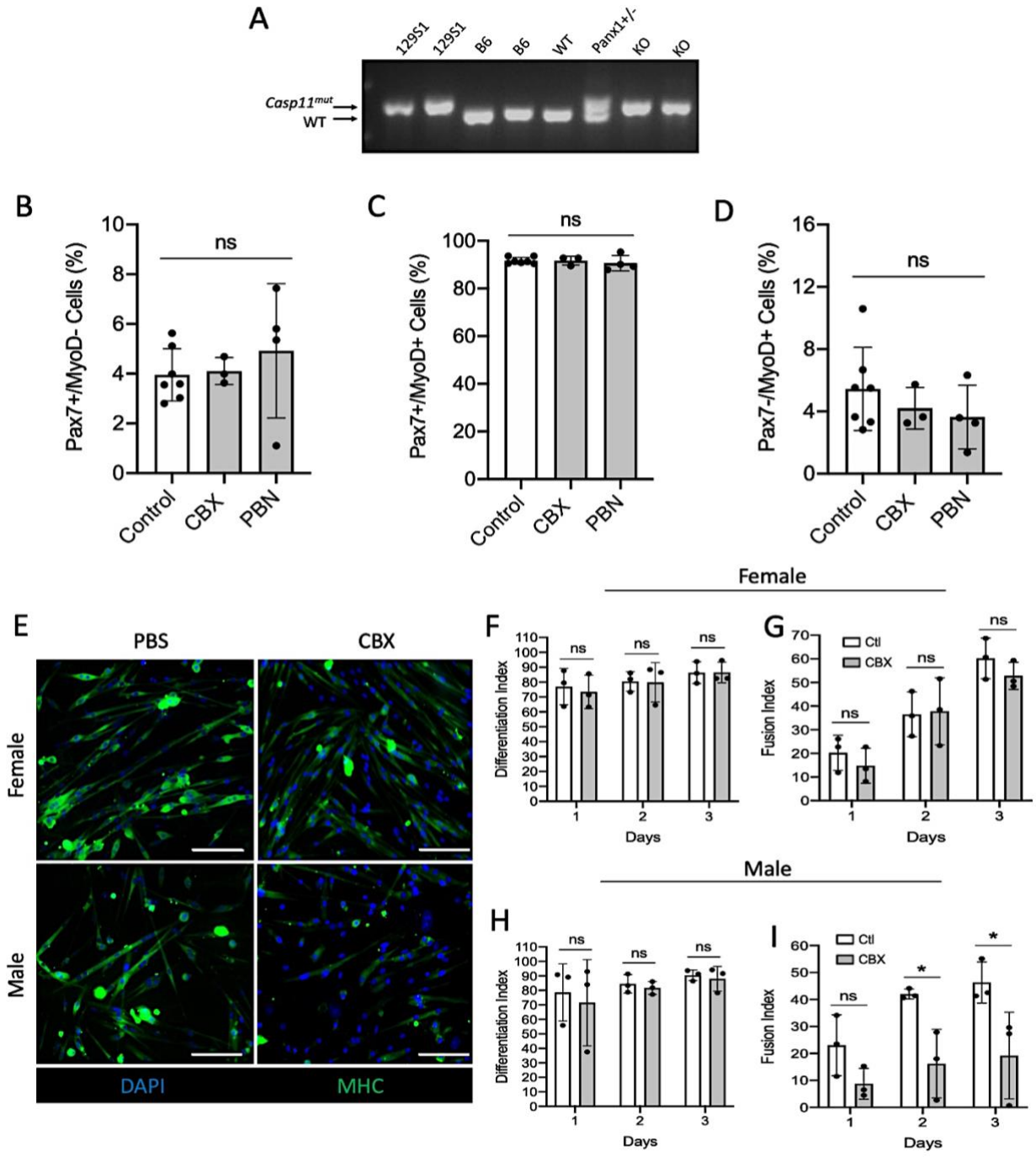

Figure 3.6: Impairment of fusion in myoblasts from male *Panx1* KO mice is due to loss of *Panx1* and not the *Casp11*^{mut}.

A) Genotyping analysis of *Panx1*$^{+/+}$ (WT) mice, *Panx1*$^{+/-}$ mice, and *Panx1*$^{-/-}$ (KO) mice for *Casp11* deletion (129S1 mice: positive control; B6: negative control mice). Myofiber isolated from male WT mice were treated with Panx1 inhibitors carbenoxolone (CBX;25 µm) and probenecid (PBN;1 mM), fixed at 48 h and assessed for the proportion of **B)** self-renewing (Pax7^{+}/MyoD^{-}), **C)** proliferating (Pax7^{+}/MyoD^{+}), and **D)** differentiating (Pax7^{-}/MyoD^{+}) cells (n=3-7; One-way ANOVA followed by Tukey's post hoc test). **E)** Representative images of

female and male WT myoblasts differentiated for 3 days. Myoblasts were stained for DAPI (blue) and MHC (green). Scale bar = 100 μm. Female myoblasts were assessed for **F)** differentiation index (percent of MHC positive cells/total nuclei) and **G)** fusion index (nuclei in myotubes/total nuclei) indexes for days 1-3 of differentiation (n=3; Two way-ANOVA followed by Sidak's post hoc test). Male myoblasts were differentiated for 3 days and the **H)** differentiation and **I)** fusion index was measured each day (n=3; Two way-ANOVA followed by Sidak's post hoc test). Data represent mean ± s.d., n.s.: non-significant.

3.3.6 Male and Female *Panx1* KO Mice both show an Increase in the Number of Regenerating Fibers during Early Stages of Skeletal Muscle Regeneration

Based on the sex-dependent role of Panx1 in regulating SC number and myoblast fusion, we then wanted to examine the role of Panx1 in skeletal muscle regeneration *in vivo* following cardiotoxin-induced injury. Injury was induced in 6-week-old mice as we have previously shown an increase in Panx1 levels during TA regeneration of wild-type mice using this model (Pham et al. 2018). Following cardiotoxin injection, TAs were collected at days 4, 7, and 14 post injury. First, the percentage of regenerating fibers, which were defined as any fiber containing centrally located nuclei (J. Liu et al. 2020), were counted at each timepoint post injury. Unexpectedly, both female and male *Panx1* KO mice showed an increased percentage of regenerating fibers at day 4 post injury, while no difference was observed at day 7 (Figure 3.7A-B). Interestingly, at day 14 post injury female *Panx1* KO mice had a small, yet significant, decrease in the proportion of regeneration fibers (Figure 3.7A), while no difference was captured in male mice at that time point (Figure 3.7B). In accordance with these data, injured TAs from both female and male *Panx1* KO mice had significantly more fibers/mm^2 than that of WT mice on day 4 post injury (Figure 3.7C-D). On days 7 and 14 post injury, female *Panx1* KO mice had a similar number of fibers to that of WT mice (Figure 3.7C). Male *Panx1* KO mice however had significantly more fibers/mm^2 on day 7 post injury (Figure 3.7D). To confirm the increase in regenerating fibers seen at day 4 post injury, TA cross-

sections were stained for embryonic myosin heavy chain 3 (Myh3), a marker of naïve muscle fibers (Schiaffino et al. 2015). In accordance with our data, injured TAs from both female and male *Panx1* KO mice had significantly more Myh3-positive fibers than that of WT mice (Figure 3.7E-G).

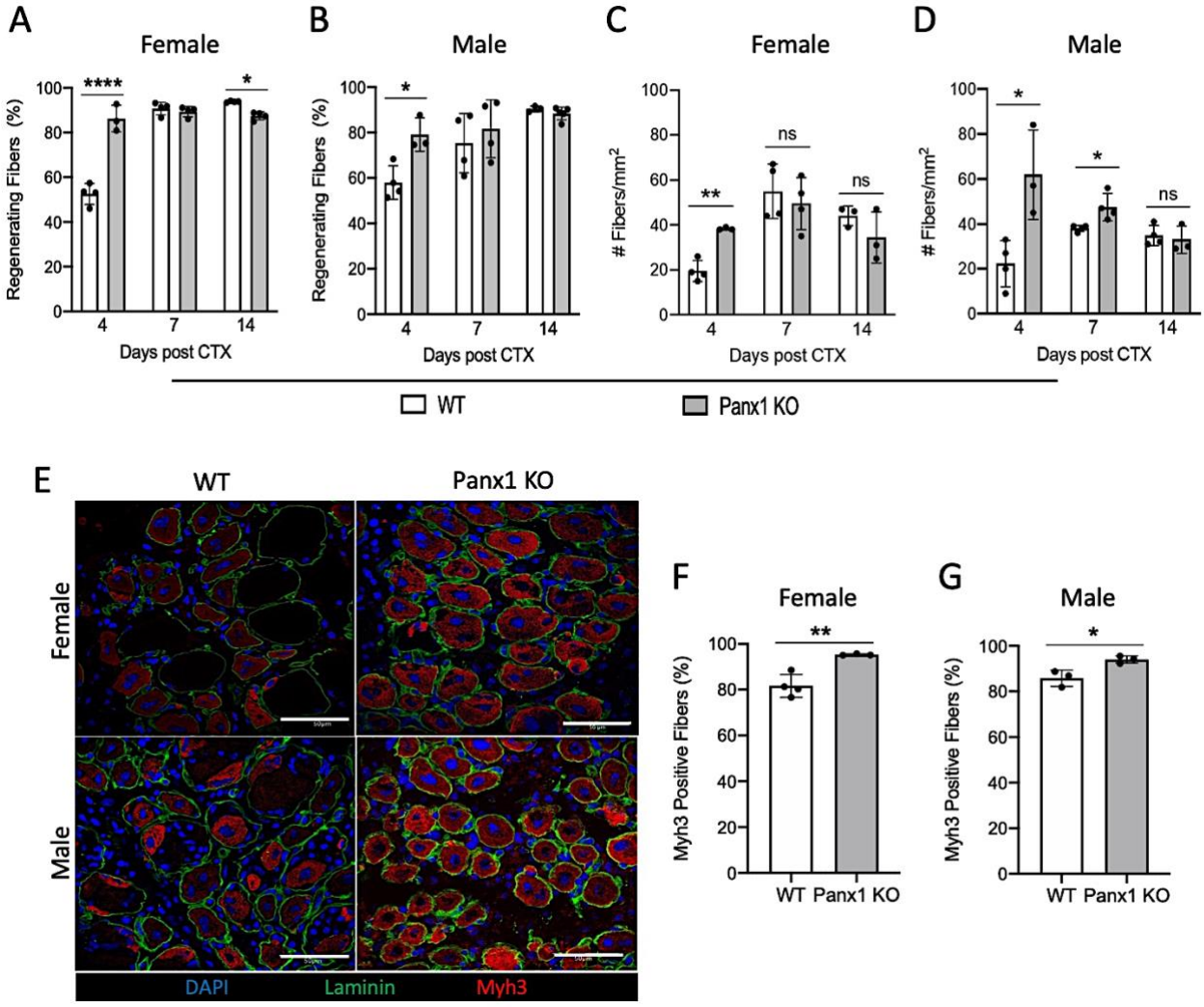

Figure 3.7:Male and female *Panx1* KO mice have an increased number of regenerating fibers during early stages of muscle regeneration.

Injury was induced in the TA muscles of male and female mice using cardiotoxin. TAs were then harvested 4-, 7-, and 14-days post injury. The percentage of regenerating fibers in **A)** females (n=3-4; Two-way ANOVA followed by Sidak's post hoc) and **B)** males (n=3-4; Two-way ANOVA followed by Sidak's post hoc) were counted at each day post injury. The total number of fibers per mm^2 was assessed at each time point in **C)** female and **D)** male TA muscles (n=3-4; Two-way ANOVA followed by Sidak's post hoc). **E)** Representative images of cross-sections stained on day 4 post injury for DAPI (blue), laminin (green), and Myh3 (red). Scale bar = 50 µm. Quantification of the number of Myh3 positive fibers in **F)** female and **G)** male TA muscles on day 4 post cardiotoxin injury (n=3-4; unpaired two-tailed student's *t*-test). Data represent mean ± s.d. **P*<0.05, ***P*<0.01, *****P*<0.0001, n.s.: non-significant.

3.3.7 *Panx1* Loss Results in Smaller New Fibers following Skeletal Muscle Injury in Male, but not Female, Mice

As we have shown here that the SC number is reduced in uninjured muscles from male but not female Panx1 KO mice, we wanted to determine whether *Panx1* deletion also affects the number of SCs during muscle regeneration in a sex-dependent manner. Since SC activation and proliferation are most active during the early stages of regeneration, TA muscle sections collected at day 4 post injury were labeled for Pax7 and the number of Pax7-positive cells/mm^2 were counted (Figure 3.8A) (Ciciliot and Schiaffino 2010). While there was no effect in female mice (Figure 3.8B), injured TA muscles from male *Panx1* KO mice had ~35 % less SCs at day 4 post injury than that of WT mice (Figure 3.8C).

Growing evidence suggests a role for Panx1 in the recruitment of inflammatory cells (Jorquera et al. 2021; Makarenkova, Shah, and Shestopalov 2018; Silverman et al. 2009). Given that recruiting various cell populations to the site of damage is a critical step in muscle regeneration, we sought to determine if loss of *Panx1* influences cell recruitment following cardiotoxin injury (Ciciliot and Schiaffino 2010; Howard et al. 2020). To this end cross-sections of CTX injured male and female TA muscles were stained for CD68 which marks both macrophages and fibro/adipogenic precursors (FAPS) (B. Deng et al. 2012; Jensen et al. 2021) and assessed for the percentage of CD68 positive area on day 4 post injury (Figure 3.8D). Markedly, female *Panx1* KO mice had significantly more CD68 positive area than that of their WT littermates (Figure 3.8E). Male *Panx1* KO mice however had comparable CD68 positive area to their WT counterparts (Figure 3.8F).

Based on our data showing that myoblast fusion and muscle maturation are impeded in male but not female *Panx1* KO mice in the uninjured context, we then wanted to determine whether newly formed fibers in male muscles following injury are smaller than that of WT mice. Therefore, the CSA of TA myofibers were measured at 4, 7, and 14 post CTX injury. Female mice showed comparable mean CSA between WT and *Panx1* KO mice at all timepoints (Figure 3.8G). However, in male mice, the newly formed fibers were significantly smaller in the *Panx1* KO mice compared to that of WT mice at days 7 and 14 post injury (Figure 3.8H). Together, these data demonstrate that genetic ablation of *Panx1* increases $CD68^+$ cells in females and increases the number of regenerating fibers during early stages of muscle regeneration in both female and male mice. However, the newly formed fibers in muscles from male *Panx1* KO mice are smaller than that from the control mice, possibly due to their reduced SC number and altered fusion capacity.

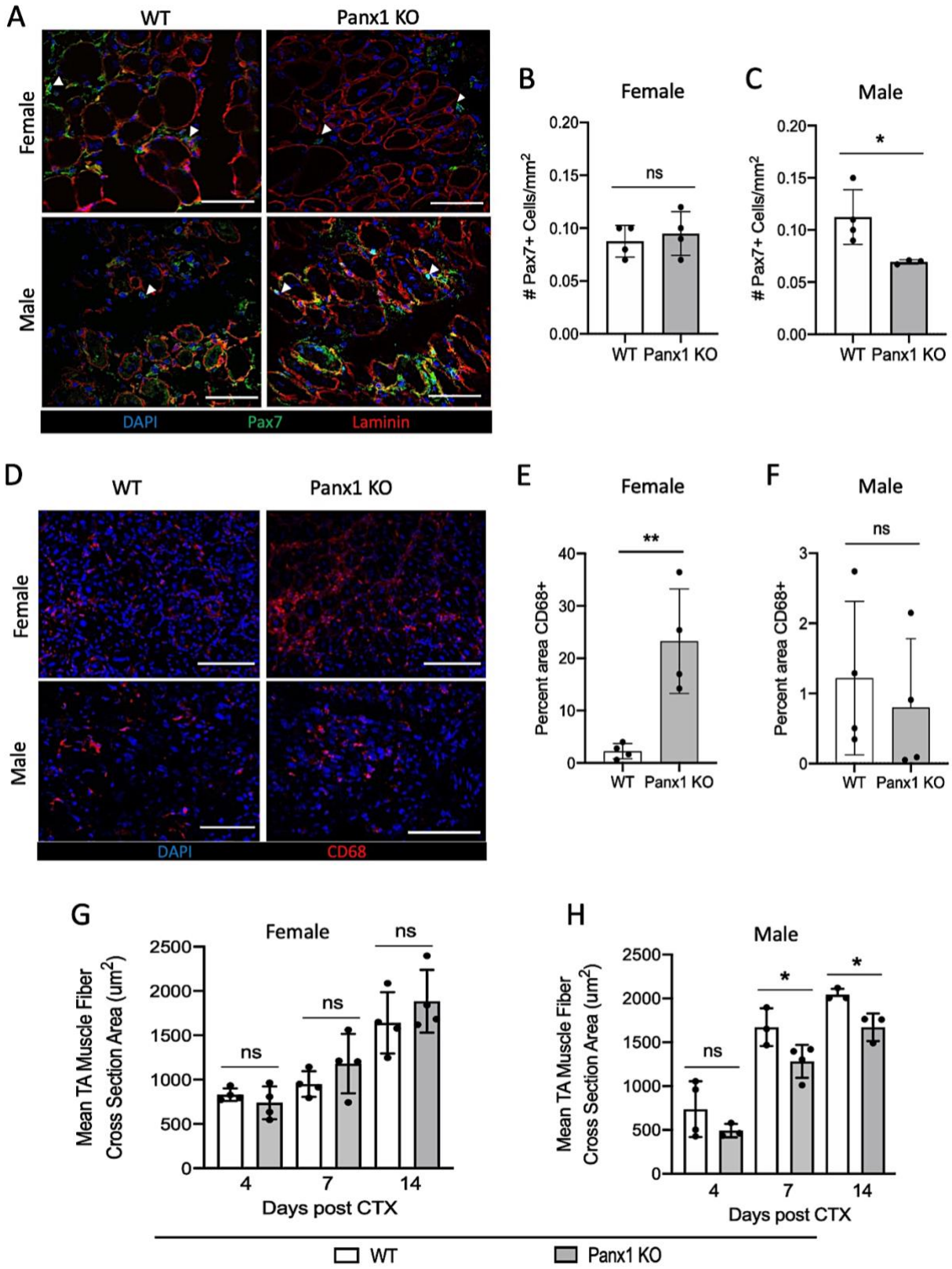

**** Figure caption on next page**

Figure 3.8:Regenerating muscle from male *Panx1* KO mice have less satellite cells and form smaller fibers.

A) Representative cross-sections of TA muscles on day 4 post injury stained for DAPI (blue), Pax7 (green), and laminin (red). Arrowhead points to satellite cells. Scale bar = 50 µm. Quantification of the number of satellite cells on day 4 post injury in **B)** females (n=4; unpaired two tailed student's *t*-test) and **C)** males (n= 3-4; unpaired two-tailed student's *t*-test). **D)** Representative TA cross-sections on day 4 post injury stained for DAPI (blue) and CD68 (red). Scale bar = 100 µm. The parentage of area positive for CD68 staining in **E)** female (n=4; unpaired two-tailed student's *t*-test) and **F)** male cross-sections (n=4; unpaired two-tailed students t-test). The mean fiber cross-sectional area (CSA) was measured on days 4, 7, and 14 post injury in **G)** female and **H)** male TA muscles (n=3-4; two-way ANOVA followed by Sidak's post hoc). Data represent mean ± s.d. **P*<0.05, n.s.: non-significant.

Chapter 4 : Results Part 2; Pannexin 1 Dysregulation in Duchenne Muscular Dystrophy and its Exacerbation of Dystrophic Features in *mdx* mice

Authors: Emily Freeman, Stéphanie Langlois, Marcos F. Leyba, Tarek Ammar, Shumei Zhong, Arul Vadivel, Zacharie Léger, Hugh J. McMillan, Jean-Marc Renaud, Bernard Thébaud, Bernard J. Jasmin, Kyle N. Cowan

Status: Most of this Chapter has been submitted to the journal of human molecular genetics

4.1 Author Contributions and Acknowledgements

I would like to thank Dr. Stéphanie Langlois for her assistance in the acquisition of data, specifically for the survival and body weight measurements over time (Figure 4.2A and B) and for the pole tests in Figure 4.6, her critical review of this chapter and for the generation of the *Panx1*$^{-/-}$*/mdx* mouse model and maintenance of the mouse colony. Dr. Marcos F. Leyba assisted with cross-sectioning and image analysis throughout the chapter. Dr. Tarek Ammar and Dr. Jean-Marc Renaud assisted in collection, analysis and data interpretation for the maximum force and force frequency curve experiments from Figures 4.3 and 4.6. Other collaborators included Shumei Zong and Dr. Arul Vadivel from the Dr. Bernard Thébaud laboratory who performed lung function experiments in figure 4.6, alongside Dr. Hugh McMillan who provided the human muscle biopsy samples in figure 4.1 and critical review of the manuscript based on this chapter. I would also like to thank our co-op student Zacharie Léger (BSc) for his assistance with image analysis for the diaphragm in figure 4.3. Dr. Kyle Cowan and Dr. Bernard Jasmin aided with study design and project supervision. We gratefully acknowledge Alexandra Welten (MSc.) for her technical assistance, Dr. Xiao Xiang for the development of the PANX1 lentivector, Dr. Bénédicte Chazaud for her kind gift of the patient derived HSMM, and Dr. Leslie Hamilton for her help in retrieving the patient samples. We are also thankful for the staff at the University of Ottawa Animal Behaviour Core, and the Histology and Staining services provided by the Louise Pelletier Histology Core Facility at the University of Ottawa.

This study was supported by grants from the Association Française contre les Myopathies (AFM-Telethon), the CIHR Institute of Musculoskeletal Health and Arthritis (IMHA), the Department of Surgery at the Children's Hospital of Eastern Ontario, and the

Children's Hospital of Eastern Ontario Research Institute. This project was also funded by the Queen Elizabeth II Graduate Scholarship in Science and Technology and the Dr. Alex Mackenzie Trainee Grant.

.

4.2 Background and Rationale

In chapter 3 of this thesis, we demonstrated that Panx1 plays a significant role in regulating muscle size, strength, and regeneration, as well as progenitor number and fusion in male, but not in female mice (Freeman et al. 2022). This highlighted Panx1 as a therapeutic target of interest for the male predominant disorder Duchenne muscular dystrophy (DMD). In addition, previous data from our laboratory suggests that Panx1 expression is decreased in the skeletal muscle from a severe murine DMD model (*utrophin*$^{-/-}$*/mdx*), while it was only slightly affected in muscles from *mdx* mice, representing a mild model of DMD. These data suggest that Panx1 levels may be correlated with disease severity (Pham et al. 2018). In healthy skeletal muscle, Panx1 co-immunoprecipitated with dystrophin as part of a multiprotein complex involved in excitation-transcription coupling (Arias-Calderón et al. 2016; Valladares et al. 2013). This led to the notion that a loss of dystrophin may disrupt Panx1 associated functions and, similar to male *Panx1* KO mice, have deleterious effects in muscle thus exacerbating dystrophic symptoms. However, the influence of Panx1 on DMD and its progression remained to be investigated.

4.3 Results

4.3.1 PANX1 Channel Function is Reduced in Immortalized Myoblasts from DMD Patients

To gain insight into how PANX1 may contribute to DMD pathogenesis, we first sought to establish whether PANX1 localisation or expression is altered in skeletal muscles from dystrophic patients. To this end, skeletal muscle biopsies collected from one donor without neuromuscular disease, one donor diagnosed with DMD, and one with an intermediate phenotype of DMD/BMD (complete absence of dystrophin staining on immunohistochemistry) were cross-sectioned and stained for PANX1. As shown Figure 4.1A, the healthy skeletal muscle displayed punctate and equally distributed PANX1 immunostaining, a pattern previously observed for Panx1 in this tissue (Pham et al., 2018). Conversely, the skeletal muscle sections from dystrophic patients displayed uneven staining throughout the tissue. These findings infer that PANX1 distribution may be altered in skeletal muscles from dystrophic patients, however due to the difficulties in acquiring such samples, additional biological replicates could not be attained. Thus, we then used immortalized human skeletal muscle myoblasts (HSMM) isolated from three healthy (Ctl 1-3) and 8 dystrophic donors (DMD 1-8) (Massenet et al. 2020) and analyzed PANX1 levels via western blotting. Myoblasts from healthy donors displayed relatively similar PANX1 protein levels. Interestingly, myoblasts from dystrophic donors expressed varying levels of PANX1 (Figure 4.1B-C), suggesting that PANX1 expression may be regulated differently from patient to patient.

Next, we wanted to determine if PANX1 channel activity is altered in myoblasts from dystrophic patients. To this end, PANX1 channel activity was assessed via sulforhodamine B (4 mg/ml) dye uptake, a dye permeable to PANX1 channels, after incubation in a either a low [K^+] solution or the PANX1 activating high [K^+] solution (Silverman et al. 2009). First, we confirmed the specificity of this assay by knocking down PANX1 levels using siRNA (*PANX1*

siRNA) in Ctl myoblasts. As shown in Figure 4.1D, PANX1-knock down myoblasts displayed a significant reduction in dye uptake in the presence of high [K^+] compared to their control counterparts.

We then selected dystrophic myoblasts that express PANX1 levels that are lower (DMD7), similar (DMD1), and higher (DMD2) than control myoblasts to assess PANX1 channel activity. As anticipated, no dye uptake was observed in any Ctl or DMD cell lines after incubation in the low [K^+] solution. Conversely, Ctl cells exposed to high [K^+] displayed dye uptake incidences above 80 % (Figure 4.1E). Notably, all three dystrophic cell lines displayed a significantly lower incidence of dye uptake than that of the Ctl cells (Figure 4.1E). Together, these data demonstrate that despite varying PANX1 protein levels among dystrophic patient cell lines, PANX1 channel activity is significantly impaired.

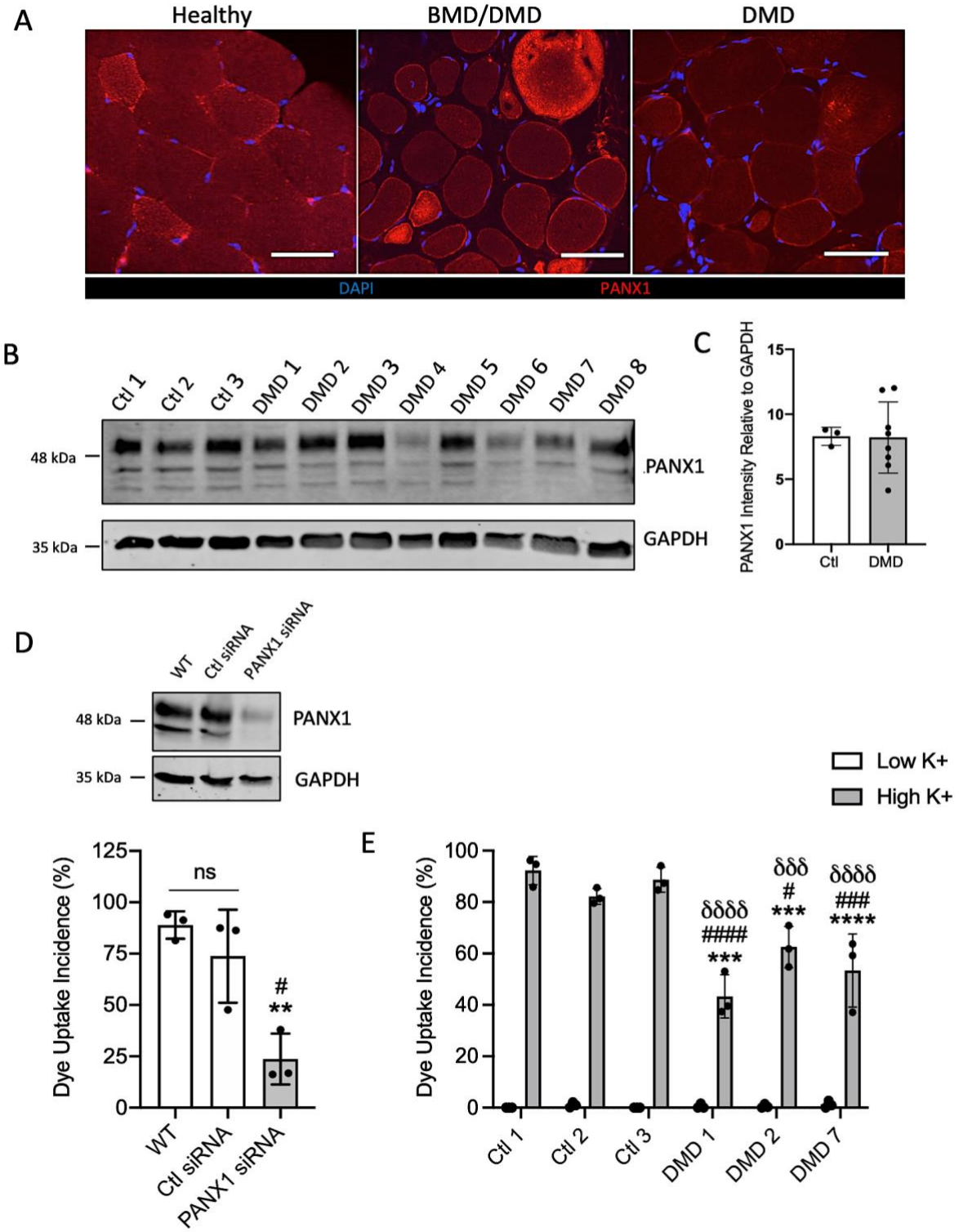

Figure 4.1:PANX1 Channel Function is Reduced in Immortalized Myoblasts from DMD Patients.

A) Representative images of human biopsy samples collected from a healthy donor, a patient diagnosed with DMD, and one with BMD/DMD stained for PANX1 (red), and DAPI (blue). Scale bar = 50 μm. **B)** Western blots of PANX1 levels in immortalized human skeletal muscle

myoblasts isolated from 3 healthy (Ctl) and 8 dystrophic (DMD) donors and **C)** the respective quantification. GAPDH was used as a loading control. **D)** Representative western blot of Ctl myoblasts that were treated with either siRNA targeting *PANX1* (*PANX1* siRNA), a scrambled control (Ctl siRNA), or were untreated (WT: wild-type) (top). The incidence of dye uptake (%) in WT, Ctl siRNA, and *PANX1* siRNA cells in high [K^+] (bottom) (n=3; one-way ANOVA followed by Tukey's multiple comparisons test). Data represents mean ± s.d. ** P<0.01 in comparison to WT; # P<0.05 in comparison to Ctl siRNA; ns: non-significant. **E)** Incidence of dye uptake in cell lines Ctl1-3 and DMD1, DMD2, and DMD7 in the presence of either low [K^+] or high [K^+] (n=3; one-way ANOVA followed by Tukey's multiple comparisons test). Data are represented as mean ± s.d. While not indicated on the graph, the difference between low [K^+] and high [K^+] was statistically significant for all cell lines (P<0.0001). There was no statistical difference between the various cell lines in low [K^+]. The statistical significance between the Ctl and DMD cell lines in high [K^+] are indicated on the graph: *** P<0.001 and **** P<0.0001 in comparison to Ctl 1; # P<0.05, ### P<0.001, #### P<0.0001 in comparison to Ctl 2; ððð P<0.001 and ðððð P<0.0001 in comparison to Ctl 3 in high [K^+].

4.3.2 Panx1$^{-/-}$/mdx mice Have a Reduced Life Span, Body Weight, and Lean Mass

To further study the role of Panx1 in dystrophic muscles, *Panx1*$^{-/-}$ and *mdx* mice were crossed to generate *Panx1*$^{-/-}$*/mdx* mice and their *Panx1*$^{+/+}$*/mdx* littermate controls. The *mdx* mouse is the most widely used preclinical model for DMD (Duddy et al. 2015). Given that Panx1 has a predominant influence in male murine skeletal muscle (Freeman et al. 2022) and since DMD primarily affects males (Bushby et al. 2016; Gumerson J. 2011), only male mice were considered for this report. Genetic ablation of *Panx1* in *mdx* mice was associated with a significantly reduced survival as after 12 months the probability of survival in *Panx1*$^{-/-}$*/mdx* mice decreased by ~50 %. In contrast, the probability of survival in the *Panx1*$^{+/+}$*/mdx* littermates only decreased by ~10 % (Figure 4.2A). The total body weight of *Panx1*$^{-/-}$*/mdx* mice was significantly lower than that of their *Panx1*$^{+/+}$*/mdx* littermates (Figure 4.2B). To determine if the decrease in body weight was associated with a decrease in muscle mass the *tibialis anterior* (TA), *extensor digitorum longus* (EDL), *Soleus* (Sol), *gastrocnemius* (GA), and *quadriceps* (Quad) of 12-week-old *Panx1*$^{+/+}$*/mdx* and *Panx1*$^{-/-}$*/mdx* mice were isolated

and the wet muscle masses measured. While most muscles assessed showed comparable weights between both genotypes, the TA muscle weight of *Panx1*$^{-/-}$*/mdx* (mean: 2.66 mg/g body weight) was significantly lower than that of their *Panx1*$^{+/+}$*/mdx* counterparts (mean: 2.33 mg/g) (Figure 4.2C).

To gain insight into the full body composition, *Panx1*$^{+/+}$*/mdx* and *Panx1*$^{-/-}$*/mdx* mice were subjected to EchoMRI analysis at 3, 6, and 12 months of age (Figure 4.2D-L). In line with the above findings, 3-, 6- and 12-month-old *Panx1*$^{-/-}$*/mdx* mice utilized for the EchoMRI had significantly lower body weight than that of *Panx1*$^{+/+}$*/mdx* mice (Figure 4.2D, 4.2G, 4.2J). Remarkably, the lean mass was significantly lower in *Panx1*$^{-/-}$*/mdx* mice compared to their *Panx1*$^{+/+}$*/mdx* counterparts (Figure 4.2E, 4.2H, 4.2K) at all three ages, while there were no significant changes in the fat mass (Figure 4.2F, 4.2I, 4.2L). Together, these data implicate that loss of *Panx1* is associated with a deficit in lean and wet muscle mass in dystrophic mice.

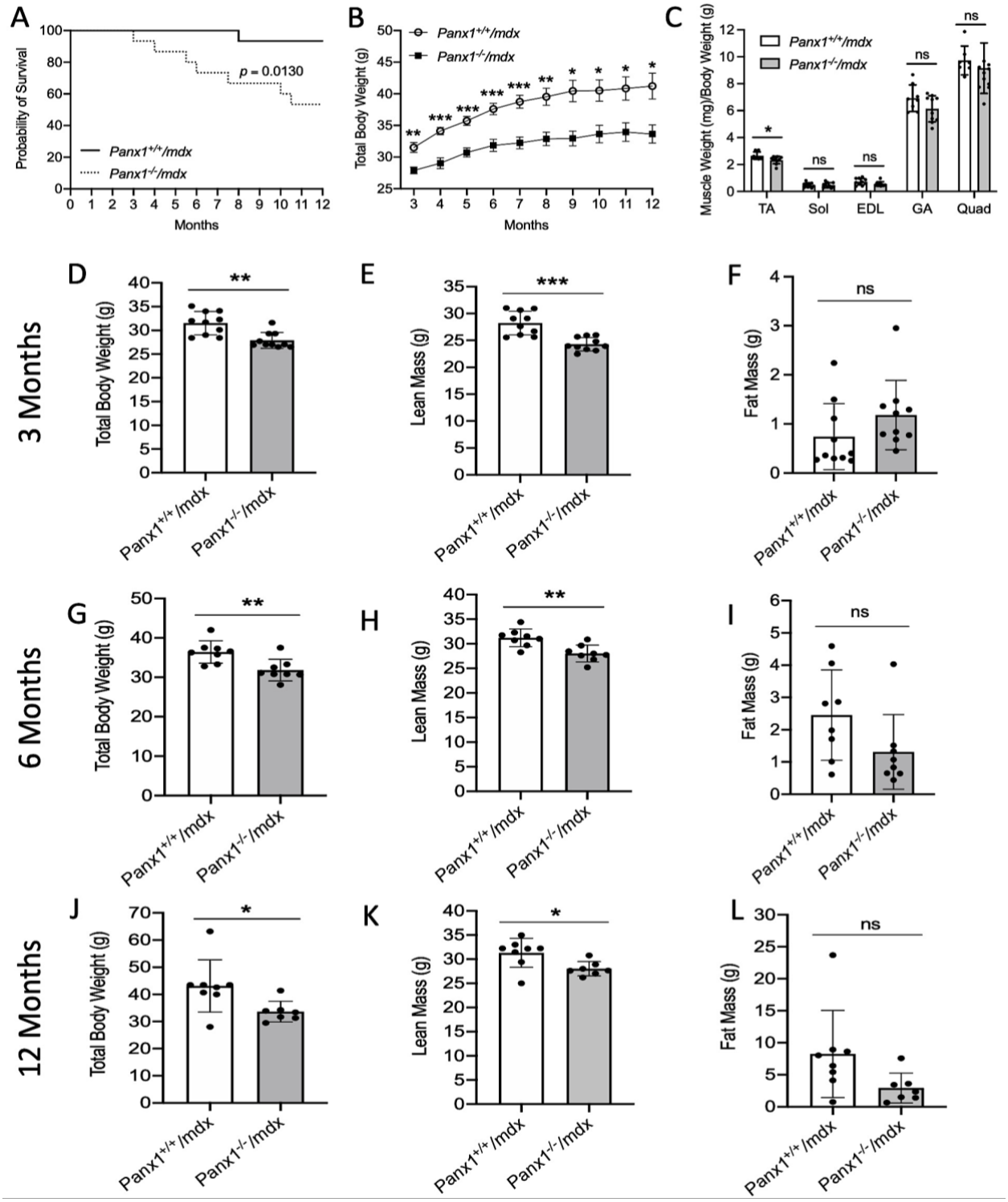

Figure 4.2:*Panx1$^{-/-}$/mdx* mice Have a Reduced Life Span, Body Weight, and Lean Mass.

A) Survival curve of *Panx1$^{-/-}$/mdx* and *Panx1$^{+/+}$/mdx* mice (n=15; Log-rank test). **B)** Total body weight of *Panx1$^{-/-}$/mdx* and *Panx1$^{+/+}$/mdx* mice from 3-12 months of age (n=8-15; two-tailed unpaired student's *t*-tests for each time point). **C)** Wet muscle weight of the *Tibialis anterior* (TA), *Soleus* (Sol), *Extensor digitorum longus* (EDL), *Gastrocnemius* (GA), and

Quadriceps (Quad) normalized to body weight from 12-week-old mice (n=7-12; two-way ANOVA followed by Tukeys post hoc test). EchoMRI analysis displaying the **D)** total body weight, **E)** lean mass, and **F)** fat mass of 3 month old mice (n=10; two-tailed unpaired student's *t*-test), **G)** total body weight, **H)** lean mass, and **I)** fat mass respectively for 6 month old mice (n=8; two-tailed unpaired student's *t*-test) and **J)** total body weight, **K)** lean mass, and **L)** fat mass respectively for 12 month old mice (n=8; two-tailed unpaired student's *t*-test). Data represents mean ± s.d., except for panel B that is shown as mean ± s.e.m. * P<0.05, ** *P*<0.01, *** *P*<0.001, ns: non-significant.

4.3.3 *Panx1*$^{-/-}$*/mdx* mice Have Normal Diaphragm Function and Improved Respiratory Function

Since the majority of dystrophic patients die from respiratory failure and the diaphragm muscle is one of the most affected muscles in DMD (Mead et al. 2014), we sought to examine whether loss of *Panx1* in *mdx* mice is associated with changes in their diaphragm and respiratory function. As death of mice was first observed at 12 weeks of age in the *Panx1*$^{-/-}$*/mdx* group, mice were analyzed at 12-week-old for the remainder of this study unless otherwise stated. To determine whether diaphragm structure and function are altered, cross-sections of *Panx1*$^{+/+}$*/mdx* and *Panx1*$^{-/-}$*/mdx* diaphragms were assessed for fiber cross-sectional area (CSA) and number following H&E staining (Figure 4.3A). *Panx1*$^{-/-}$*/mdx* had significantly more fibers in the smallest size range (0-500 μm^2) (Figure 4.3B), which was reflected in the significantly reduced mean fiber size (Figure 4.3C). The *Panx1*$^{-/-}$*/mdx* diaphragms also displayed a higher number of myofibers when compared to diaphragms of their *Panx1*$^{+/+}$*/mdx* counterparts (Figure 4.3D). We also assessed the presence of centrally located nuclei in the diaphragm muscle fibers, as it marks myofibers undergoing regeneration (J. Liu et al. 2020) and found no difference between the two genotypes (Figure 4.3E). Next, we sought to establish whether the diaphragm force was reduced in *Panx1*$^{-/-}$*/mdx* mice. While no shifts were observed in the force frequency curve to indicate that *Panx1*$^{-/-}$*/mdx* diaphragms had a fiber type

composition shift (and perhaps fatigue characteristics), there was a consistent trend to a reduction in the force generated at all frequencies between 20-200 Hz (Figure 4.3F). Contrary to normal muscles including diaphragm for which maximum tetanic force occurs at 200 Hz, maximum force in both *Panx1*$^{-/-}$*/mdx* and *Panx1*$^{+/+}$*/mdx* diaphragms peaked at 70-80 Hz. When comparing the maximum force generated by the diaphragm based on the curve, this force was comparable between both genotypes (Figure 4.3G).

The PV-loop curve was used to assess respiratory function and is important to note that two curves for each genotype were generated by the PV-loop curve as one is generated during the forced filling of the lungs and the other during expiration. We found that both *Panx1*$^{-/-}$*/mdx* and *Panx1*$^{+/+}$*/mdx* genotypes had a significant downward shift in the pressure-volume (PV)-loop curve in comparison to WT mice. However, this decrease was significantly lower in *Panx1*$^{+/+}$*/mdx* than in *Panx1*$^{-/-}$*/mdx* mice (Figure 4.3H). Using the PV-loop curve, a significantly higher compliance was calculated in *Panx1*$^{-/-}$*/mdx* mice than in *Panx1*$^{+/+}$*/mdx* with both genotypes being significantly lower than that of WT mice (Figure 4.3I). Similarly, WT mice recorded the highest residual volume, followed by *Panx1*$^{-/-}$*/mdx* mice which had a significantly higher residual volume than that of *Panx1*$^{+/+}$*/mdx* mice (Figure 4.3J). In all these data suggest that in contrary to reduced survival rates, loss of *Panx1* seems to improve the respiration function in dystrophic mice.

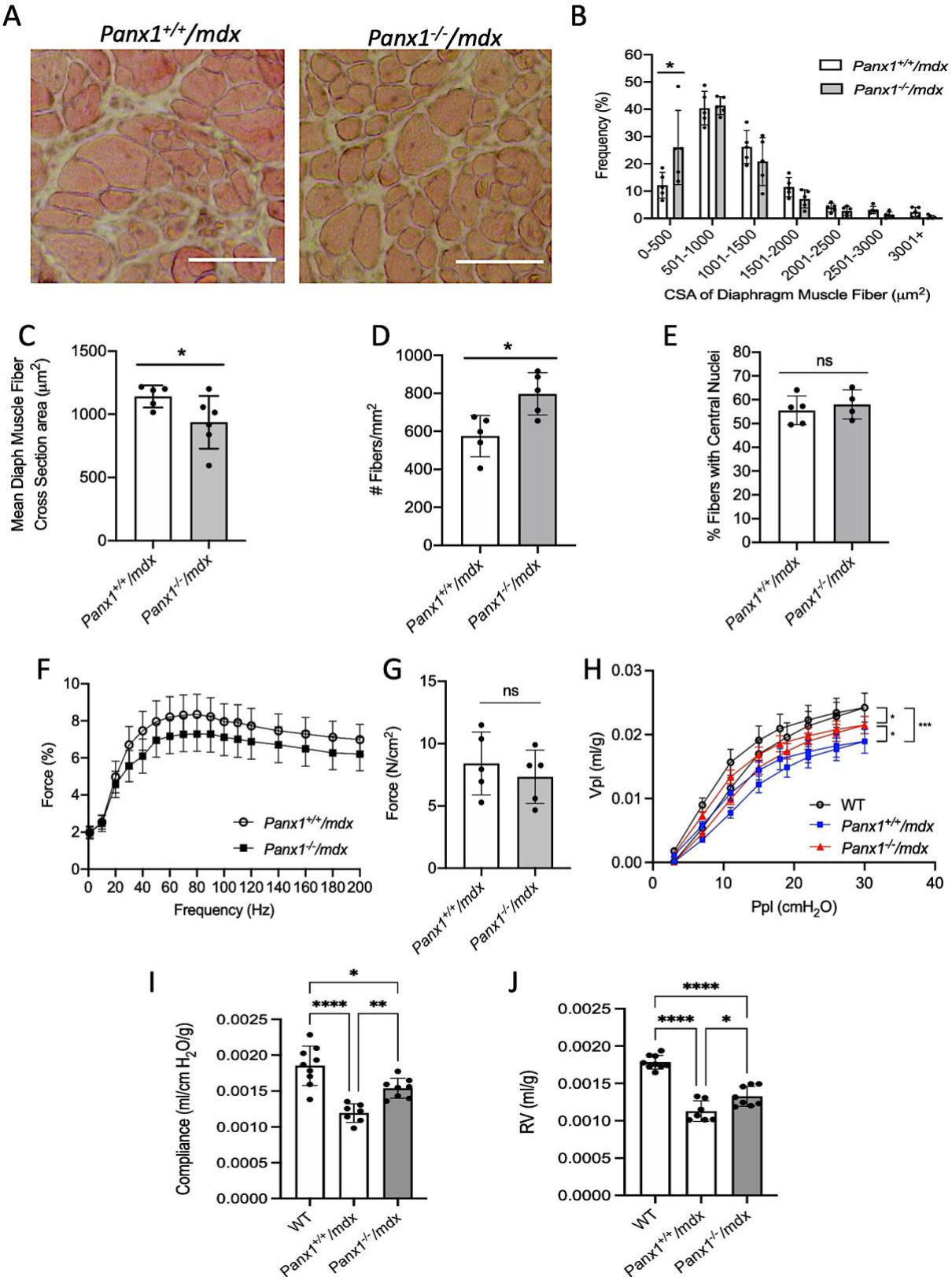

**** Figure Caption on Next Page**

Figure 4.3: Altered Respiration in *Panx1*$^{-/-}$*/mdx* mice is not Linked to Fiber Damage or Impaired Strength in the Diaphragm.

A) Representative images of diaphragm cross-sections stained with H&E. Scale bar = 100 μm. Diaphragms were then analyzed for **B)** distribution curve (%) based on fiber cross-sectional area (CSA) (n=5; two-way ANOVA followed by Sidak's *post hoc* tests; data represents mean ± s.d.). **C)** Mean CSA of diaphragm fibers (n=5-6; unpaired two-tailed student's *t*-test), **D)** the number of fibers per mm^2 in the diaphragm cross-sections (n=5; unpaired two-tailed student's *t*-test), and the **E)** percentage of fibers containing centrally located nuclei (n=4-5; unpaired two-tailed student's *t*-test) were also determined (data represents mean ± s.d.). **F)** The force-frequency curve of diaphragm strips (data represents mean ± s.e.m. instead of s.d. to better visualize the curves) and the **G)** average maximum force (n=5; unpaired two-tailed student's *t*-test; data represents mean ± s.d.). Mice were subjected to forced ventilation and the **H)** pressure volume loop (n=7-8; two-way ANOVA followed by Sidak's *post hoc* test; data represents mean ± s.e.m.), I**)** compliance (ml/cm H_2O) normalized to body weight (g)) (n=7-8; One-way ANOVA followed by Tuckey's *Post hoc*; data represents mean ± s.d.), and **J)** residual volume (RV) (n=7-8; One-way ANOVA followed by Tuckey's *Post hoc*; data represents mean ± s.d.) were determined. * $P<0.05$, *** $P<0.001$, ns: non-significant.

4.3.4 Genetic Ablation of *Panx1* in *mdx* mice Alters Muscle Fiber Size Distribution, Reduces Fiber Number, and Increases the Proportion of Fibers with Centrally Located Nuclei

We next selected one fast-twitch and one slow-twitch muscle which we previously characterized in the *Panx1* knockout mouse model (Freeman et al. 2022), namely the TA and Sol muscles respectively, for further investigation into the muscle histology of the *Panx1*$^{-/-}$*/mdx* mice. The characterization of the two muscles is also informative as fast-twitch, but not slow-twitch, muscles in *mdx* mice have an increased susceptibility to contraction-induced injury (Kiriaev et al. 2021). The TA and Sol muscles were subjected to H&E staining for the analysis of fiber size, number, and presence of centrally located nuclei (Figure 4.4A, top panels) and to Masson trichrome staining to analyze accumulation of fibrotic tissue (Figure 4.4A, lower panels). While not evident by looking at the average CSA (Figure 4.4B), the fiber size distribution in the TA of Panx*1*$^{-/-}$*/mdx* mice showed a significantly increased proportion

of fibers over 7000 μm^2 (Figure 4.4C). These data were accompanied by a significant drop in the number of muscle fibers per mm^2 in the *Panx1*$^{-/-}$*/mdx* TAs (Figure 4.4D). In the Sol, no significant differences in fiber CSA or fiber number were observed between the two genotypes (Figure 4.4E-G). These data infer that loss of Panx1 in the *mdx* mouse model alters the myofiber size and reduces the myofiber number in the fast twitch TA muscle.

We then assessed cross-sections of the TA and Sol for the percentage of fibers with centrally located nuclei, which represent myofibers undergoing regeneration and also indicative of diseased muscle (Cadot, Gache, and Gomes 2015; Folker and Baylies 2013). Sections were also subjected to Masson trichrome staining as an indicator of fibrosis (Van De Vlekkert, Machado, and d'Azzo 2020). Both the TA and Sol muscles from *Panx1*$^{-/-}$*/mdx* mice displayed significantly more fibers with centrally located nuclei compared to that of *Panx1*$^{+/+}$*/mdx* mice (Figure 4.4H-I). Intriguingly, while the muscle area stained with Masson trichrome was low for both genotypes, the TA of *Panx1*$^{-/-}$*/mdx* mice displayed less Masson trichrome staining than the *Panx1*$^{+/+}$*/mdx* controls (Figure 4.4J). No significant difference was observed for the Sol muscle (Figure 4.4K). These data suggest that loss of *Panx1* may reduce fibrotic accumulation in the TA of *mdx* mice but increases the proportion of myofibers with central nuclei in the TA and Sol muscles.

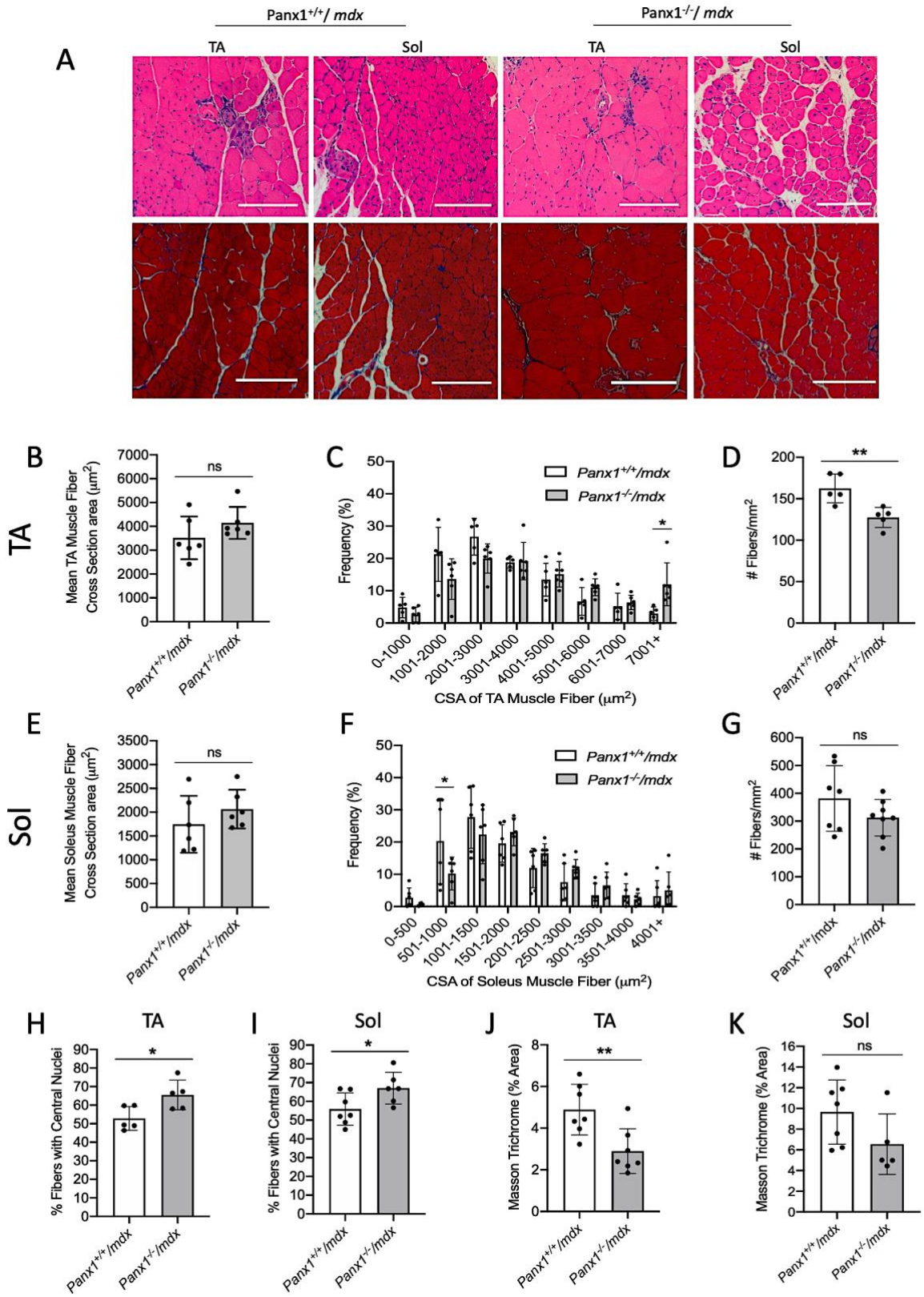

****Figure Caption on Next Page**

Figure 4.4:Genetic Ablation of *Panx1* in *mdx* mice Alters Muscle Fiber Size Distribution, Reduces Fiber Number, and Increases the Proportion of Fibers with Centrally Located Nuclei.

A) Representative images of the TA and Sol muscles of *Panx1*$^{-/-}$*/mdx* and *Panx1*$^{+/+}$*/mdx* cross-sections stained with H&E (top) and Masson trichrome (bottom). Scale bars = 200 μm. In the TA, the **B)** mean CSA (n=6; two-tailed unpaired student's *t*-test), **C)** fiber CSA distribution (n=6; two-way ANOVA followed by Sidak's *post hoc* tests), and **D)** number of fibers per mm^2 (n=5; unpaired two-tailed student's *t*-test) were measured. The Sol **E)** mean CSA (n=6; unpaired two-tailed student's *t*-test), **F)** fiber CSA distribution (n=6; two-way ANOVA followed by Sidak's *post hoc* tests), and **G)** number of fibers per mm^2 (n=7-8; unpaired two-tailed student's *t*-test) were also assessed. The percentage of fibers containing centrally located nuclei for **H)** the TA (n=5; unpaired two-tailed student's *t*-test), and **I)** the Sol (n=6-7; two-tailed unpaired student's *t*-test). From the Masson trichrome staining the percentage of fibrotic area was calculated in the **J)** TA (n=7; two-tailed unpaired student's *t*-test), and the **K)** Sol (n=5-7; two-tailed unpaired student's *t*-test). Data represents mean ± s.d. **P*<0.05, ** *P*<0.01, ns: non-significant.

4.3.5 The Tibialis Anterior Muscles of *Panx1*$^{-/-}$*/mdx* mice have Fewer SCs

Since increased myofiber damage often corresponds to increased fat accumulation in dystrophic muscle, we further assessed the TA and Sol sections for percentage of area covered by lipids via Oil Red O staining (Biltz and Meyer 2017) (Figure 4.5A). In line with our EchoMRI data, there were no significant changes in fat accumulation between the Panx*1*$^{+/+}$*/mdx* and *Panx1*$^{-/-}$*/mdx* TA and Sol muscles (Figure 4.5B-C). We next sought to establish whether muscles from *Panx1*$^{-/-}$*/mdx* mice had more necrotic fibers via IgG staining (Bencze et al. 2019) (Figure 4.5D, top panels). We also looked for any changes in the SC pool via Pax7 staining (Figure 4.5D, bottom panels) as loss of SCs can be associated with increased muscle damage (Evano and Tajbakhsh 2018). The percentage of IgG-positive fibers were very low in the TA and Sol muscles and similar for both genotypes (Figure 4.5E-F). While the SC numbers in the Sol muscle were comparable for both groups, genetic ablation of *Panx1* significantly decreased the SC number in the TA muscle of *mdx* mice (Figure 4.5G-H).

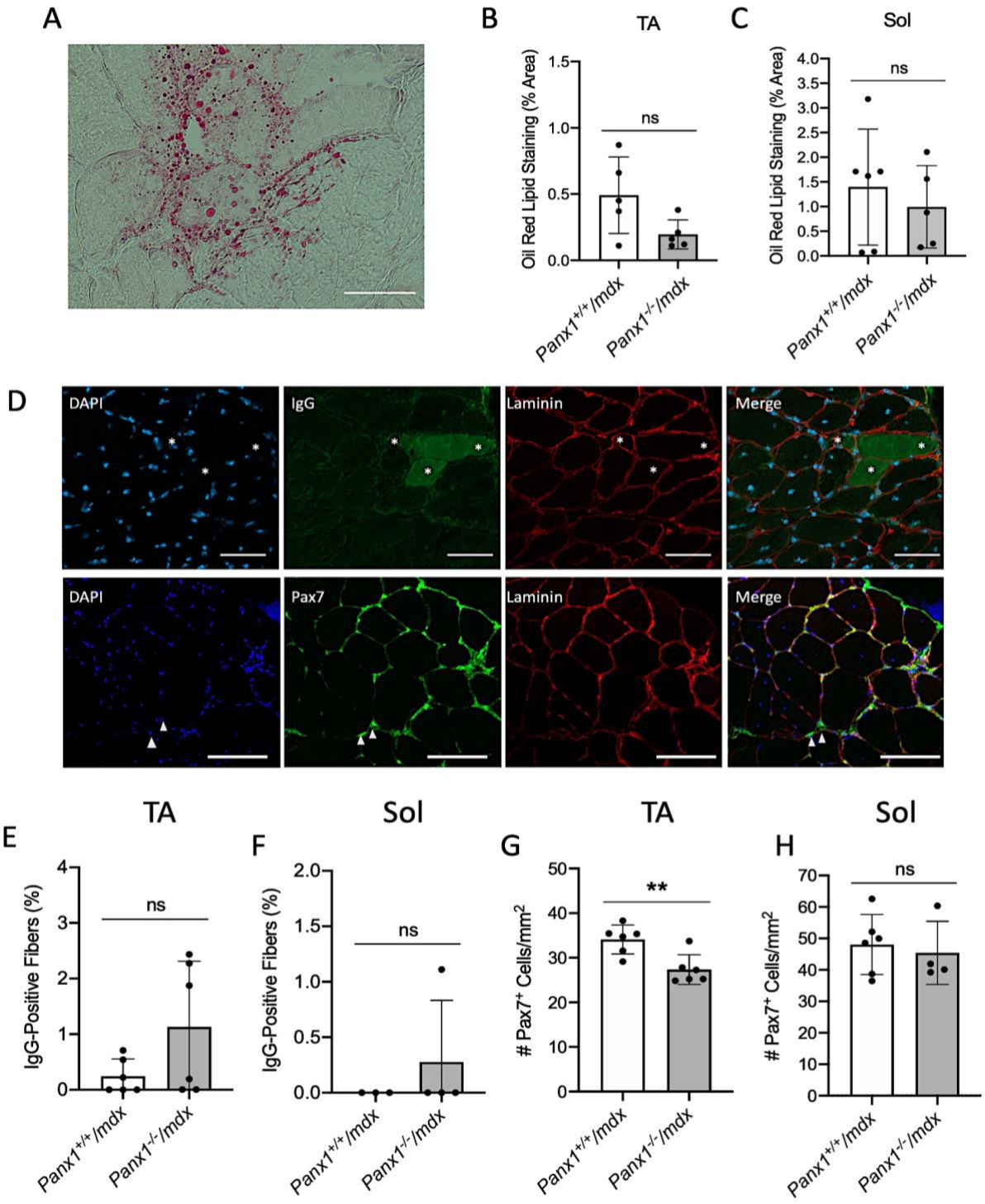

Figure 4.5: The Tibialis Anterior Muscles of *Panx1*$^{-/-}$*/mdx* mice have fewer SCs.

A) Representative image of Oil Red O staining performed on a *Panx1*$^{+/+}$*/mdx* TA. Scale bar = 50um. Quantification of percent area covered by Oil Red O stain in the **B)** TA and **C)** Sol (n=5-6; unpaired, two tailed student's t-test). **D)** Representative pictures of cross-sections of the TA muscles stained for DAPI (blue), necrotic fibers (IgG positive; green), and laminin

(red) (top). They were also stained for DAPI (blue), Pax7 (green), and laminin (red) as shown in the representative pictures (bottom). Scale bar = 100 μm. Cross-sections were then analyzed for the percentage of IgG positive fibers for the **E)** TA (n=6; two-tailed unpaired student's *t*-test) and **F)** Sol (n=3-4; two-tailed unpaired student's *t*-test). The number of SCs per mm^2, identified by Pax7 staining, was measured in **G)** TA (n=6; two-tailed unpaired student's *t*-test) and **H)** Sol muscles (n=4-6; two-tailed unpaired student's *t*-test). Data represents mean ± s.d. ***P*<0.01, ns: non-significant.

4.3.6 Panx1$^{-/-}$/mdx mice Display Reduced Muscle Strength and Locomotor Function

As DMD involves muscle weakness, we sought to establish if *Panx1$^{-/-}$/mdx* mice present with a reduction in muscle function. First, we selected the Sol muscle to assess for maximum force. Due to its anatomical nature and the requirement of attaching the muscle tendon to tendon, the TA was not suitable for these tests. No shift was observed in the force frequency curve indicating that likely muscle fatigability was similar in the Sol muscles of the two groups of mice (Figure 4.6A). When comparing the maximum force generated based on the curve, Sol muscles from *Panx1$^{-/-}$/mdx* mice displayed a significant reduction in maximum force generation when compared to that of *Panx1$^{+/+}$/mdx* (Figure 4.6B).

Grip strength and pole tests were then used to further assess *in vivo* muscle strength and locomotor function. In line with the contraction data, *Panx1$^{-/-}$/mdx* mice had significantly reduced grip strength than the *Panx1$^{+/+}$/mdx* controls (Figure 4.6C). When subjected to the pole test, *Panx1$^{-/-}$/mdx* mice took a significantly longer time to turn around and descend the pole than the *Panx1$^{+/+}$/mdx* mice (Figure 4.6D-E). These findings, taken alongside the reduced contractile force observed in the Sol muscle, implicate that loss of Panx1 reduces muscle force and overall locomotor function.

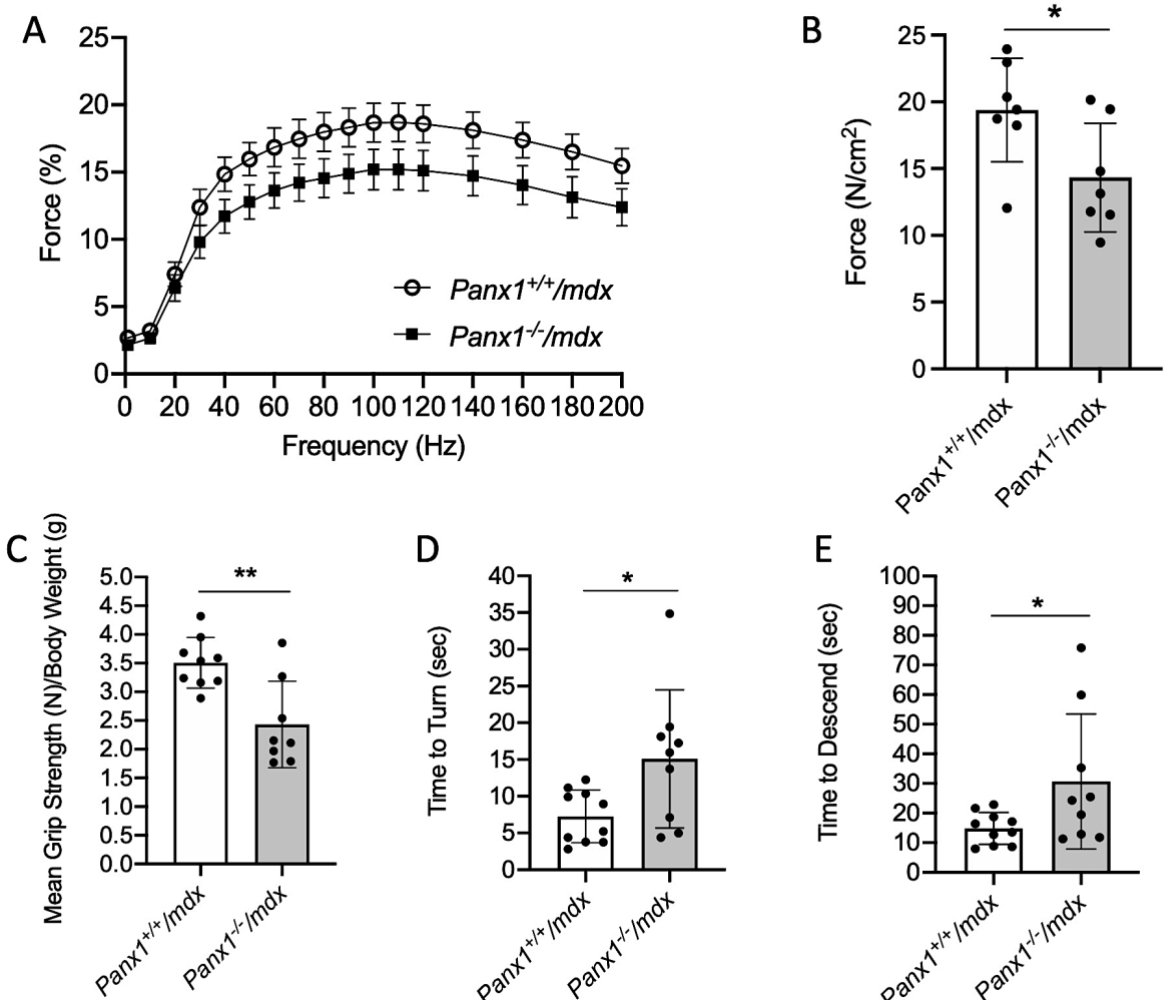

Figure 4.6: *Panx1*$^{-/-}$*/mdx* mice Display Reduced Muscle Strength and Locomotor Function.

The soleus muscle was subjected to force measurements and the **A)** force-frequency curve were recorded and **B)** average maximum force determined based on the curves (n=7; two-tailed unpaired student's *t*-test). **C)** Mean forelimb grip strength of *Panx1*$^{-/-}$*/mdx* and *Panx1*$^{+/+}$*/mdx* mice was measured (n=8-9; two-tailed unpaired student's *t*-test). Mice were also subjected to a pole test where the **D)** time to turn around and **E)** time to descend the pole were measured (n=9-10; two-tailed unpaired student's *t*-test). Data represents mean ± s.d. except for panel A where data represents mean ± s.e.m. to better visualize the curves. **P*<0.05, ***P*<0.01.

4.3.7 P2Y1 Levels are Increased in the Soleus Muscle of *Panx1*$^{-/-}$*/mdx* mice.

Given the significant role of P2 receptors in mediating Panx1-based signaling, including those involved in cytoskeletal rearrangements and muscle differentiation (Riquelme et al. 2015; Suarez-Berumen et al. 2021), we assessed the expression of P2Y1 in the TA, Sol, and diaphragms of *Panx1*$^{-/-}$*/mdx* and *Panx1*$^{+/+}$*/mdx* mice. We selected to assess the P2Y1 receptor as P2Y1 agonists have been demonstrated to regulate the expression of genes related to cell death in dystrophic fibers (Valladares et al. 2013). In the TA, two species were detected using the anti-P2Y1 antibody: one at 90 kDa and the second one at 114 kDa. These species have been previously identified as the dimer (90 kDa) and glycosylated dimer (114 kDa) (Ju et al. 2003) of the P2Y1 receptor. Levels of both species were slightly decreased in the *Panx1*$^{-/-}$*/mdx* TA compared to that of the *Panx1*$^{+/+}$*/mdx* mice (Figure 4.7 A-C). In the Sol and diaphragm only the 90 kDa P2Y1 species was detected. When compared to *Panx1*$^{+/+}$*/mdx* mice, *Panx1*$^{-/-}$*/mdx* mice had significantly more P2Y1 expression in their Sol muscle, while no statistical difference was observed in the diaphragm (P=0.06 as determined by two-tailed unpaired student's t-test) (Figure 4.7 D-E).

As elevation in P2Y1 levels have been suggested to correlate with increased in apoptosis in dystrophic tissue (Valladares et al. 2013), we assessed apoptosis using antibodies against the active (cleaved) form of caspase 3 (Porter and Jänicke 1999). We found that the TA muscles of *Panx1*$^{-/-}$*/mdx* and *Panx1*$^{+/+}$*/mdx* mice had comparable levels of cleaved caspase 3 (Figure 4.7 F-G), while it was not expressed at a detectable level in the Sol in either genotype (Figure 4.7F). These data imply that P2Y1 levels do not correlate with the apoptotic state of dystrophic muscles, nor does loss of *Panx1* trigger myofiber apoptosis.

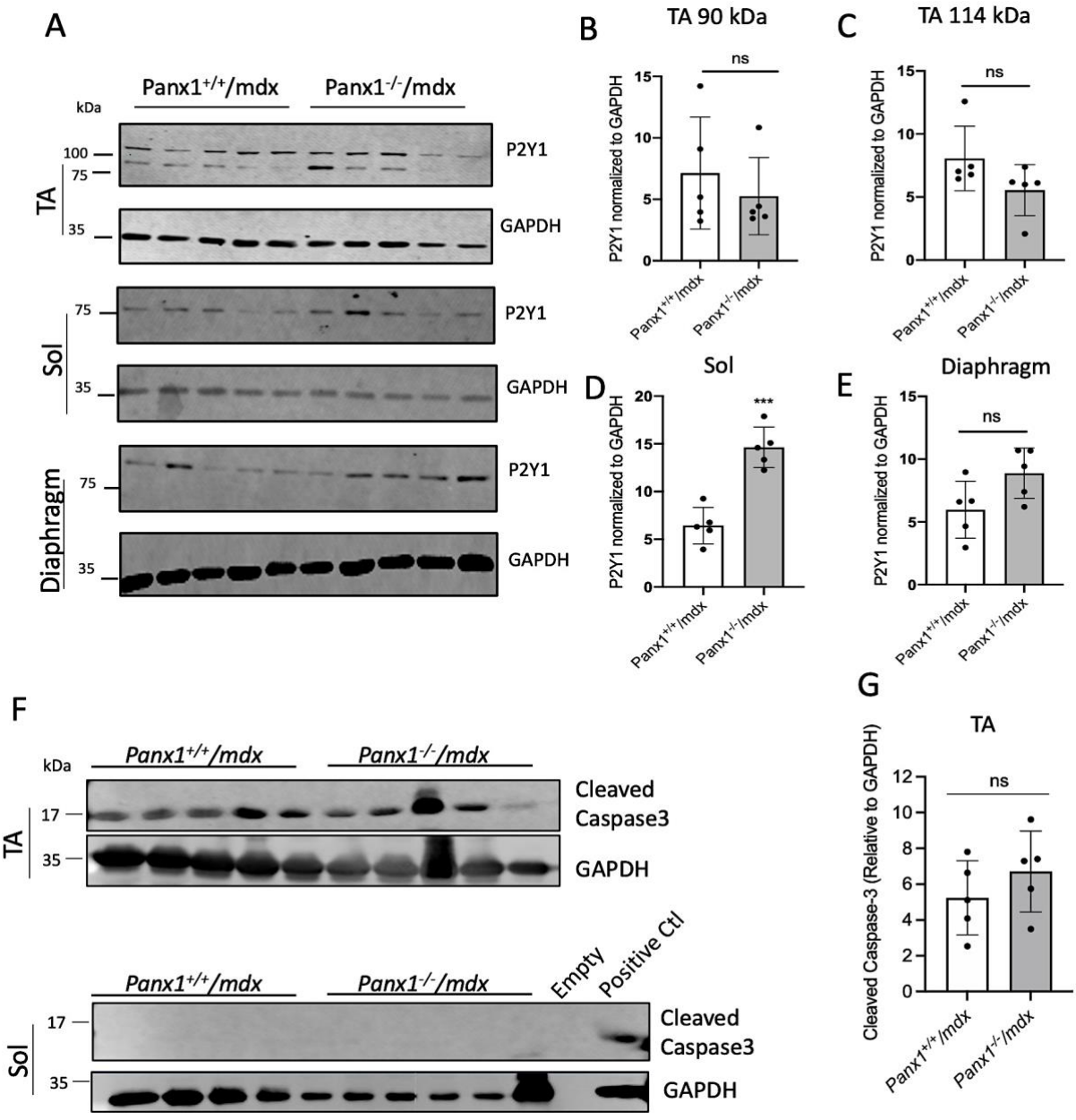

Figure 4.7: P2Y1 levels are increased in Soleus muscle of *Panx1$^{-/-}$/mdx* mice.

A) Representative western blot of P2Y1 levels and their quantification normalized to GAPDH for the **B)** TA (90 kDa species), **C)** TA (114 kDa species), **D)** Sol, and **E)** diaphragm muscles (n=5; unpaired two-tailed student's *t*-test). **F)** Western blots of cleaved caspase-3 and GAPDH in the TA and Sol of Panx*1$^{-/-}$/mdx* and *Panx1$^{+/+}$/mdx* mice. Sol muscles did not display detectable levels of cleaved caspase 3 for either genotype. Positive control consisted of bone marrow derived macrophages treated with lipopolysaccharide to induce apoptosis. **G)** Quantification of cleaved caspase-3 protein levels normalized to GAPDH in the TA muscles (n=5; unpaired two-tailed student's *t*-test). Data represents mean ± s.d. ***$P < 0.001$, ns: non-significant.

4.3.8 SC Number, Proliferation, and Differentiation are Unaltered in *Panx1*$^{-/-}$*/mdx* mice

To determine if loss of Panx1 in *mdx* mice alters SC numbers as it does in *Panx1* KO mice (Freeman et al. 2022), myofibers from the EDL of 8-week-old *Panx1*$^{-/-}$*/mdx* and *Panx1*$^{+/+}$*/mdx* mice were isolated and immediately assessed for SC number via Pax7 immunostaining. In contrast to our findings in TA-sections, *Panx1*$^{-/-}$*/mdx* and *Panx1*$^{+/+}$*/mdx* mice had similar numbers of SC cells per fiber (Figure 4.8A). Fibers were then fixed after 48 hours of culture and co-stained with Pax7 and MyoD to assess for the percentage of cells that are self-renewing (Pax7^{+}/MyoD^{-}), proliferating (Pax7^{+}/MyoD^{+}), and differentiating (Pax7^{-}/MyoD^{+}) (Figure 4.8B). *Panx1*$^{-/-}$*/mdx* fibers had significantly more self-renewing cells compared that of *Panx1*$^{+/+}$*/mdx* mice (Figure 4.8C). However, no significant differences were observed in the proportion of proliferating and differentiating progenitors between *Panx1*$^{-/-}$*/mdx* and *Panx1*$^{+/+}$*/mdx* mice (Figure 4.8D-E). When fibers were fixed 72 hours post isolation, the percentage of cells expressing the terminal differentiation marker MyoG was again comparable between both genotypes (Figure 4.8F). As muscle differentiation was seemingly unaffected we wanted to determine if loss of the major contractile protein MHC was contributing to muscle weakness. To this end, we assessed MHC levels in the TA, Sol, and Diaphragm of *Panx1*$^{-/-}$*/mdx* and *Panx1*$^{+/+}$*/mdx* mice at 12 weeks of age. MHC levels were similar between *Panx1*$^{-/-}$*/mdx* and *Panx1*$^{+/+}$*/mdx* mice in all muscles selected indicating that muscle weakness was not induced by a loss of MHC (Figure 4.8G-I).

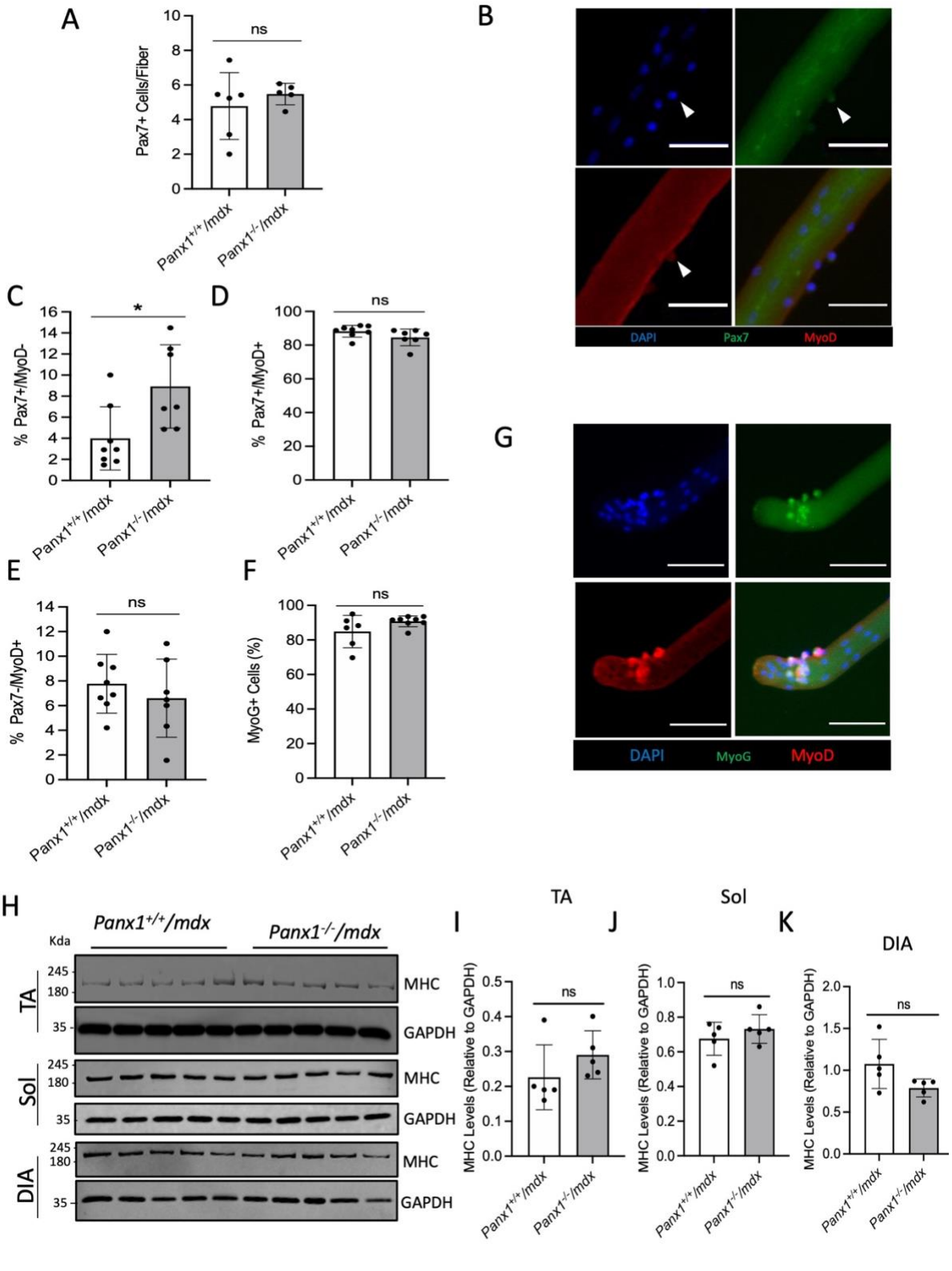

**** Figure Caption on Next Page**

Figure 4.8: *Panx1*$^{-/-}$*/mdx* mice have unaltered SC number, proliferation, and differentiation.

A) Myofibers were isolated from the EDL of 8-week-old *Panx1*$^{+/+}$*/mdx* and *Panx1*$^{-/-}$*/mdx* mice and immediately assessed (0 hours) for the number of Pax7 positive cells per fiber (n=5-6; unpaired two-tailed student's *t*-test). **B)** Representative image of myofibers fixed 48 hours (h) after culture and stained for DAPI (blue), Pax7 (green), and MyoD (red). Arrow depicts a Pax7^{+}/MyoD^{+} myogenic precursor. Scale bar = 50 µm. Myofibers fixed 48 h after culture were assessed for the proportion of **C)** self-renewing (Pax7^{+}/MyoD^{-}), **D)** proliferating (Pax7^{+}/MyoD^{+}), and **E)** differentiating (Pax7^{-}/MyoD^{+}) cells (n=7-8; unpaired two-tailed student's *t*-test). **F)** Myofibers fixed 72h after culture were stained for the proportion of MyoG positive cells (n=7-8; unpaired two-tailed student's *t*-test). **G)** Representative image of myofibers fixed at 72 h of culture and stained for DAPI (blue), MyoG (green), and MyoD (red). Scale bar = 50 µm. **H)** Western blots displaying MHC and GAPDH levels in *Panx1*$^{+/+}$*/mdx* and *Panx1*$^{-/-}$*/mdx* TA, Sol, and DIA muscles. Quantification of MHC protein levels normalized to GAPDH for the **I)** TA, **(J)** Sol, and **K)** DIA muscles (n=5; unpaired two-tailed student's *t*-test). Data represents mean ± s.d. **P*< 0.05, ns: non-significant.

4.3.9 Panx1/PANX1 Regulates the Fusion of Murine and Human Dystrophic Myoblasts

We and others have previously shown that loss or inhibition of Panx1 does not affect the differentiation of normal primary myoblasts from male mice, but inhibits their fusion (Freeman et al. 2022; Suarez-Berumen et al. 2021). To evaluate whether Panx1 regulates dystrophic cell differentiation and fusion, myoblasts isolated from 8-week-old *Panx1*$^{+/+}$*/mdx* mice were differentiated for 3 days in the presence of either PBS (Ctl) or 25 µm carbenoxolone (CBX) to inhibit Panx1 channels (Figure 4.9A). This concentration of CBX was utilized as it was previously demonstrated to block Panx1 channels in myoblasts without inducing cell toxicity (Suarez-Berumen et al. 2021). CBX treatment had no significant effect on the differentiation index (Figure 4.9B), but significantly reduced dystrophic murine myoblast fusion at days 1 and 2 post differentiation (Figure 4.9C).

We next sought to establish whether increasing PANX1 levels in DMD patient-derived myoblasts could improve their differentiation and fusion. To this end, dystrophic myoblasts

were transduced with either a PANX1 overexpression lentivector or a GFP lentivector as a control. Myoblasts overexpressing PANX1 displayed increased differentiation and fusion indices when compared to their controls (Figure 4.9E-G). These data demonstrate that increasing PANX1 levels promote the differentiation and fusion of human dystrophic myoblasts.

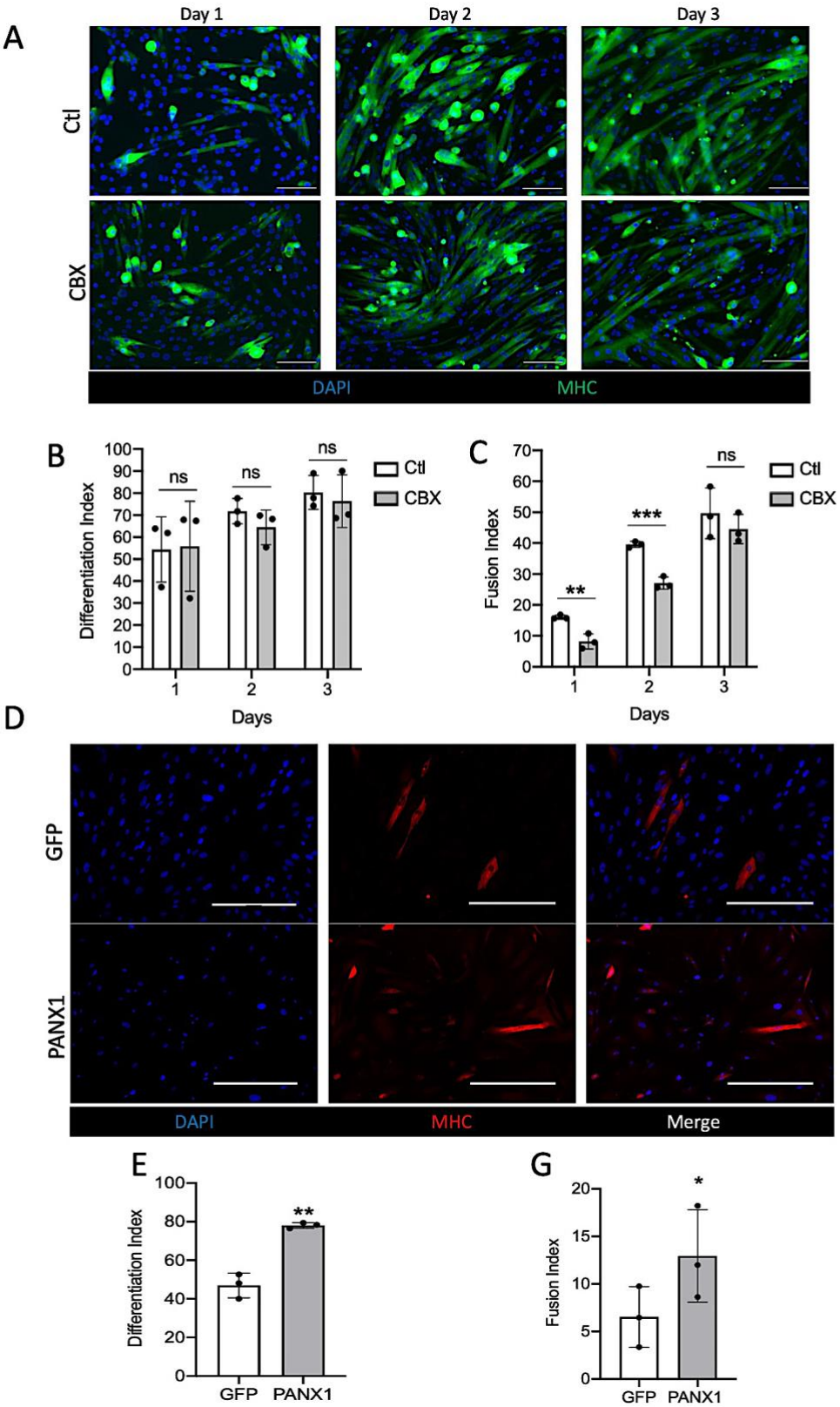

****Figure caption on next page**

Figure 4.9: Panx1/PANX1 Regulates the Fusion of Murine and Human Dystrophic Myoblasts.

A) Primary myoblasts isolated from *Panx1*$^{+/+}$*/mdx* mice were differentiated for 3 days in the presence of either PBS (Ctl) or 25 μM carbenoxolone (CBX). At each day, cells were fixed and then stained with DAPI (blue) and MHC (green). Scale bar = 400 μm. **B)** The differentiation and **C)** fusion indices were calculated at each time point (n=3; paired two-tailed student's *t*-test for each time point). **D)** Dystrophic human skeletal muscle myoblasts derived from patients (namely DMD1, DMD2 and DMD7) were treated with a lentivector containing either a GFP or PANX1 overexpression construct. Cells were differentiated for 6 days then stained for DAPI (blue) and MHC (red). Representative images shown. Scale bar = 400 μm. Myoblasts were then analyzed for the **E)** differentiation (n=3; paired two-tailed student's *t*-test) and **F)** fusion index (n=3; paired two-tailed student's *t*-test). Data represents mean ± s.d. * $P<0.05$, ** $P<0.01$, ns: non-significant.

Chapter 5 : General Discussion

In the studies presented in this thesis, we have found that Panx1 regulates skeletal muscle function, and regeneration in a sex-dependant manner in the context of normal muscle. Specifically, Panx1 is required for the establishment of fiber size, strength, and the SC pool in male but not in female muscle. Most effects observed in this setting, including the decreased CSA and the increased number of muscle fibers during regeneration, might be attributed to the significant impairment of myoblast fusion present in the male *Panx1* KO mice. Importantly, the use of Panx1 pharmacological inhibitors recapitulated these effects indicating that the reduction of myoblast fusion was due to the loss of *Panx1* and not caused by any passenger mutations, such as the *casp11* mutation found in the *Panx1* KO model. In DMD, a disease predominantly affecting males, Panx1 protein levels varied amongst patient derived samples. Regardless of the PANX1 protein level, PANX1 channel function was significantly hindered in dystrophic samples suggesting that PANX1 function is altered in DMD. While the specific mechanisms involved remain to be explored, the genetic ablation of *Panx1* in the dystrophic *mdx* mouse model was associated with increased signs of myofiber specific damage marked by increased presence of centrally located nuclei and significant myofiber loss. These mice also display a significantly reduced lifespan. Conversely, increasing Panx1 levels in patient derived cell lines showed significant improvement in myoblast fusion, highlighting that increasing PANX1 levels may have therapeutic benefit for patients with DMD.

5.1 Panx1 has Sex-Dependant Roles in Skeletal Muscle.

This study is the first to report that Panx1 regulates skeletal muscle size, function, and regeneration in a sex-dependant manner. Genetic ablation of *Panx1* resulted in smaller skeletal

muscle fibers, weaker muscle function, reduced satellite cell numbers, and delays in early SC differentiation preferentially in male mice. Furthermore, in primary myoblasts isolated from male mice, we show that the absence of *Panx1* does not alter terminal differentiation, however, significantly reduces myoblasts fusion. Importantly, these effects were minimal or absent in female mice indicating that the influence of Panx1 on skeletal muscle may be sex-dependent. Following cardiotoxin-induced skeletal muscle injury, male muscles showed reduced SC numbers; an effect that was not observed in female mice. Intriguingly in both male and female *Panx1* null mice, early stages of *in vivo* muscle regeneration showed increased fiber number, however, these fibers were smaller in male, but not in female mice, further suggesting a sex-specific effect of impaired fusion.

The current *Panx1* KO model (CMV-Cre/Panx1$^{fl/fl}$) uses a *Panx1* allele with floxed exons 3-4 which when crossed with transgenic mice containing the cytomegalovirus (CMV) promoter and Cre-recombinase generates a global knockout (Dvoriantchikova et al. 2012). However, this model carries a passenger mutation deleting Caspase 11 and as evident from our genotyping data is not removed via backcrossing. While not detectable in healthy muscle, Caspase 11 is expressed in macrophages during injury response and therefore its loss poses a concern during muscle regeneration and/or disease when macrophages are most active in muscle tissue (S. J. Kang et al. 2000). Our data demonstrated that treatment with the Panx1 inhibitor carbenoxolone in primary WT myoblasts recapitulates our differentiation and fusion findings from *Panx1* KO myoblasts inferring that these effects were not influenced by loss of *Casp11*. Furthermore, Suarez-Berumen and colleagues recently compared the current *Panx1* KO model with both, *Casp11*$^{-/-}$ mice and the Panx1KO/B6 knockout model which does not contain the *Casp*11 mutation. In accordance with our findings, they showed that following

neotoxin induced injury, the TA had reduced fiber sizes in both *Panx1* KO models (Suarez-Berumen et al. 2021). Together, these data infer that the effects reported in this study are due to a loss of Panx1 and not secondary to the *Casp11* mutation.

Here, we investigated the role of Panx1 in regulating SC number and function and found that myofibers from male *Panx1* KO mice have a reduced number of SCs compared to that of their WT controls. Notably, this effect was not observed in female *Panx1* KO mice. After 48 hours in culture, the proportion of self-renewing cells was increased in male *Panx1* KO myofibers possibly to replenish the reduced SC pool in these mice. Conversely, the proportion of differentiating cells was significantly decreased in myofibers from male *Panx1* KO mice after 48h, suggesting a differentiation defect caused by the absence of Panx1. However, this suspected differentiation delay was rescued by 72 hours as reflected by the proportion of cells expressing MyoG. These effects are likely a consequence of the low number of SCs in fibers from male *Panx1* KO mice as the increase in self-renewal or decrease in early differentiation were not observed when single fibers from WT male mice were cultured in the presence of probenecid or carbenoxolone.

The influence of sex-specific androgens testosterone and estrogen in skeletal muscle has been well characterized. Sex based differences have been reported to influence muscle progenitor proliferation and differentiation (Singh et al. 2003; Z et al. 2001; Mangan et al. 2014), muscle development, hypertrophy (Griggs et al. 1989; Vingren et al. 2010), strength and fiber typing (Vingren et al. 2010; Moran et al. 2007; Srinivas-Shankar et al. 2010). Conversely, the sex-dependant functions of Panx1 are just beginning to emerge. Genetic ablation of *Panx1* revealed that its presence impairs recovery from ischemic injury in female but not male mice (Freitas-Andrade et al. 2017). More recent studies have also revealed sex-

dependant responses of Panx1 in bone resorption (Deosthale et al. 2022) and metformin treatment in diabetic models (Luetić et al. 2021). One study of particular interest is that of Aguilar-Perez and colleagues who reported that osteocytic specific knockout of Panx1 increased muscle mass without altering muscle strength in female mice (Aguilar-Perez et al. 2019). Conversely, male mice had no changes in muscle mass but displayed significantly weaker muscles. Here they concluded that Panx1 mediated release of metabolites from osteocytes influences muscle in a sex-dependent fashion (Aguilar-Perez et al. 2019).

The male dominant influence Panx1 exerts on skeletal muscle was particularly surprising considering previous reports demonstrating male and female skeletal muscle express similar levels of Panx1 (Pham et al. 2018). While no difference was observed between the female *Panx1* KO and WT mice for most of the assessments in this study, two differences were recorded at day 4 post cardiotoxin injury. There were significantly more newly formed myofibers as indicated by increased Myh3 positive myofibers and increased $CD68^+$ positive myofibers in the *Panx1* KO females. These findings could be in line with fusion deficiencies which commonly associate with increased fiber numbers (Howard et al. 2020). Furthermore, around day 4 post-injury the number macrophages present in muscle begins to diminish. Thus, increased amounts of $CD68^+$ cells can be indicative of a regeneration delay (Howard et al. 2020). However, the current study did not assess whether these $CD68^+$ are early appearing pro-inflammatory macrophages, the subsequently acting anti-inflammatory macrophages or the later appearing FAPS and therefore, the extent of this suspected regeneration delay remains undetermined. Nonetheless, the lack of effects at later post-injury timepoints and the lack of changes in female *Panx1 KO* muscle histology and function in comparison to that of WT muscle indicates that the effects of global *Panx1* loss is minimal in female skeletal muscle.

The influence sex has on Panx1 remains to be investigated in detail however, one report has suggested that sex-specific androgens may regulate Panx1 expression. In 2014, Dufresne and Cyr demonstrated that Panx1 is significantly upregulated in orchiectomized rats and this correlated with increased levels of the Panx1 transcriptional promoter, ETS variant transcription factor 4 (ETV4) (Dufresne and Cyr 2014). These findings led to the notion that male specific androgens can regulate Panx1 transcription. Unfortunately, this does not explain the differences observed in our current study as we have previously reported that Panx1 transcript and protein levels are equally expressed in male and female TA and Sol muscles (Pham et al. 2018). More recently, Panx3 transcripts have been detected in female but not male skeletal muscle (Wakefield and Penuela 2022). It is thus possible that Panx3 compensates for loss of Panx1 only in female muscle describing our sex-specific effects observed here (Wakefield and Penuela 2022). However, the lack of a specific Panx3 antibody prevents us from confirming this in our mice but would be of interest for future studies. Furthermore, it is possible that signaling cascades downstream from Panx1. act in a sex-dependent manner. For instance, sex-specific androgens have opposing roles in the regulation of muscle mass via TGF- β signaling, a known downstream Panx1 signaling cascade (Haizlip, Harrison, and Leinwand 2015; W. Liu et al. 2019).

5.2 Panx1 is Dysregulated in DMD and Panx1 loss Exacerbates Dystrophic features in *mdx* Mice.

The work detailed in this aim revealed that while PANX1 levels varied amongst the dystrophic patient-derived myoblast cell lines assessed, PANX1 channel activity was significantly reduced. Consistent with this data, Valladares et al (2013) have previously shown that dystrophic fibers from *mdx* mice are unable to activate Panx1-mediated ATP release after

electrical stimulation (Valladares et al. 2013). Taking into consideration that both Panx1 and dystrophin reside together within a multi-protein complex (Arias-Calderón et al. 2016), alongside the reduced Panx1 protein levels in muscles from severely dystrophic mice (Pham et al. 2018), these findings suggest that Panx1 is dysregulated in DMD. To decipher the role Panx1 plays in DMD and its progression, our laboratory generated the first dystrophic (*mdx*) mouse model that lacks Panx1 (*Panx1*$^{-/-}$*/mdx*).

Upon initial observations, *Panx1*$^{-/-}$*/mdx* mice had a significant reduction in body weight that was attributed to loss of lean body mass, potentially indicating muscle wasting. In favor of this, the TA of these mice also displayed less myofibers and significantly reduced wet muscle weight. Histological analysis of the *Panx1*$^{-/-}$*/mdx* mice further revealed increased signs of myofiber specific damage as seen by the elevated number of fibers containing centrally located nuclei in both the TA and Sol muscles. The presence of myofibers with central nuclei is common to many neuromuscular disorders or diseases and is a common indicator of muscle weakness and increased disease progression (Folker and Baylies 2013). This increase in myofiber specific damage of *Panx1*$^{-/-}$*/mdx* mice was associated with lower maximum force of the Sol, reduced grip strength, and impaired locomotor function. Together these data infer that absence of Panx1 may increase myofiber susceptibility to dystrophic damage, ultimately resulting in muscle weakness and wasting.

The *mdx* model commonly displays poor accumulation of fibrotic tissue during the early months of life (3-12 weeks old) however, it is at these stages that dystrophic symptoms are most active. Thus, this likely accounts for the low amount of fibrotic tissue within the skeletal muscle observed in this study. Interestingly, *Panx1*$^{-/-}$*/mdx* had an even lower amount of fibrotic tissue compared to their *Panx1*$^{+/+}$*mdx* littermates. These data are in keeping with

previous reports demonstrating that genetic ablation of *Panx1* reduces fibroblast activation and subsequently fibrosis accumulation in the liver (Crespo Yanguas et al. 2018) and cardiomyocytes (Dolmatova et al. 2012). Interestingly, reduced fibrosis commonly leads to improved lung compliance, higher lung residual volumes, and overall improved respiratory function which were all observed here in the *Panx1*$^{-/-}$*/mdx* mice (Giovarelli et al. 2022; Shafa et al. 2018; Vanoirbeek et al. 2010). *Panx1*$^{-/-}$*/mdx* diaphragms did have significantly smaller myofibers and higher numbers of fibers which may be indicative of fiber splitting and subsequently fiber damage (Murach et al. 2019). However, it is evident from the normal diaphragm strength and unaltered numbers of centrally located nuclei that this potential damage may be minimal and does not seem to alter diaphragm function at least by the assessments we used and at the age we examined. While reduced fibrosis and improved respiratory function would typically be of benefit to dystrophic mice, the drastically reduced lifespan of *Panx1*$^{-/-}$*/mdx* mice indicates that other mechanisms at play are counteracting these slightly advantageous effects.

As we have focused this study on skeletal muscle, we did not assess the cardiac health of *Panx1*$^{-/-}$*/mdx* mice. Cardiomyopathy presents itself in the majority of DMD patients, and in 8% of DMD female carriers. Furthermore, it is the main clinical complication of BMD patients (Mavrogeni et al. 2015; Palladino et al. 2016; Rajdev and Groh 2015). Indeed, a study by Petric and colleagues (2016) demonstrated that *Panx1* KO mice have increased susceptibility to atrial fibrillation (Petric et al. 2016). These findings are in corroboration with those describing that atrial fibrillation can contribute to cardiac failure in DMD patients (Branco et al. 2007; Chen et al. 2013; Palladino et al. 2016; Rajdev and Groh 2015; Waldmann et al. 2020). It is thus tempting to speculate that the cause of premature death in the *Panx1*$^{-/-}$*/mdx*

mice may be linked to increased cardiac failure emphasizing the need for further investigation into the cardiac health of *Panx1*$^{-/-}$*/mdx* mice.

5.3 Differences Between Panx1 KO and *Panx1*$^{-/-}$*/mdx* Muscle Histology and SC Proportions May Be Linked To *mdx* Disease Progression

Unlike the *Panx1* KO males, *Panx1*$^{-/-}$*/mdx* males demonstrated a significant decrease in total body mass reflected by losses in lean body mass, a shift towards increased fiber cross-sectional area and no change in SC numbers in cultured EDL myofibers. Most of these differences can be attributed to the *mdx* mouse model. For instance, given that fusion defects are present following pharmacological Panx1 inhibition in both WT and *Panx1*$^{+/+}$*/mdx* myoblasts, it was expected that male *Panx1*$^{-/-}$*/mdx* myofibers may also display smaller fiber CSA. However, *Panx1*$^{-/-}$*/mdx* myofibers had comparable mean CSA to that of their *Panx1*$^{+/+}$*/mdx* littermates. Indeed, the *mdx* mouse model does not perfectly reflect the muscle wasting observed in human DMD and progressive myofiber hypertrophy in the *mdx* mouse takes place as early as 6-weeks of age (Duddy et al. 2015). Therefore, it is likely that this fiber hypertrophy present in *mdx* mice counteracts the reduction in fiber size observed in male *Panx1* KO mice. Furthermore, the significant increase in the number of fibers over 7000µm in the TA of *Panx1*$^{-/-}$*/mdx* mice might indicate that this hypertrophy present in the *mdx* mouse model is slightly amplified following loss of Panx1. Findings from Duddy and colleagues (2015) demonstrated that increased myofiber sizes in the *mdx* mouse model is associated with increased lysosomal structures and may indicate a pre-necrotic state of the myofiber (Duddy et al. 2015). Therefore, these data would further imply that *Panx1*$^{-/-}$*/mdx* mice have increased signs of myofiber stress.

Typically, in absence of dystrophy, *Panx1* KO mice display increased fat mass (Lee et al. 2018). Nevertheless, we found no changes in total body fat nor any signs of lipid accumulation in the muscles of *Panx1*$^{-/-}$*/mdx* mice. Interestingly, despite their increased weight in comparison to their WT counterparts, *mdx* mice do not typically display fat accumulation. Rather, their weight differences are typically attributed to increases in muscle hypertrophy and changes in bone size (Radley-Crabb et al. 2014). Indeed, Panx1 KO mice have been reported to have perturbed load-induced bone growth indicating that Panx1 has roles in regulation of bone size (Seref-Ferlengez et al. 2019). Thus, it is important to note that while *Panx1*$^{-/-}$*/mdx* mice had significantly lower total body weight and reduced lean mass in contrast to their *mdx* counterparts, other tissues aside from muscle may contribute to these body weight changes.

Here we found the *Panx1*$^{-/-}$*/mdx* mice to have similar SC numbers to that of their *Panx1*$^{+/+}$*/mdx* littermates, whereas our previous findings in the *Panx1* KO mouse suggest that loss of *Panx1* decreases male SC number in both the TA during regeneration and in the uninjured EDL myofibers. While *mdx* mice are known to have heightened regenerative responses, this is an effect that is not observed in the human disease. These heightened regenerative responses may also reduce the influence of factors that would otherwise regulate progenitor populations in healthy skeletal muscle (Massopust et al. 2020; Mázala et al. 2020). Specifically, the *mdx* model used in this study has been previously reported to have abnormally high SC cell expansion, which may account for why the EDL myofibers of *Panx1*$^{-/-}$*/mdx* mice do not display the typical decrease in SC number seen with the *Panx1* KO mice (Kottlors and Kirschner 2010; Mázala et al. 2020). Furthermore, the *Panx1*$^{-/-}$*/mdx* males had no delay in differentiation unlike that seen in the *Panx1* KO male myofibers 48 hours after isolation, an effect attributed to decreased SC numbers. Interestingly, the difference in SC number seems

to be muscle specific, as we observed decreased SC numbers in the uninjured TA of *Panx1*$^{-/-}$*/mdx* mice. Alternatively, this may be related to Panx1 expression in the *mdx* mouse model. Our laboratory has previously reported that Panx1 levels are downregulated in the EDL but not the TA muscle of *mdx* mice (Pham et al. 2018). Therefore, it is likely that muscle specific downregulation of Panx1 in the *mdx* model accounts for the muscle specific changes observed here, and these effects were not accentuated by the complete loss of *Panx1*. Indeed, we observed muscle specific differences in the *Panx1* KO mouse as well in relation to MHC expression in which only the Gastroc muscle displayed a reduction following loss of *Panx1*, further indicating that the influence of Panx1 may vary from muscle to muscle. These muscle specific changes may be linked to fiber type variance between muscles a topic which is discussed further in the next section (section 5.4).

It is possible that the D2 *mdx* mouse would be a better model for assessing the role of Panx1 in progenitor populations as they behave in a manner that more closely resembling that reported in the human disease (Kottlors and Kirschner 2010). However, the D2 *mdx* mouse holds an additional mutation in LTBP4 (latent transforming binding growth factor 4) which increases the amount of active TGF-β (transforming growth factor beta) present during inflammation (Hammers et al. 2020; van Putten et al. 2019). While the D2 *mdx* mouse has a reduced regenerative response closer to that of the human disease, it does not recapitulate the genetic changes observed in human DMD, and further alters the immune response making some measurements, such as macrophage and IgG staining, inaccurate (Hammers et al. 2020; Kottlors and Kirschner 2010; van Putten et al. 2019).

5.4 Effects of Panx1 May be Fiber Type Specific

One common phenomenon observed between both the male *Panx1* KO and the *Panx1*$^{-/-}$*/mdx* mice is that fast-twitch muscles, namely the TA, are seemingly more effected by loss of Panx1 than in the Sol, a slow-twitch muscle. These findings were surprising considering that we have shown here and previously that Panx1 is more abundant in slow-twitch muscles such as the Sol (Freeman et al. 2022; Pham et al. 2018). Additionally, findings from Jorquera et al (2013) suggested that Panx1 may be involved in the specification of slow-twitch fibers (Jorquera et al. 2013). Together, these studies would lead one to believe that slow-twitch fibers may be more affected by Panx1 loss. However, we demonstrate here that reduction in fiber size, decreases in the SC pool and signs of dystrophic damage including increased centrally located nuclei are more prominent in the TA of Panx1 KO and *Panx1*$^{-/-}$*/mdx* mice.

Typically, the TA muscle consists of a low (~4 %) (Lexell et al. 1994) percentage of slow type I fibers unlike the Sol which is comprised of ~75 % type I fibers (Barclay and Weber 2004). The diaphragm however contains relatively equal parts of type I and fast type II fibers and this may contribute to the minimal effects observed in the diaphragms of our *Panx1*$^{-/-}$*/mdx* mice (Atkin et al. 2005). Interestingly, female skeletal muscle expresses higher proportions of slow-twitch muscle fibers than that of male muscle (Haizlip, Harrison, and Leinwand 2015) Therefore, it is possible that the compensatory mechanisms occurring in slow-twitch muscle could be similar or the same to those occurring in female *Panx1* KO mice. Additionally, slow-twitch fibers have a lower demand for ATP, the most studied Panx1 released metabolite, during muscle contraction (Medina et al. 2020; Szentesi et al. 2001). This is further supported by Riquelme et al (2013) who showed that Panx1-mediated ATP release promotes contraction potentiation through P2Y1 receptor activation in the fast-twitch EDL but not in the Sol muscle

further indicating that the requirement for Panx1 may differ between slow- and fast-twitch muscles (Riquelme et al. 2013).

5.5 Panx1/PANX1 Might Influence Muscle in a Species and Muscle Specific Manner

Our results from *ex vivo* cultured myofibers demonstrating that genetic ablation of *Panx1* does not alter myogenic progenitor proliferation are consistent with our previous report demonstrating that pharmacological inhibition of PANX1 channel function had no effect on primary human skeletal muscle myoblast (HSMM) proliferation (Langlois et al. 2014). Previous data using HSMM showed that treatment with probenecid or carbenoxolone reduced the percentage of MHC-positive HSMM, and thus impaired differentiation (Langlois et al. 2014). Despite reduced fiber sizes in males, we found no significant changes in MHC protein levels in the TA and Sol muscles from male and female *Panx1* KO mice. However, *Panx1* KO mice did have significantly lower MHC protein levels in the Gastroc indicating the relationship between Panx1 and MHC might vary from muscle to muscle. It is possible that the primary HSMM used in our previous study were isolated from a muscle type in which PANX1 exhibits more effect or could be due to sex-based differences in the donors. However, neither sex nor the muscle type of the HSMM donors were disclosed by the vendor. In keeping with previous findings from our lab using HSMM from a healthy donor (Langlois et al. 2014), my data also showed that over-expression of PANX1 in myoblasts from male DMD donors promotes their differentiation and fusion. While a difference in differentiation may exist between murine and human myoblasts, inhibition of PANX1/Panx1 channels significantly reduced HSMM fusion (Langlois et al., 2014), as well as fusion of myoblasts from male WT and *mdx* mice. In all,

these findings highlight the need for a thorough investigation into the muscle-specific and species-specific differences Panx1/PANX1 may have to fully grasp potential clinical impacts.

5.6 Proposed Mechanism of Panx1 in Skeletal Muscle might involve Cytoskeleton Organization

Results from this thesis showed that loss of Panx1 in healthy and dystrophic mice reduces muscle strength and leaves it more susceptible to damage particularly in males, which may further exacerbate DMD pathology. Accumulating evidence around Panx1 signaling suggests a mechanism that works through Panx1 mediated activation of P2 receptors. For instance, Valladares et al implicated that elevated P2Y1 levels may increase mRNA expression of pro-apoptotic genes suggesting these muscles could also be poised for increased cell death (Valladares et al. 2013). However, here we did not find such correlation as while P2Y1 levels increased in the *Panx1*$^{-/-}$*/mdx* Sol muscle, we could not detect any cleaved (active) caspase 3, a marker of apoptosis. Similar to Panx1, P2Y1 levels have been detected in activated SCs further implicating a role for it in muscle development and regeneration (May et al. 2006; M.-J. Wang et al. 2023). However, P2Y receptors are not extensively studied in skeletal muscle and therefore further investigations are required to determine the significance of this relationship.

Alternatively, Suarez-Berman and colleagues (2021) demonstrated Panx1 channels promote male myoblast fusion by activating P2X7R which leads to the generation of lysophosphatidic acid (Suarez-Berumen et al. 2021). Lipid signaling, via lysophosphatidic acid, activates the Rho-associated kinase (ROCK) that then initiates cytoskeletal changes that promote membrane “blebbing”, an amoeboid like movement required for efficient myoblast fusion (Suarez-Berumen et al. 2021). It is important to note that the authors of this report only

considered male mice for their study and thus whether female myoblasts can initiate this process in the absence of Panx1 remains unknown. These findings, infer that Panx1 regulates the cytoskeleton of muscle progenitors contributing at least in part to some of its roles in skeletal muscle. Our Preliminary investigations found that that loss of *Panx1* in male *mdx* mice does not alter the total levels of the cytoskeletal components actin nor tubulin. We did observe that over 50 % of fibers in the *Panx1*$^{-/-}$*/mdx* TA presented abnormal F-actin patterning however resolution limits of our microscope prevented us from fully grasping the degree of F-actin mis-organization (Appendix I Figure 1).

Similar to our observations in *Panx1*$^{-/-}$*/mdx* mice, MAP6 (microtubule associated protein 6) KO mice display increased muscle weakness and a loss of TA muscle mass. MAP6 KO mice also have significantly reduced fiber sizes an effect observed in our *Panx1* KO mice. These changes in MAP6 KO myofibers were attributed to mis-organized cytoskeletal components rather than their loss (Sébastien et al. 2018). Pharmacologically induced cytoskeletal disorganization in *mdx* mice has been identified to disrupt Ca^{2+} and reactive oxygen species (ROS) signaling which was further linked to decreased muscle strength and myofiber instability (Khairallah et al. 2012; Lindsay et al. 2019). Indeed, organization of the cytoskeleton plays a pivotal role in muscle health and any disruptions in its organization can exasperate dystrophic symptoms.

Interestingly, our laboratory identified the PANX1 proximome by BioID (Biotin Identification) in rhabdomyosarcoma, a sarcoma thought to originate from skeletal muscle, using two patient-derived cell lines, one of each sub-type (alveolar and embryonal) (Xiang et al. 2021) (Appendix I Figure 2A). PANTHER gene ontology (GO) analysis of the top-ranked 215 proteins (>2-fold enrichment in PANX1 over-expressing cells) classified 37 proteins (17.2

%) as cytoskeletal or cytoskeleton-associated proteins (Appendix I Figure 2B). These 37 proteins were further processed using STRING interaction network analysis, which placed these cytoskeletal proteins in a primarily actin- and tubulin-related protein interaction network (Appendix I Figure 2C and Table 1). One particularly interesting hit was Septin 9, a pseudopodial protein involved in generating "ameboid like" cell movements (Shankar et al. 2010), similar to the Panx1-dependent myoblast movements described by Suarez-Berman et al (Suarez-Berumen et al. 2021). These in silico analyses suggest a PANX1-proximome involving many cytoskeletal proteins and thus may provide insight into a potential mechanism, for further exploration, by which Panx1 regulates myofibers in both healthy and dystrophic tissue.

Several groups have implicated roles for Panx1 mediated P2 activation in cytoskeletal re-arrangements (Bhalla-Gehi et al. 2010; Boyce, Wicki-Stordeur, and Swayne 2014; Wicki-Stordeur and Swayne 2013). Bao and colleagues (2012) demonstrated that Panx1 mediated activation of P2 receptors drove aggregation of C6 rat glioma cells, a process reliant on actin cytoskeletal rearrangements (Bao et al. 2012). Panx1 has also been shown in N2a cells to bind and sequester collapsin response mediator 2 protein (Crmp2), a positive regulator of microtubules (Xu et al. 2018). In this study, Panx1 inhibition led to the release of Crmp2 which promoted microtubule stability via tubulin polymerization (Xu et al. 2018). Furthermore, in neural progenitors Panx1 has been shown to directly interact with actin-related protein 3 (ARP3), a major component of the ARP2/3 complex regulating actin cytoskeletal rearrangements in a variety of processes including determination of cell shape, cell migration, and proliferation (Boyce, Wicki-Stordeur, and Swayne 2014; Goley and Welch 2006; Swaney and Li 2016; Wicki-Stordeur and Swayne 2013). Interestingly, this interaction was found via

GO analysis which revealed that about 10 % of Panx1 interacting hits were classified under the term “Cytoskeleton”(Wicki-Stordeur and Swayne 2013). Clearly, Panx1 has many cytoskeletal interactors and in-depth analysis of these hits and their relation to Panx1 may reveal if the regulation of muscle progenitor fusion and myofiber strength by Panx1 involves a reorganization of the cytoskeleton.

Chapter 6 : Future Directions & Conclusions

Overall, this study revealed a sex-based role for Panx1 in skeletal muscle size, regeneration, and strength. Many of these effects were attributed to impaired progenitor fusion and were observed in male but not female mice. This study also found that Panx1 contributes to myofiber maintenance in DMD and its loss leaves myofibers more susceptible to damage resulting in weaker muscles and a significantly shorter lifespan of *mdx* mice. This thesis proposes a potential link between Panx1 and cytoskeletal organization in dystrophic myofibers indicating this may be one mechanism by which Panx1 contributes to muscle health. Indeed, cytoskeletal rearrangements via Panx1 signaling have been implicated in myoblast fusion (Suarez-Berumen et al. 2021). Therefore, it would be of interest to examine the relationship between Panx1 and the cytoskeleton, and to determine whether this may be a mechanism by which Panx1 maintains myofiber stability in healthy muscles and how this may be altered in DMD and contributes to its progression.

One limitation of the current study is that all mouse assessments utilized a global *Panx1* knockout model. With the ubiquitous expression of Panx1, it is challenging to determine if loss from Panx1 in the muscle alone contributed to our findings or if influence from other tissues is also at play. Here our *in vitro* data demonstrate clear effects on myoblast fusion in the absence of other tissues. However, with regards to our *in vivo* data it is unclear

whether loss of Panx1 from other tissues influences our data. Indeed, muscle is in constant communication with other tissues including the blood, and bone which can govern muscle size and function (Bonetto, Andersson, and Waning 2015; Rudnicki and Williams 2015; Aguilar-Perez et al. 2019).For example report from Aguilar-Perez and colleagues showing that osteocytic *Panx1* deletion alters muscle strength in females raised the possibility that some of the skeletal muscle phenotype we observed here in global *Panx1* KO mice could result from Panx1 deletion in tissues other than skeletal muscle (Aguilar-Perez et al. 2019). This emphasizes the need to assess a muscle specific *Panx1* knockout model to confirm whether Panx1 expression in muscle is responsible for the effects reported here. Indeed, our laboratory has generated a skeletal muscle specific *Panx1* knockout mouse model which we are currently characterizing however preliminary data suggests that muscle specific loss of *Panx1* may recapitulate some of the results presented in this thesis.

This present study revealed a role for Panx1 in maintenance of myofiber size, however it did not establish if this is due to developmental defects or altered hypertrophy of the muscle fiber. Interestingly, P2Y2 activation via ATP has been demonstrated to activate mTOR signaling and contribute to muscle hypertrophy (Ito, Ruegg, and Takeda 2018). In fact, removal of extracellular ATP was associated with loss of muscle fiber size and muscle atrophy. Given that Panx1 is a major source of ATP release in myofibers and that majority of Panx1 signaling pathways engage P2 receptors it is imperative that future studies assess the role of Panx1 in muscle hypertrophy (Valladares et al. 2013; Riquelme et al. 2013; 2015; Burnstock 2018). Such studies may involve assessing the presence and activation state of hypertrophy associated signaling including members of the mTOR pathway.

This study found that lentiviral based overexpression of PANX1 in dystrophic patient-derived myoblasts promotes their fusion and differentiation highlighting the therapeutic potential of increasing PANX1 levels for DMD. However, the use of lentivectors for clinical treatment poses many challenges and thus the FDA and European medicine agency require extensive testing prior to clinical use (Milone and O'Doherty 2018). Alternatively, our lab has identified the clinic ready supplement quercetin to promote PANX1 expression in rhabdomyosarcoma, by binding to the 5' untranslated region of the *PANX1* transcript (Xiang et al. 2022). Furthermore, quercetin treatment in *Panx1*$^{+/+}$/*mdx* primary myoblasts significantly increased Panx1 expression (Appendix I Figure 3). Remarkably, Hollinger et al (2015) demonstrated that quercetin treatment improves dystrophic symptoms in *mdx* mice via an unknown mechanism (Hollinger et al. 2015). Future experimental investigations should thus involve treating both *Panx1*$^{+/+}$/*mdx and Panx1*$^{-/-}$/*mdx* mice with quercetin to establish first if quercetin can target Panx1 *in vivo* and second if the ability of quercetin to reduce dystrophic symptoms is dependent upon Panx1. These studies will provide insight into the role Panx1 plays in the mechanism of action for quercetin treatment in *mdx* mice.

In all, the results presented here bring significant new knowledge to the evolving field of Panx1 in the skeletal muscle by demonstrating that Panx1 channels play a key role in regulating skeletal muscle maintenance, regeneration, strength, and SC number and function in healthy males. The discovery that Panx1 has distinct sex-dependent functions in skeletal muscle highlights the importance of considering sex when evaluating potential roles of Panx1 in skeletal muscle in health and disease. Moreover, these results are among the first to demonstrate that the mechanism of action for Panx1 in male skeletal muscle is through regulating myoblast fusion. In the context of dystrophy, our findings suggest that PANX1 is

dysregulated in DMD, exacerbating several features of the disorder such as myofiber specific damage and myofiber loss, reduction of muscle strength and locomotion, and a significantly shortened lifespan as revealed using our dystrophic mouse model that lacks *Panx1*. Additionally, our data suggest a potential therapeutic benefit to increasing PANX1 levels in muscles of dystrophic patients to promote muscle formation and protect myofibers from the damage induced by the absence of dystrophin.

References:

Abitbol, J. M., B. L. O'Donnell, C. B. Wakefield, E. Jewlal, J. J. Kelly, K. Barr, K. E. Willmore, B. L. Allman, and S. Penuela. 2019. "Double Deletion of Panx1 and Panx3 Affects Skin and Bone but Not Hearing." *Journal of Molecular Medicine* 97 (5): 723–36. https://doi.org/10.1007/s00109-019-01779-9.

Aguilar-Perez, Alexandra, Rafael Pacheco-Costa, Emily G Atkinson, Padmini Deosthale, Hannah M Davis, Alyson L Essex, Julian E Dilley, et al. 2019. "Age- and Sex-Dependent Role of Osteocytic Pannexin1 on Bone and Muscle Mass and Strength." *Scientific Reports* 9 (1): 13903–13903. https://doi.org/10.1038/s41598-019-50444-1.

Allen, Hugh D., Kevin M. Flanigan, Philip T. Thrush, Igor Dvorchik, Han Yin, Charles Canter, Anne M. Connolly, et al. 2013. "A Randomized, Double-Blind Trial of Lisinopril and Losartan for the Treatment of Cardiomyopathy in Duchenne Muscular Dystrophy." *PLoS Currents* 5 (December): ecurrents.md.2cc69a1dae4be7dfe2bcb420024ea865. https://doi.org/10.1371/currents.md.2cc69a1dae4be7dfe2bcb420024ea865.

Ambrosi, Cinzia, Oliver Gassmann, Jennifer N. Pranskevich, Daniela Boassa, Amy Smock, Junjie Wang, Gerhard Dahl, Claudia Steinem, and Gina E. Sosinsky. 2010. "Pannexin1 and Pannexin2 Channels Show Quaternary Similarities to Connexons and Different Oligomerization Numbers from Each Other." *The Journal of Biological Chemistry* 285 (32): 24420–31. https://doi.org/10.1074/jbc.M110.115444.

Ammar, Tarek, Wei Lin, Amanda Higgins, Lawrence J. Hayward, and Jean Marc Renaud. 2015. "Understanding the Physiology of the Asymptomatic Diaphragm of the M1592V Hyperkalemic Periodic Paralysis Mouse." *Journal of General Physiology* 146 (6): 509–25. https://doi.org/10.1085/jgp.201511476.

Anne-Gaëlle Borycki, Brian Brunk, Shahragim Tajbakhsh, Margaret Buckingham, Chin Chiang, and Charles P. Emerson. 1999. "Sonic Hedgehog Controls Epaxial Muscle Determination through Myf5 Activation." *Development* 126: 4053–63.

Annemieke Aartsma-Rus, Ieke B Ginjaar, and Kate Bushby. 2016. "The Importance of Genetic Diagnosis for Duchenne Muscular Dystrophy." *Journal of Medical Genetics* 53 (3): 145. https://doi.org/10.1136/jmedgenet-2015-103387.

Arias-Calderón, Manuel, Gonzalo Almarza, Alexis Díaz-Vegas, Ariel Contreras-Ferrat, Denisse Valladares, Mariana Casas, Héctor Toledo, Enrique Jaimovich, and Sonja Buvinic. 2016. "Characterization of a Multiprotein Complex Involved in Excitation-Transcription Coupling of Skeletal Muscle." *Skeletal Muscle* 6 (April): 15–15. https://doi.org/10.1186/s13395-016-0087-5.

Atkin, Julie D., Rachel L. Scott, Jan M. West, Elizabeth Lopes, Alvin K.J. Quah, and Surindar S. Cheema. 2005. "Properties of Slow- and Fast-Twitch Muscle Fibres in a Mouse

Model of Amyotrophic Lateral Sclerosis." *Neuromuscular Disorders* 15 (5): 377–88. https://doi.org/10.1016/j.nmd.2005.02.005.

Bachman, John F., Alanna Klose, Wenxuan Liu, Nicole D. Paris, Roméo S. Blanc, Melissa Schmalz, Emma Knapp, and Joe V. Chakkalakal. 2018. "Prepubertal Skeletal Muscle Growth Requires Pax7-Expressing Satellite Cell-Derived Myonuclear Contribution." *Development (Cambridge, England)* 145 (20). https://doi.org/10.1242/dev.167197.

Bao, Brian A., Charles P. Lai, Christian C. Naus, and Jeffrey R. Morgan. 2012. "Pannexin1 Drives Multicellular Aggregate Compaction via a Signaling Cascade That Remodels the Actin Cytoskeleton." *The Journal of Biological Chemistry* 287 (11): 8407–16. https://doi.org/10.1074/jbc.M111.306522.

Baranova, Ancha, Dmitry Ivanov, Nadezda Petrash, Anya Pestova, Mikhail Skoblov, Ilya Kelmanson, Dmitry Shagin, et al. 2004. "The Mammalian Pannexin Family Is Homologous to the Invertebrate Innexin Gap Junction Proteins." *Genomics* 83 (4): 706–16. https://doi.org/10.1016/j.ygeno.2003.09.025.

Barclay, C. J., and C. L. Weber. 2004. "Slow Skeletal Muscles of the Mouse Have Greater Initial Efficiency than Fast Muscles but the Same Net Efficiency." *The Journal of Physiology* 559 (Pt 2): 519–33. https://doi.org/10.1113/jphysiol.2004.069096.
Baxter, Peter. 2010. "Diagnosis and Management of Duchenne Muscular Dystrophy." *Developmental Medicine and Child Neurology* 52 (4): 313–313. https://doi.org/10.1111/j.1469-8749.2010.03634.x.

Bencze, Maximilien, Baptiste Periou, Yasmine Baba-Amer, and Francois J. Authier, dirs. 2019. *Immunolabelling Myofiber Degeneration in Muscle Biopsies.* United States. https://doi.org/10.3791/59754.

Bhalla-Gehi, Ruchi, Silvia Penuela, Jared M. Churko, Qing Shao, and Dale W. Laird. 2010. "Pannexin1 and Pannexin3 Delivery, Cell Surface Dynamics, and Cytoskeletal Interactions." *The Journal of Biological Chemistry* 285 (12): 9147–60. https://doi.org/10.1074/jbc.M109.082008.

Biltz, Nicole K., and Gretchen A. Meyer. 2017. "A Novel Method for the Quantification of Fatty Infiltration in Skeletal Muscle." *Skeletal Muscle* 7 (1): 1. https://doi.org/10.1186/s13395-016-0118-2.

Blake, D. J., J. M. Tinsley, and K. E. Davies. 1996. "Utrophin: A Structural and Functional Comparison to Dystrophin." *Brain Pathology (Zurich, Switzerland)* 6 (1): 37–47. https://doi.org/10.1111/j.1750-3639.1996.tb00781.x.

Boassa, Daniela, Cinzia Ambrosi, Feng Qiu, Gerhard Dahl, Guido Gaietta, and Gina Sosinsky. 2007. "Pannexin1 Channels Contain a Glycosylation Site That Targets the Hexamer to the Plasma Membrane." *Journal of Biological Chemistry* 282 (43): 31733–43. https://doi.org/10.1074/jbc.M702422200.

Bonetto, Andrea, Daniel C Andersson, and David L Waning. 2015. “Assessment of Muscle Mass and Strength in Mice.” *BoneKEy Reports* 4 (August): 732–732. https://doi.org/10.1038/bonekey.2015.101.

Boyce, Andrew K. J., Leigh E. Wicki-Stordeur, and Leigh Anne Swayne. 2014. “Powerful Partnership: Crosstalk between Pannexin 1 and the Cytoskeleton.” *Frontiers in Physiology* 5: 27. https://doi.org/10.3389/fphys.2014.00027.

Boyce, Andrew K.J., Anna L. Epp, Archana Nagarajan, and Leigh Anne Swayne. 2018. “Transcriptional and Post-Translational Regulation of Pannexins.” *Gap Junction Proteins* 1860 (1): 72–82. https://doi.org/10.1016/j.bbamem.2017.03.004.

Branco, Dorothy M., Cordula M. Wolf, Megan Sherwood, Peter E. Hammer, Peter B. Kang, and Charles I. Berul. 2007. “Cardiac Electrophysiological Characteristics of the Mdx5cvmouse Model of Duchenne Muscular Dystrophy.” *Journal of Interventional Cardiac Electrophysiology* 20 (1): 1–7. https://doi.org/10.1007/s10840-007-9168-z.

Brun, Caroline E, Yu Xin Wang, and Michael A Rudnicki. 2018. “Single EDL Myofiber Isolation for Analyses of Quiescent and Activated Muscle Stem Cells.” In *Cellular Quiescence: Methods and Protocols*, edited by H Daniel Lacorazza, 149–59. New York, NY: Springer New York. https://doi.org/10.1007/978-1-4939-7371-2_11.

Bruzzone, Roberto, Sheriar G. Hormuzdi, Michael T. Barbe, Anne Herb, and Hannah Monyer. 2003. “Pannexins, a Family of Gap Junction Proteins Expressed in Brain.” *Proceedings of the National Academy of Sciences of the United States of America* 100 (23): 13644–49. https://doi.org/10.1073/pnas.2233464100.

Buas, Matthew F., Shara Kabak, and Tom Kadesch. 2010. “The Notch Effector Hey1 Associates with Myogenic Target Genes to Repress Myogenesis.” *The Journal of Biological Chemistry* 285 (2): 1249–58. https://doi.org/10.1074/jbc.M109.046441.

Buckingham, M. 2001. “Skeletal Muscle Formation in Vertebrates.” *Current Opinion in Genetics & Development* 11 (4): 440–48. https://doi.org/10.1016/s0959-437x(00)00215-x.

Buono, Roberta, Chiara Vantaggiato, Viviana Pisa, Emanuele Azzoni, Maria Teresa Bassi, Silvia Brunelli, Clara Sciorati, and Emilio Clementi. 2012. “Nitric Oxide Sustains Long-Term Skeletal Muscle Regeneration by Regulating Fate of Satellite Cells via Signaling Pathways Requiring Vangl2 and Cyclic GMP.” *Stem Cells (Dayton, Ohio)* 30 (2): 197–209. https://doi.org/10.1002/stem.783.

Burnstock, Geoffrey. 2018. “Purine and Purinergic Receptors.” *Brain and Neuroscience Advances* 2 (December): 2398212818817494. https://doi.org/10.1177/2398212818817494.
Burnstock, Geoffrey, Timothy R. Arnett, and Isabel R. Orriss. 2013. “Purinergic Signalling in the Musculoskeletal System.” *Purinergic Signalling* 9 (4): 541–72. https://doi.org/10.1007/s11302-013-9381-4.

Bushby, Katharine, Richard Finkel, David J Birnkrant, Laura E Case, Paula R Clemens, Linda Cripe, Ajay Kaul, et al. 2016. “Diagnosis and Management of Duchenne Muscular Dystrophy, Part 1: Diagnosis, and Pharmacological and Psychosocial Management.” *The Lancet Neurology* 9 (1): 77–93. https://doi.org/10.1016/S1474-4422(09)70271-6.

Buvinic, Sonja, Gonzalo Almarza, Mario Bustamante, Mariana Casas, Javiera López, Manuel Riquelme, Juan Carlos Sáez, Juan Pablo Huidobro-Toro, and Enrique Jaimovich. 2009. “ATP Released by Electrical Stimuli Elicits Calcium Transients and Gene Expression in Skeletal Muscle.” *The Journal of Biological Chemistry* 284 (50): 34490–505. https://doi.org/10.1074/jbc.M109.057315.

Cadot, Bruno, Vincent Gache, and Edgar R Gomes. 2015. “Moving and Positioning the Nucleus in Skeletal Muscle – One Step at a Time.” *Nucleus* 6 (5): 373–81. https://doi.org/10.1080/19491034.2015.1090073.

Campbell, Kevin P., and Steven D. Kahl. 1989. “Association of Dystrophin and an Integral Membrane Glycoprotein.” *Nature* 338 (6212): 259–62. https://doi.org/10.1038/338259a0.

Celetti, Steven J., Kyle N. Cowan, Silvia Penuela, Qing Shao, Jared Churko, and Dale W. Laird. 2010. “Implications of Pannexin 1 and Pannexin 3 for Keratinocyte Differentiation.” *Journal of Cell Science* 123 (8): 1363–72. https://doi.org/10.1242/jcs.056093.

Chang, Natasha C., Marie-Claude Sincennes, Fabien P. Chevalier, Caroline E. Brun, Melanie Lacaria, Jessica Segalés, Pura Muñoz-Cánoves, Hong Ming, and Michael A. Rudnicki. 2018. “The Dystrophin Glycoprotein Complex Regulates the Epigenetic Activation of Muscle Stem Cell Commitment.” *Cell Stem Cell* 22 (5): 755-768.e6. https://doi.org/10.1016/j.stem.2018.03.022.

Chekeni, Faraaz B., Michael R. Elliott, Joanna K. Sandilos, Scott F. Walk, Jason M. Kinchen, Eduardo R. Lazarowski, Allison J. Armstrong, et al. 2010. “Pannexin 1 Channels Mediate ‘find-Me’ Signal Release and Membrane Permeability during Apoptosis.” *Nature* 467 (7317): 863–67. https://doi.org/10.1038/nature09413.

Chen, Lin Y., Nona Sotoodehnia, Petra Bůžková, Faye L. Lopez, Laura M. Yee, Susan R. Heckbert, Ronald Prineas, et al. 2013. “Atrial Fibrillation and the Risk of Sudden Cardiac Death: The Atherosclerosis Risk in Communities Study and Cardiovascular Health Study.” *JAMA Internal Medicine* 173 (1): 29–35. https://doi.org/10.1001/2013.jamainternmed.744.
Ciciliot, Stefano, and Stefano Schiaffino. 2010. “Regeneration of Mammalian Skeletal Muscle. Basic Mechanisms and Clinical Implications.” *Current Pharmaceutical Design* 16 (8): 906–14. https://doi.org/10.2174/138161210790883453.

Clow, Charlene, and Bernard J Jasmin. 2010. “Brain-Derived Neurotrophic Factor Regulates Satellite Cell Differentiation and Skeltal Muscle Regeneration.” *Molecular Biology of the Cell* 21 (13): 2182–90. https://doi.org/10.1091/mbc.e10-02-0154.

Collins, Charlotte A., Irwin Olsen, Peter S. Zammit, Louise Heslop, Aviva Petrie, Terence A. Partridge, and Jennifer E. Morgan. 2005. “Stem Cell Function, Self-Renewal, and Behavioral Heterogeneity of Cells from the Adult Muscle Satellite Cell Niche.” *Cell* 122 (2): 289–301. https://doi.org/10.1016/J.CELL.2005.05.010.

Condrea, Eleonora. 1974. “Membrane-Active Polypeptides from Snake Venom: Cardiotoxins and Haemocytotoxins.” *Experientia* 30 (2): 121–29. https://doi.org/10.1007/BF01927688.

Constantin, Bruno. 2014. “Dystrophin Complex Functions as a Scaffold for Signalling Proteins.” *Reciprocal Influences between Cell Cytoskeleton and Membrane Channels, Receptors and Transporters* 1838 (2): 635–42. https://doi.org/10.1016/j.bbamem.2013.08.023.

Crespo Yanguas, Sara, Tereza C. da Silva, Isabel V. A. Pereira, Michaël Maes, Joost Willebrords, Valery I. Shestopalov, Bruna M. Goes, et al. 2018. “Genetic Ablation of Pannexin1 Counteracts Liver Fibrosis in a Chemical, but Not in a Surgical Mouse Model.” *Archives of Toxicology* 92 (8): 2607–27. https://doi.org/10.1007/s00204-018-2255-3.

DeLalio, Leon J., Marie Billaud, Claire A. Ruddiman, Scott R. Johnstone, Joshua T. Butcher, Abigail G. Wolpe, Xueyao Jin, et al. 2019. “Constitutive SRC-Mediated Phosphorylation of Pannexin 1 at Tyrosine 198 Occurs at the Plasma Membrane.” *The Journal of Biological Chemistry* 294 (17): 6940–56. https://doi.org/10.1074/jbc.RA118.006982.

Deng, Bo, Michelle Wehling-Henricks, S. Armando Villalta, Ying Wang, and James G. Tidball. 2012. “IL-10 Triggers Changes in Macrophage Phenotype That Promote Muscle Growth and Regeneration.” *Journal of Immunology (Baltimore, Md. : 1950)* 189 (7): 3669–80. https://doi.org/10.4049/jimmunol.1103180.

Deng, Zengqin, Zhihui He, Grigory Maksaev, Ryan M. Bitter, Michael Rau, James A. J. Fitzpatrick, and Peng Yuan. 2020. “Cryo-EM Structures of the ATP Release Channel Pannexin 1.” *Nature Structural & Molecular Biology* 27 (4): 373–81. https://doi.org/10.1038/s41594-020-0401-0.

Deosthale, Padmini, Jung Min Hong, Alyson L Essex, Wilyaret Rodriguez, Dua Tariq, Harmandeep Sidhu, Alejandro Marcial, Angela Bruzzaniti, and Lilian I Plotkin. 2022. “Sex-Specific Differences in Direct Osteoclastic versus Indirect Osteoblastic Effects Underlay the Low Bone Mass of Pannexin1 Deletion in TRAP-Expressing Cells in Mice.” *Bone Reports* 16 (January): 101164–101164. https://doi.org/10.1016/j.bonr.2021.101164.

Der Vartanian, Audrey, Marie Quétin, Stéphanie Michineau, Frédéric Auradé, Shinichiro Hayashi, Christelle Dubois, Didier Rocancourt, et al. 2019. “PAX3 Confers Functional Heterogeneity in Skeletal Muscle Stem Cell Responses to Environmental Stress.” *Cell Stem Cell* 24 (6): 958-973.e9. https://doi.org/10.1016/j.stem.2019.03.019.

Dolmatova, Elena, Gaelle Spagnol, Daniela Boassa, Jennifer R. Baum, Kimberly Keith, Cinzia Ambrosi, Maria I. Kontaridis, Paul L. Sorgen, Gina E. Sosinsky, and Heather S. Duffy. 2012. "Cardiomyocyte ATP Release through Pannexin 1 Aids in Early Fibroblast Activation." *American Journal of Physiology. Heart and Circulatory Physiology* 303 (10): H1208-1218. https://doi.org/10.1152/ajpheart.00251.2012.

Duan, Dongsheng. 2019. "Micro-Utrophin Therapy for Duchenne Muscular Dystrophy." *Molecular Therapy* 27 (11): 1872–74. https://doi.org/10.1016/j.ymthe.2019.10.011.

Duddy, William, Stephanie Duguez, Helen Johnston, Tatiana V. Cohen, Aditi Phadke, Heather Gordish-Dressman, Kanneboyina Nagaraju, Viola Gnocchi, SiewHui Low, and Terence Partridge. 2015. "Muscular Dystrophy in the Mdx Mouse Is a Severe Myopathy Compounded by Hypotrophy, Hypertrophy and Hyperplasia." *Skeletal Muscle* 5 (1): 16. https://doi.org/10.1186/s13395-015-0041-y.

Dufresne, Julie, and Daniel G. Cyr. 2014. "Regulation of the Pannexin-1 Promoter in the Rat Epididymis1." *Biology of Reproduction* 91 (6): 143, 1–13. https://doi.org/10.1095/biolreprod.114.122168.

Dumont, Nicolas A, C Florian Bentzinger, Marie-Claude Sincennes, and Michael A Rudnicki. 2015. "Satellite Cells and Skeletal Muscle Regeneration." *Comprehensive Physiology* 5 (3): 1027–59. https://doi.org/10.1002/cphy.c140068.

Dumont, Nicolas A, and Michael A Rudnicki. 2016. "Targeting Muscle Stem Cell Intrinsic Defects to Treat Duchenne Muscular Dystrophy." *Npj Regenerative Medicine* 1 (April): 16006–16006. https://doi.org/10.1038/npjregenmed.2016.6.

Dumont, Nicolas A, Yu Xin Wang, Julia von Maltzahn, Alessandra Pasut, C Florian Bentzinger, Caroline E Brun, and Michael A Rudnicki. 2015. "Dystrophin Expression in Muscle Stem Cells Regulates Their Polarity and Asymmetric Division." *Nature Medicine* 21 (12): 1455–63. https://doi.org/10.1038/nm.3990.

Dunckley, M. G., D. J. Wells, F. S. Walsh, and G. Dickson. 1993. "Direct Retroviral-Mediated Transfer of a Dystrophin Minigene into Mdx Mouse Muscle in Vivo." *Human Molecular Genetics* 2 (6): 717–23. https://doi.org/10.1093/hmg/2.6.717.
Dvoriantchikova, Galina, Dmitry Ivanov, David Barakat, Alexander Grinberg, Rong Wen, Vladlen Z. Slepak, and Valery I. Shestopalov. 2012. "Genetic Ablation of Pannexin1 Protects Retinal Neurons from Ischemic Injury." *PLOS ONE* 7 (2): e31991. https://doi.org/10.1371/journal.pone.0031991.

Evano, Brendan, and Shahragim Tajbakhsh. 2018. "Skeletal Muscle Stem Cells in Comfort and Stress." *NPJ Regenerative Medicine* 3: 24. https://doi.org/10.1038/s41536-018-0062-3.

Folker, Eric S., and Mary K. Baylies. 2013. "Nuclear Positioning in Muscle Development and Disease." *Frontiers in Physiology* 4 (December): 363. https://doi.org/10.3389/fphys.2013.00363.

Frederiksen, Simona D, Leigh E Wicki-Stordeur, Juan C Sanchez-Arias, and Leigh Anne Swayne. 2019. “Exploring the Pannexin 1 Interactome: In Silico Cross-Analyses with Postsynaptic Proteins and Neuropsychiatric Disorder Susceptibility Genes.” *bioRxiv*, January, 801563. https://doi.org/10.1101/801563.

Freeman, Emily, Stéphanie Langlois, Kaylee Scott, Aymeric Ravel-Chapuis, Bernard J. Jasmin, and Kyle N. Cowan. 2022. “Sex-Dependent Role of Pannexin 1 in Regulating Skeletal Muscle and Satellite Cell Function.” *Journal of Cellular Physiology* 10 (237): 3944–59. https://doi.org/10.1002/jcp.30850.

Freitas-Andrade, Moises, John F Bechberger, Brian A MacVicar, Victor Viau, and Christian C Naus. 2017. “Pannexin1 Knockout and Blockade Reduces Ischemic Stroke Injury in Female, but Not in Male Mice.” *Oncotarget* 8 (23): 36973–83. https://doi.org/10.18632/oncotarget.16937.

Frontera, Walter R., and Julien Ochala. 2015. “Skeletal Muscle: A Brief Review of Structure and Function.” *Calcified Tissue International* 96 (3): 183–95. https://doi.org/10.1007/s00223-014-9915-y.

Fu, Wenxiang, Patrik Asp, Brian Canter, and Brian David Dynlacht. 2014. “Primary Cilia Control Hedgehog Signaling during Muscle Differentiation and Are Deregulated in Rhabdomyosarcoma.” *Proceedings of the National Academy of Sciences of the United States of America*, 1–6. https://doi.org/10.1073/pnas.1323265111.

Füchtbauer, Ernst-Martin, and Heiner Westphal. 1992. “MyoD and Myogenin Are Coexpressed in Regenerating Skeletal Muscle of the Mouse.” *Developmental Dynamics* 193 (1): 34–39. https://doi.org/10.1002/aja.1001930106.

Garbincius, Joanne F., and Daniel E. Michele. 2015. “Dystrophin–Glycoprotein Complex Regulates Muscle Nitric Oxide Production through Mechanoregulation of AMPK Signaling.” *Proceedings of the National Academy of Sciences* 112 (44): 13663–68. https://doi.org/10.1073/pnas.1512991112.
Gehi, Ruchi, Qing Shao, and Dale W Laird. 2011. “Pathways Regulating the Trafficking and Turnover of Pannexin1 Protein and the Role of the C-Terminal Domain.” *The Journal of Biological Chemistry* 286 (31): 27639–53. https://doi.org/10.1074/jbc.M111.260711.

Giovarelli, Matteo, Francesca Arnaboldi, Silvia Zecchini, Laura B. Cornaghi, Ambra Nava, Michele Sommariva, Emilio G. Clementi, and Nicoletta Gagliano. 2022. “Characterisation of Progressive Skeletal Muscle Fibrosis in the Mdx Mouse Model of Duchenne Muscular Dystrophy: An In Vivo and In Vitro Study.” *International Journal of Molecular Sciences* 23 (15). https://doi.org/10.3390/ijms23158735.

Giraldo, Genesys, Mieu Brooks, Benoit I. Giasson, and Christopher Janus. 2018. “Locomotor Differences in Mice Expressing Wild-Type Human α-Synuclein.” *Neurobiology of Aging* 65 (May): 140–48. https://doi.org/10.1016/j.neurobiolaging.2018.01.020.

Goley, Erin D., and Matthew D. Welch. 2006. “The ARP2/3 Complex: An Actin Nucleator Comes of Age.” *Nature Reviews Molecular Cell Biology* 7 (10): 713–26. https://doi.org/10.1038/nrm2026.

Goulding, M., A. Lumsden, and A.J. Paquette. 1994. “Regulation of Pax-3 Expression in the Dermomyotome and Its Role in Muscle Development.” *Development* 120 (4): 957–71. https://doi.org/10.1242/dev.120.4.957.

Graber, Ted G., Lisa Ferguson-Stegall, Jong-Hee Kim, and LaDora V. Thompson. 2013. “C57BL/6 Neuromuscular Healthspan Scoring System.” *The Journals of Gerontology. Series A, Biological Sciences and Medical Sciences* 68 (11): 1326–36. https://doi.org/10.1093/gerona/glt032.

Gramolini, A. O., and B. J. Jasmin. 1999. “Expression of the Utrophin Gene during Myogenic Differentiation.” *Nucleic Acids Research* 27 (17): 3603–9. https://doi.org/10.1093/nar/27.17.3603.

Griggs, R. C., W. Kingston, R. F. Jozefowicz, B. E. Herr, G. Forbes, and D. Halliday. 1989. “Effect of Testosterone on Muscle Mass and Muscle Protein Synthesis.” *Journal of Applied Physiology (Bethesda, Md. : 1985)* 66 (1): 498–503. https://doi.org/10.1152/jappl.1989.66.1.498.

Gumerson J., & Michele D. 2011. “The Dystrophin-Glycoprotein Complex in the Prevention of Muscle Damage.” *J. of Biomed Biochtech* 10: 210797–210797.

Haizlip, K. M., B. C. Harrison, and L. A. Leinwand. 2015. “Sex-Based Differences in Skeletal Muscle Kinetics and Fiber-Type Composition.” *Physiology* 30 (1): 30–39. https://doi.org/10.1152/physiol.00024.2014.

Hammers, David W., Cora C. Hart, Michael K. Matheny, Lillian A. Wright, Megan Armellini, Elisabeth R. Barton, and H. Lee Sweeney. 2020. “The D2.Mdx Mouse as a Preclinical Model of the Skeletal Muscle Pathology Associated with Duchenne Muscular Dystrophy.” *Scientific Reports* 10 (1): 14070. https://doi.org/10.1038/s41598-020-70987-y.

Hernandez-Hernandez, M, E Garcia-Gonzalez, Caroline E Brun, and Michael A. Rudnicki. 2017. “The Myogenic Regulatory Factors, Determinants of Muscle Development, Cell Identity and Regeneration.” *Seminars in Cell & Developmental Biology* 72: 10–18.

Hollinger, Katrin, R. Andrew Shanely, John C. Quindry, and Joshua T. Selsby. 2015. “Long-Term Quercetin Dietary Enrichment Decreases Muscle Injury in Mdx Mice.” *Clinical Nutrition (Edinburgh, Scotland)* 34 (3): 515–22. https://doi.org/10.1016/j.clnu.2014.06.008.

Howard, Emily E., Stefan M. Pasiakos, Christopher N. Blesso, Maya A. Fussell, and Nancy R. Rodriguez. 2020. “Divergent Roles of Inflammation in Skeletal Muscle Recovery From Injury.” *Frontiers in Physiology* 11: 87. https://doi.org/10.3389/fphys.2020.00087.

Ito, Naoki, Urs T. Ruegg, and Shin'ichi Takeda. 2018. "ATP-Induced Increase in Intracellular Calcium Levels and Subsequent Activation of mTOR as Regulators of Skeletal Muscle Hypertrophy." *International Journal of Molecular Sciences* 19 (9). https://doi.org/10.3390/ijms19092804.

Jensen, Jonas B., Andreas B. Møller, Jesper Just, Maike Mose, Frank V. de Paoli, Tine B. Billeskov, Rikard G. Fred, et al. 2021. "Isolation and Characterization of Muscle Stem Cells, Fibro-Adipogenic Progenitors, and Macrophages from Human Skeletal Muscle Biopsies." *American Journal of Physiology-Cell Physiology* 321 (2): C257–68. https://doi.org/10.1152/ajpcell.00127.2021.

Jiang, Jean X, and Silvia Penuela. 2016. "Connexin and Pannexin Channels in Cancer." *BMC Cell Biology* 17 Suppl 1 (Suppl 1): 12–12. https://doi.org/10.1186/s12860-016-0094-8.

Jin, Qiuheng, Bo Zhang, Xiang Zheng, Ningning Li, Lingyi Xu, Yuan Xie, Fangjun Song, et al. 2020. "Cryo-EM Structures of Human Pannexin 1 Channel." *Cell Research* 30 (5): 449–51. https://doi.org/10.1038/s41422-020-0310-0.

Jorquera, Gonzalo, Francisco Altamirano, Ariel Contreras-Ferrat, Gonzalo Almarza, Sonja Buvinic, Vincent Jacquemond, Enrique Jaimovich, and Mariana Casas. 2013. "Cav1.1 Controls Frequency-Dependent Events Regulating Adult Skeletal Muscle Plasticity." *Journal of Cell Science* 126 (5): 1189–98. https://doi.org/10.1242/jcs.116855.
Jorquera, Gonzalo, Roberto Meneses-Valdés, Giovanni Rosales-Soto, Denisse Valladares-Ide, Cristian Campos, Mónica Silva-Monasterio, Paola Llanos, Gonzalo Cruz, Enrique Jaimovich, and Mariana Casas. 2021. "High Extracellular ATP Levels Released through Pannexin-1 Channels Mediate Inflammation and Insulin Resistance in Skeletal Muscle Fibres of Diet-Induced Obese Mice." *Diabetologia* 64 (6): 1389–1401. https://doi.org/10.1007/s00125-021-05418-2.

Ju, Yue-Kun, Wenbing Huang, Lele Jiang, Julian A. Barden, and David G. Allen. 2003. "ATP Modulates Intracellular Ca2+ and Firing Rate through a P2Y1 Purinoceptor in Cane Toad Pacemaker Cells." *The Journal of Physiology* 552 (Pt 3): 777–87. https://doi.org/10.1113/jphysiol.2003.052258.

Kang, Martin H., Laura P. van Lieshout, Liqun Xu, Jakob M. Domm, Arul Vadivel, Laurent Renesme, Christian Mühlfeld, et al. 2020. "A Lung Tropic AAV Vector Improves Survival in a Mouse Model of Surfactant B Deficiency." *Nature Communications* 11 (1): 3929. https://doi.org/10.1038/s41467-020-17577-8.

Kang, S. J., S. Wang, H. Hara, E. P. Peterson, S. Namura, S. Amin-Hanjani, Z. Huang, et al. 2000. "Dual Role of Caspase-11 in Mediating Activation of Caspase-1 and Caspase-3 under Pathological Conditions." *The Journal of Cell Biology* 149 (3): 613–22. https://doi.org/10.1083/jcb.149.3.613.

Keller, Charles, and Denis C Guttridge. 2013. “Mechanisms of Impaired Differentiation in Rhabdomyosarcoma.” *The FEBS Journal* 280 (17): 4323–34. https://doi.org/10.1111/febs.12421.

Khairallah, Ramzi J., Guoli Shi, Francesca Sbrana, Benjamin L. Prosser, Carlos Borroto, Mark J. Mazaitis, Eric P. Hoffman, et al. 2012. “Microtubules Underlie Dysfunction in Duchenne Muscular Dystrophy.” *Science Signaling* 5 (236): ra56. https://doi.org/10.1126/scisignal.2002829.

Kiriaev, Leonit, Sindy Kueh, John W. Morley, Peter J. Houweling, Stephen Chan, Kathryn N. North, and Stewart I. Head. 2021. “Dystrophin-Negative Slow-Twitch Soleus Muscles Are Not Susceptible to Eccentric Contraction Induced Injury over the Lifespan of the Mdx Mouse.” *American Journal of Physiology. Cell Physiology* 321 (4): C704–20. https://doi.org/10.1152/ajpcell.00122.2021.

Klingler, Werner, Karin Jurkat-Rott, Frank Lehmann-Horn, and Robert Schleip. 2012. “The Role of Fibrosis in Duchenne Muscular Dystrophy.” *Acta Myologica : Myopathies and Cardiomyopathies : Official Journal of the Mediterranean Society of Myology* 31 (3): 184–95.

Kottlors, Michael, and Janbernd Kirschner. 2010. “Elevated Satellite Cell Number in Duchenne Muscular Dystrophy.” *Cell and Tissue Research* 340 (3): 541–48. https://doi.org/10.1007/s00441-010-0976-6.

Kuang, Shihuan, Kazuki Kuroda, Fabien Le Grand, and Michael A. Rudnicki. 2007. “Asymmetric Self-Renewal and Commitment of Satellite Stem Cells in Muscle.” *Cell* 129 (5): 999–1010. https://doi.org/10.1016/j.cell.2007.03.044.

Langlois, Stéphanie, Marie-Eve St-Pierre, Stephen H. Holland, Xiao Xiang, Emily Freeman, Hisham Mohamed, Ahmet Cem Dural, et al. 2023. “Inhibition of PANX1 Channels Reduces the Malignant Properties of Human High-Risk Neuroblastoma.” *Journal of Cancer* 14 (5): 689–706. https://doi.org/10.7150/jca.79552.

Langlois, Stéphanie, Xiao Xiang, Kelsey Young, Bryce J Cowan, Silvia Penuela, and Kyle N Cowan. 2014. “Pannexin 1 and Pannexin 3 Channels Regulate Skeletal Muscle Myoblast Proliferation and Differentiation.” *The Journal of Biological Chemistry* 289 (44): 30717–31. https://doi.org/10.1074/jbc.M114.572131.

Lazure, Felicia, Darren M. Blackburn, Aldo H. Corchado, Korin Sahinyan, Nabila Karam, Ahmad Sharanek, Duy Nguyen, et al. 2020. “Myf6/MRF4 Is a Myogenic Niche Regulator Required for the Maintenance of the Muscle Stem Cell Pool.” *EMBO Reports* 21 (12): e49499. https://doi.org/10.15252/embr.201949499.

Lee, Vanessa R., Kevin J. Barr, John J. Kelly, Danielle Johnston, Cody F.C. Brown, Kevin P. Robb, Samar Sayedyahossein, et al. 2018. “Pannexin 1 Regulates Adipose Stromal Cell Differentiation and Fat Accumulation.” *Scientific Reports* 8 (1). https://doi.org/10.1038/s41598-018-34234-9.

Leikina, Evgenia, Dilani G. Gamage, Vikram Prasad, Joanna Goykhberg, Michael Crowe, Jiajie Diao, Michael M. Kozlov, Leonid V. Chernomordik, and Douglas P. Millay. 2018. "Myomaker and Myomerger Work Independently to Control Distinct Steps of Membrane Remodeling during Myoblast Fusion." *Developmental Cell* 46 (6): 767-780.e7. https://doi.org/10.1016/j.devcel.2018.08.006.

Lexell, J., J. C. Jarvis, J. Currie, D. Y. Downham, and S. Salmons. 1994. "Fibre Type Composition of Rabbit Tibialis Anterior and Extensor Digitorum Longus Muscles." *Journal of Anatomy* 185 (Pt 1) (Pt 1): 95–101.

Lindsay, Angus, William M. Southern, Preston M. McCourt, Alexie A. Larson, James S. Hodges, Dawn A. Lowe, and James M. Ervasti. 2019. "Variable Cytoplasmic Actin Expression Impacts the Sensitivity of Different Dystrophin-Deficient Mdx Skeletal Muscles to Eccentric Contraction." *The FEBS Journal* 286 (13): 2562–76. https://doi.org/10.1111/febs.14831.

Liu, Haofeng, Min Yuan, Yanxue Yao, Dandan Wu, Shuying Dong, and Xuhui Tong. 2019. "In Vitro Effect of Pannexin 1 Channel on the Invasion and Migration of I-10 Testicular Cancer Cells via ERK1/2 Signaling Pathway." *Biomedicine & Pharmacotherapy* 117 (September): 109090. https://doi.org/10.1016/j.biopha.2019.109090.
Liu, Jianming, Zhan-Peng Huang, Mao Nie, Gang Wang, William J. Silva, Qiumei Yang, Paula P. Freire, et al. 2020. "Regulation of Myonuclear Positioning and Muscle Function by the Skeletal Muscle-Specific CIP Protein." *Proceedings of the National Academy of Sciences* 117 (32): 19254. https://doi.org/10.1073/pnas.1922911117.

Liu, Wenjing, Demao Zhang, Xin Li, Liwei Zheng, Chen Cui, Yujia Cui, Jianxun Sun, Jing Xie, and Xuedong Zhou. 2019. "TGF-B1 Facilitates Cell–Cell Communication in Osteocytes via Connexin43- and Pannexin1-Dependent Gap Junctions." *Cell Death Discovery* 5 (1): 141. https://doi.org/10.1038/s41420-019-0221-3.

Ljubicic, Vladimir, and Bernard J. Jasmin. 2015. "Metformin Increases Peroxisome Proliferator-Activated Receptor γ Co-Activator-1α and Utrophin a Expression in Dystrophic Skeletal Muscle." *Muscle and Nerve* 52 (1): 139–42. https://doi.org/10.1002/mus.24692.

Locovei, Silviu, Li Bao, and Gerhard Dahl. 2006. "Pannexin 1 in Erythrocytes: Function without a Gap." *Proceedings of the National Academy of Sciences of the United States of America* 103 (20): 7655–59. https://doi.org/10.1073/pnas.0601037103.

Lohman, Alexander W., Marie Billaud, Adam C. Straub, Scott R. Johnstone, Angela K. Best, Monica Lee, Kevin Barr, Silvia Penuela, Dale W. Laird, and Brant E. Isakson. 2012. "Expression of Pannexin Isoforms in the Systemic Murine Arterial Network." *Journal of Vascular Research* 49 (5): 405–16. https://doi.org/10.1159/000338758.

Luetić, Martina, Genia Kretzschmar, Maximilian Grobe, Leo Jerčić, Ivana Bota, Vedrana Ivić, Marta Balog, et al. 2021. "Sex-Specific Effects of Metformin and Liraglutide on Renal

Pathology and Expression of Connexin 45 and Pannexin 1 Following Long-Term High-Fat High-Sugar Diet." *Acta Histochemica* 123 (8): 151817. https://doi.org/10.1016/j.acthis.2021.151817.

Makarenkova, Helen P., Sameer B. Shah, and Valery I. Shestopalov. 2018. "The Two Faces of Pannexins: New Roles in Inflammation and Repair." *Journal of Inflammation Research* 11: 273–88. https://doi.org/10.2147/JIR.S128401.

Mangan, G., E. Bombardier, A. S. Mitchell, J. Quadrilatero, and P. M. Tiidus. 2014. "Oestrogen-Dependent Satellite Cell Activation and Proliferation Following a Running Exercise Occurs via the PI3K Signalling Pathway and Not IGF-1." *Acta Physiologica (Oxford, England)* 212 (1): 75–85. https://doi.org/10.1111/apha.12317.

Mansouri, A., A. Stoykova, M. Torres, and P. Gruss. 1996. "Dysgenesis of Cephalic Neural Crest Derivatives in Pax7-/- Mutant Mice." *Development (Cambridge, England)* 122 (3): 831–38. https://doi.org/10.1242/dev.122.3.831.

Massenet, Jimmy, Cyril Gitiaux, Mélanie Magnan, Sylvain Cuvellier, Arnaud Hubas, Patrick Nusbaum, F Jeffrey Dilworth, Isabelle Desguerre, and Bénédicte Chazaud. 2020. "Derivation and Characterization of Immortalized Human Muscle Satellite Cell Clones from Muscular Dystrophy Patients and Healthy Individuals." *Cells* 9 (8): 1780–1780. https://doi.org/10.3390/cells9081780.

Massopust, Ryan T., Young il Lee, Anna L. Pritchard, Van-Khoa M. Nguyen, Dylan A. McCreedy, and Wesley J. Thompson. 2020. "Lifetime Analysis of Mdx Skeletal Muscle Reveals a Progressive Pathology That Leads to Myofiber Loss." *Scientific Reports* 10 (1): 17248. https://doi.org/10.1038/s41598-020-74192-9.

Mavrogeni, Sophie, George Markousis-Mavrogenis, Antigoni Papavasiliou, and Genovefa Kolovou. 2015. "Cardiac Involvement in Duchenne and Becker Muscular Dystrophy." *World Journal of Cardiology* 7 (7): 410–14. https://doi.org/10.4330/wjc.v7.i7.410.

May, Christopher, Lukas Weigl, Anton Karel, and Martin Hohenegger. 2006. "Extracellular ATP Activates ERK1/ERK2 via a Metabotropic P2Y1 Receptor in a Ca2+ Independent Manner in Differentiated Human Skeletal Muscle Cells." *Biochemical Pharmacology* 71 (10): 1497–1509. https://doi.org/10.1016/j.bcp.2006.02.003.

Mázala, Davi A.G., James S. Novak, Marshall W. Hogarth, Marie Nearing, Prabhat Adusumalli, Christopher B. Tully, Nayab F. Habib, et al. 2020. "TGF-β–Driven Muscle Degeneration and Failed Regeneration Underlie Disease Onset in a DMD Mouse Model." *JCI Insight* 5 (6). https://doi.org/10.1172/jci.insight.135703.

McGreevy, Joe W., Chady H. Hakim, Mark A. McIntosh, and Dongsheng Duan. 2015. "Animal Models of Duchenne Muscular Dystrophy: From Basic Mechanisms to Gene Therapy." *DMM Disease Models and Mechanisms* 8 (3): 195–213. https://doi.org/10.1242/dmm.018424.

Mead, A. F., M. Petrov, A. S. Malik, M. A. Mitchell, M. K. Childers, J. R. Bogan, G. Seidner, J. N. Kornegay, and H. H. Stedman. 2014. “Diaphragm Remodeling and Compensatory Respiratory Mechanics in a Canine Model of Duchenne Muscular Dystrophy.” *Journal of Applied Physiology (Bethesda, Md. : 1985)* 116 (7): 807–15. https://doi.org/10.1152/japplphysiol.00833.2013.

Medina, Christopher B., Parul Mehrotra, Sanja Arandjelovic, Justin S. A. Perry, Yizhan Guo, Sho Morioka, Brady Barron, et al. 2020. “Metabolites Released from Apoptotic Cells Act as Tissue Messengers.” *Nature* 580 (7801): 130–35. https://doi.org/10.1038/s41586-020-2121-3.

Michalski, Kevin, Johanna L Syrjanen, Erik Henze, Julia Kumpf, Hiro Furukawa, and Toshimitsu Kawate. 2020. “The Cryo-EM Structure of Pannexin 1 Reveals Unique Motifs for Ion Selection and Inhibition.” Edited by Kenton J Swartz, Raimund Dutzler, and Ming Zhou. *eLife* 9 (February): e54670. https://doi.org/10.7554/eLife.54670.

Millay, Douglas P., Jason R. O’Rourke, Lillian B. Sutherland, Svetlana Bezprozvannaya, John M. Shelton, Rhonda Bassel-Duby, and Eric N. Olson. 2013. “Myomaker Is a Membrane Activator of Myoblast Fusion and Muscle Formation.” *Nature* 499 (7458): 301–5. https://doi.org/10.1038/nature12343.

Miller, Iain, Mingwei Min, Chen Yang, Chengzhe Tian, Sara Gookin, Dylan Carter, and Sabrina L. Spencer. 2018. “Ki67 Is a Graded Rather than a Binary Marker of Proliferation versus Quiescence.” *Cell Reports* 24 (5): 1105-1112.e5. https://doi.org/10.1016/j.celrep.2018.06.110.

Milone, Michael C., and Una O’Doherty. 2018. “Clinical Use of Lentiviral Vectors.” *Leukemia* 32 (7): 1529–41. https://doi.org/10.1038/s41375-018-0106-0.
Mirouse, Vincent. 2023. “Evolution and Developmental Functions of the Dystrophin-Associated Protein Complex: Beyond the Idea of a Muscle-Specific Cell Adhesion Complex.” *Frontiers in Cell and Developmental Biology* 11: 1182524. https://doi.org/10.3389/fcell.2023.1182524.

Moran, Amy L., Steven A. Nelson, Rachel M. Landisch, Gordon L. Warren, and Dawn A. Lowe. 2007. “Estradiol Replacement Reverses Ovariectomy-Induced Muscle Contractile and Myosin Dysfunction in Mature Female Mice.” *Journal of Applied Physiology (Bethesda, Md. : 1985)* 102 (4): 1387–93. https://doi.org/10.1152/japplphysiol.01305.2006.

Morishima, Nobuhiro, and Keiko Nakanishi. 2015. “Significance of ER Ca(2+) Outflow during Myogenesis.” *Channels (Austin, Tex.)* 9 (4): 173–74. https://doi.org/10.1080/19336950.2015.1069504.

Murach, Kevin A., Cory M. Dungan, Charlotte A. Peterson, and John J. McCarthy. 2019. “Muscle Fiber Splitting Is a Physiological Response to Extreme Loading in Animals.”

Exercise and Sport Sciences Reviews 47 (2): 108–15. https://doi.org/10.1249/JES.0000000000000181.

Neal, Alice, Luisa Boldrin, and Jennifer Elizabeth Morgan. 2012. "The Satellite Cell in Male and Female, Developing and Adult Mouse Muscle: Distinct Stem Cells for Growth and Regeneration." *PLOS ONE* 7 (5): e37950. https://doi.org/10.1371/journal.pone.0037950.

Okada, Takashi, and Shin'ichi Takeda. 2013. "Current Challenges and Future Directions in Recombinant AAV-Mediated Gene Therapy of Duchenne Muscular Dystrophy." *Pharmaceuticals* 6 (7). https://doi.org/10.3390/ph6070813.

Olguin, Hugo C., Zhihong Yang, Stephen J. Tapscott, and Bradley B. Olwin. 2007. "Reciprocal Inhibition between Pax7 and Muscle Regulatory Factors Modulates Myogenic Cell Fate Determination." *The Journal of Cell Biology* 177 (5): 769–79. https://doi.org/10.1083/jcb.200608122.

Palladino, Alberto, Paola D'Ambrosio, Andrea Antonio Papa, Roberta Petillo, Chiara Orsini, Marianna Scutifero, Gerardo Nigro, and Luisa Politano. 2016. "Management of Cardiac Involvement in Muscular Dystrophies: Paediatric versus Adult Forms." *Acta Myologica : Myopathies and Cardiomyopathies : Official Journal of the Mediterranean Society of Myology* 35 (3): 128–34.

Panchin, Y., I. Kelmanson, M. Matz, K. Lukyanov, N. Usman, and S. Lukyanov. 2000. "A Ubiquitous Family of Putative Gap Junction Molecules." *Current Biology : CB* 10 (13): R473-474. https://doi.org/10.1016/s0960-9822(00)00576-5.

Péladeau, Christine, Nadine J. Adam, and Bernard J. Jasmin. 2018. "Celecoxib Treatment Improves Muscle Function in Mdx Mice and Increases Utrophin A Expression." *The FASEB Journal* 32 (9): 5090–5103. https://doi.org/10.1096/fj.201800081R.

Penuela, Silvia, Ruchi Gehi, and Dale W Laird. 2013. "The Biochemistry and Function of Pannexin Channels." *Biochimica et Biophysica Acta (BBA) - Biomembranes* 1828 (1): 15–22. https://doi.org/10.1016/j.bbamem.2012.01.017.

Penuela, Silvia, John J. Kelly, Jared M. Churko, Kevin J. Barr, Amy C. Berger, and Dale W. Laird. 2014. "Panx1 Regulates Cellular Properties of Keratinocytes and Dermal Fibroblasts in Skin Development and Wound Healing." *The Journal of Investigative Dermatology* 134 (7): 2026–35. https://doi.org/10.1038/jid.2014.86.

Perkins, Kelly J., and Kay E. Davies. 2002. "The Role of Utrophin in the Potential Therapy of Duchenne Muscular Dystrophy." In , 12:S78–89. Elsevier. https://doi.org/10.1016/S0960-8966(02)00087-1.

Petric, S., S. Klein, L. Dannenberg, T. Lahres, L. Clasen, K.G. Schmidt, Z. Ding, and B.C. Donner. 2016. "Pannexin-1 Deficient Mice Have an Increased Susceptibility for Atrial Fibrillation and Show a QT-Prolongation Phenotype." *Cellular Physiology and Biochemistry* 38 (2): 487–501. https://doi.org/10.1159/000438645.

Pham, Tammy L, Marie-Eve St-Pierre, Aymeric Ravel-Chapuis, Tara E C Parks, Stéphanie Langlois, Silvia Penuela, Bernard J Jasmin, and Kyle N Cowan. 2018. "Expression of Pannexin 1 and Pannexin 3 during Skeletal Muscle Development, Regeneration, and Duchenne Muscular Dystrophy." *Journal of Cellular Physiology* 233 (10): 7057–70. https://doi.org/10.1002/jcp.26629.

Porter, A. G., and R. U. Jänicke. 1999. "Emerging Roles of Caspase-3 in Apoptosis." *Cell Death and Differentiation* 6 (2): 99–104. https://doi.org/10.1038/sj.cdd.4400476.
Proulx, Alain, Peter A Merrifield, and Christian C G Naus. 1997. "Blocking Gap Junctional Intercellular Communication in Myoblasts Inhibits Myogenin and MRF4 Expression." *Developmental Genetics* 20 (2): 133–44.

https://doi.org/10.1002/(SICI)1520-6408(1997)20:2<133::AID-DVG6>3.0.CO;2-8.
Putten, Maaike van, Kayleigh Putker, Maurice Overzier, W A Adamzek, Svetlana Pasteuning-Vuhman, Jaap J Plomp, and Annemieke Aartsma-Rus. 2019. "Natural Disease History of the D2-Mdx Mouse Model for Duchenne Muscular Dystrophy." *FASEB Journal : Official Publication of the Federation of American Societies for Experimental Biology* 33 (7): 8110–24. https://doi.org/10.1096/fj.201802488R.

Quinn, Malgorzata E., Qingnian Goh, Mitsutoshi Kurosaka, Dilani G. Gamage, Michael J. Petrany, Vikram Prasad, and Douglas P. Millay. 2017. "Myomerger Induces Fusion of Non-Fusogenic Cells and Is Required for Skeletal Muscle Development." *Nature Communications* 8 (1): 15665. https://doi.org/10.1038/ncomms15665.

Radley-Crabb, Hannah G., Juan C. Marini, Horacio A. Sosa, Liliana I. Castillo, Miranda D. Grounds, and Marta L. Fiorotto. 2014. "Dystropathology Increases Energy Expenditure and Protein Turnover in the Mdx Mouse Model of Duchenne Muscular Dystrophy." *PLOS ONE* 9 (2): e89277.
https://doi.org/10.1371/journal.pone.0089277.3

Rajdev, Archana, and William J. Groh. 2015. "Arrhythmias in the Muscular Dystrophies." *Cardiac Electrophysiology Clinics* 7 (2): 303–8. https://doi.org/10.1016/j.ccep.2015.03.011.

Rando, Thomas A. 2001. "The Dystrophin–Glycoprotein Complex, Cellular Signaling, and the Regulation of Cell Survival in the Muscular Dystrophies." *Muscle & Nerve* 24 (12): 1575–94. https://doi.org/10.1002/mus.1192.

Ravel-Chapuis, Aymeric, Tara E Crawford, Marie-Laure Blais-Crépeau, Guy Bélanger, Chase T Richer, and Bernard J Jasmin. 2014. "The RNA-Binding Protein Staufen1 Impairs Myogenic Differentiation via a c-Myc-Dependent Mechanism." *Molecular Biology of the Cell* 25 (23): 3765–78. https://doi.org/10.1091/mbc.E14-04-0895.

Relaix, Frédéric, Didier Montarras, Stéphane Zaffran, Barbara Gayraud-Morel, Didier Rocancourt, Shahragim Tajbakhsh, Ahmed Mansouri, Ana Cumano, and Margaret Buckingham. 2006. "Pax3 and Pax7 Have Distinct and Overlapping Functions in Adult

Muscle Progenitor Cells." *The Journal of Cell Biology* 172 (1): 91–102. https://doi.org/10.1083/jcb.200508044.

Riquelme, Manuel A, Luis A Cea, José L Vega, Mauricio P Boric, Hannah Monyer, Michael V L Bennett, Marina Frank, Klaus Willecke, and Juan C Sáez. 2013. "The ATP Required for Potentiation of Skeletal Muscle Contraction Is Released via Pannexin Hemichannels." *Neuropharmacology* 75: 594–603. https://doi.org/10.1016/j.neuropharm.2013.03.022.

Riquelme, Manuel A, Luis A Cea, José L Vega, Carlos Puebla, Aníbal A Vargas, Kenji F Shoji, Mario Subiabre, and Juan C Sáez. 2015. "Pannexin Channels Mediate the Acquisition of Myogenic Commitment in C2C12 Reserve Cells Promoted by P2 Receptor Activation." *Frontiers in Cell and Developmental Biology* 3 (May): 25–25. https://doi.org/10.3389/fcell.2015.00025.

Romanelli, Gerardo, Rocío Varela, and Juan C. Benech. 2020. "Diabetes Induces Differences in the F-Actin Spatial Organization of Striated Muscles." *Cytoskeleton (Hoboken, N.J.)* 77 (5–6): 202–13. https://doi.org/10.1002/cm.21600.

Ruan, Zheng, Ian J. Orozco, Juan Du, and Wei Lü. 2020. "Structures of Human Pannexin 1 Reveal Ion Pathways and Mechanism of Gating." *Nature* 584 (7822): 646–51. https://doi.org/10.1038/s41586-020-2357-y.

Rudnicki, Michael A., and Bart O. Williams. 2015. "Wnt Signaling in Bone and Muscle." *Bone* 80: 60–66. https://doi.org/10.1016/j.bone.2015.02.009.

Sacco, Alessandra, Regis Doyonnas, Peggy Kraft, Stefan Vitorovic, and Helen M Blau. 2008. "Self-Renewal and Expansion of Single Transplanted Muscle Stem Cells." *Nature* 456 (7221): 502–6. https://doi.org/10.1038/nature07384

Sanchez-Arias, Juan C., Mei Liu, Catherine S. W. Choi, Sarah N. Ebert, Craig E. Brown, and Leigh Anne Swayne. 2019. "Pannexin 1 Regulates Network Ensembles and Dendritic Spine Development in Cortical Neurons." *Eneuro* 6 (3): ENEURO.0503-18.2019. https://doi.org/10.1523/ENEURO.0503-18.2019.

Sanchez-Pupo, Rafael E., Brooke L. O'Donnell, Danielle Johnston, Laszlo Gyenis, David W. Litchfield, and Silvia Penuela. 2022. "Pannexin 2 Is Expressed in Murine Skin and Promotes UVB-Induced Apoptosis of Keratinocytes." *Molecular Biology of the Cell* 33 (3): ar24. https://doi.org/10.1091/mbc.E21-08-0387.

Schiaffino, Stefano, Alberto C. Rossi, Vika Smerdu, Leslie A. Leinwand, and Carlo Reggiani. 2015. "Developmental Myosins: Expression Patterns and Functional Significance." *Skeletal Muscle* 5 (1): 22. https://doi.org/10.1186/s13395-015-0046-6.

Seale, Patrick, Anna Polesskaya, and Michael A. Rudnicki. 2003. "Adult Stem Cell Specification by Wnt Signaling in Muscle Regeneration." *Cell Cycle (Georgetown, Tex.)* 2 (5): 417–18. https://doi.org/10.4161/cc.2.5.498.

Seale, Patrick, Luc A Sabourin, Adele Girgis-Gabardo, Ahmed Mansouri, Peter Gruss, and Michael A Rudnicki. 2000. “Pax7 Is Required for the Specification of Myogenic Satellite Cells.” *Cell* 102 (6): 777–86. https://doi.org/10.1016/S0092-8674(00)00066-0.

Sébastien, Muriel, Benoit Giannesini, Perrine Aubin, Julie Brocard, Mathilde Chivet, Laura Pietrangelo, Simona Boncompagni, et al. 2018. “Deletion of the Microtubule-Associated Protein 6 (MAP6) Results in Skeletal Muscle Dysfunction.” *Skeletal Muscle* 8 (1): 30. https://doi.org/10.1186/s13395-018-0176-8.
Seref-Ferlengez, Zeynep, Marcia Urban-Maldonado, Hui B. Sun, Mitchell B. Schaffler, Sylvia O. Suadicani, and Mia M. Thi. 2019. “Role of Pannexin 1 Channels in Load-Induced Skeletal Response.” *Annals of the New York Academy of Sciences* 1442 (1): 79–90. https://doi.org/10.1111/nyas.13914.

Séror, Claire, Marie-Thérèse Melki, Frédéric Subra, Syed Qasim Raza, Marlène Bras, Héla Saïdi, Roberta Nardacci, et al. 2011. “Extracellular ATP Acts on P2Y2 Purinergic Receptors to Facilitate HIV-1 Infection.” *The Journal of Experimental Medicine* 208 (9): 1823–34. https://doi.org/10.1084/jem.20101805.

Shafa, Mehdi, Lavinia Iuliana Ionescu, Arul Vadivel, Jennifer J.P. Collins, Liqun Xu, Shumei Zhong, Martin Kang, et al. 2018. “Human Induced Pluripotent Stem Cell–Derived Lung Progenitor and Alveolar Epithelial Cells Attenuate Hyperoxia-Induced Lung Injury.” *Cytotherapy* 20 (1): 108–25. https://doi.org/10.1016/j.jcyt.2017.09.003.

Shankar, Jay, Anat Messenberg, Jackie Chan, T. Michael Underhill, Leonard J. Foster, and Ivan R. Nabi. 2010. “Pseudopodial Actin Dynamics Control Epithelial-Mesenchymal Transition in Metastatic Cancer Cells.” *Cancer Research* 70 (9): 3780–90. https://doi.org/10.1158/0008-5472.CAN-09-4439.

Shin, Jin-Hong, Chady H. Hakim, Keqing Zhang, and Dongsheng Duan. 2011. “Genotyping Mdx, Mdx3cv, and Mdx4cv Mice by Primer Competition Polymerase Chain Reaction.” *Muscle & Nerve* 43 (2): 283–86. https://doi.org/10.1002/mus.21873.

Sienkiewicz, Dorota, Wojciech Kulak, Bożena Okurowska-Zawada, Grażyna Paszko-Patej, and Katarzyna Kawnik. 2015. “Duchenne Muscular Dystrophy: Current Cell Therapies.” *Therapeutic Advances in Neurological Disorders* 8 (4): 166–77. https://doi.org/10.1177/1756285615586123.

Silverman, William R., Juan Pablo de Rivero Vaccari, Silviu Locovei, Feng Qiu, Steven K. Carlsson, Eliana Scemes, Robert W. Keane, and Gerhard Dahl. 2009. “The Pannexin 1 Channel Activates the Inflammasome in Neurons and Astrocytes.” *Journal of Biological Chemistry* 284 (27): 18143–51. https://doi.org/10.1074/jbc.M109.004804.

Singh, Rajan, Jorge N. Artaza, Wayne E. Taylor, Nestor F. Gonzalez-Cadavid, and Shalender Bhasin. 2003. “Androgens Stimulate Myogenic Differentiation and Inhibit

Adipogenesis in C3H 10T1/2 Pluripotent Cells through an Androgen Receptor-Mediated Pathway." *Endocrinology* 144 (11): 5081–88. https://doi.org/10.1210/en.2003-0741.

Skuk, Daniel, Marlyne Goulet, and Jacques P. Tremblay. 2006. "Use of Repeating Dispensers to Increase the Efficiency of the Intramuscular Myogenic Cell Injection Procedure." *Cell Transplantation* 15 (7): 659–63. https://doi.org/10.3727/000000006783981648.

Soleimani, Vahab D., Vincent G. Punch, Yoh-ichi Kawabe, Andrew E. Jones, Gareth A. Palidwor, Christopher J. Porter, Joe W. Cross, et al. 2012. "Transcriptional Dominance of Pax7 in Adult Myogenesis Is Due to High-Affinity Recognition of Homeodomain Motifs." *Developmental Cell* 22 (6): 1208–20. https://doi.org/10.1016/j.devcel.2012.03.014.

Srinivas-Shankar, Upendram, Stephen A. Roberts, Martin J. Connolly, Matthew D. L. O'Connell, Judith E. Adams, Jackie A. Oldham, and Frederick C. W. Wu. 2010. "Effects of Testosterone on Muscle Strength, Physical Function, Body Composition, and Quality of Life in Intermediate-Frail and Frail Elderly Men: A Randomized, Double-Blind, Placebo-Controlled Study." *The Journal of Clinical Endocrinology and Metabolism* 95 (2): 639–50. https://doi.org/10.1210/jc.2009-1251.

Suarez-Berumen, Katia, Henry Collins-Hooper, Anastasia Gromova, Robyn Meech, Alessandra Sacco, Phil R. Dash, Robert Mitchell, et al. 2021. "Pannexin 1 Regulates Skeletal Muscle Regeneration by Promoting Bleb-Based Myoblast Migration and Fusion Through a Novel Lipid Based Signaling Mechanism." *Frontiers in Cell and Developmental Biology* 9: 2759. https://doi.org/10.3389/fcell.2021.736813.

Swaney, Kristen F., and Rong Li. 2016. "Function and Regulation of the Arp2/3 Complex during Cell Migration in Diverse Environments." *Current Opinion in Cell Biology* 42 (October): 63–72. https://doi.org/10.1016/j.ceb.2016.04.005.

Szentesi, P., R. Zaremba, W. van Mechelen, and G. J. Stienen. 2001. "ATP Utilization for Calcium Uptake and Force Production in Different Types of Human Skeletal Muscle Fibres." *The Journal of Physiology* 531 (Pt 2): 393–403. https://doi.org/10.1111/j.1469-7793.2001.0393i.x.

Tajbakhsh, Shahragim, U Borello, E Vivarelli, R Kelly, J Papkoff, D Duprez, Margaret E Buckingham, and Giulio Cossu. 1998. "Differential Activation of Myf5 and MyoD by Different Wnts in Explants of Mouse Paraxial Mesoderm and the Later Activation of Myogenesis in the Absence of Myf5." *Development (Cambridge, England)* 125 (21): 4155–62.

Tremblay, P., S. Dietrich, M. Mericskay, F. R. Schubert, Z. Li, and D. Paulin. 1998. "A Crucial Role for Pax3 in the Development of the Hypaxial Musculature and the Long-Range Migration of Muscle Precursors." *Developmental Biology* 203 (1): 49–61. https://doi.org/10.1006/dbio.1998.9041.

Tu, Michelle K., Jacqueline B. Levin, Andrew M. Hamilton, and Laura N. Borodinsky. 2016. “Calcium Signaling in Skeletal Muscle Development, Maintenance and Regeneration.” *Cell Calcium* 59 (2–3): 91–97. https://doi.org/10.1016/j.ceca.2016.02.005.

Valladares, Denisse, Gonzalo Almarza, Ariel Contreras, Mario Pavez, Sonja Buvinic, Enrique Jaimovich, and Mariana Casas. 2013. “Electrical Stimuli Are Anti-Apoptotic in Skeletal Muscle via Extracellular ATP. Alteration of This Signal in Mdx Mice Is a Likely Cause of Dystrophy.” *PloS One* 8 (11): e75340. https://doi.org/10.1371/journal.pone.0075340.

Van De Vlekkert, Diantha, Eda Machado, and Alessandra d’Azzo. 2020. “Analysis of Generalized Fibrosis in Mouse Tissue Sections with Masson’s Trichrome Staining.” *Bio-Protocol* 10 (10): e3629. https://doi.org/10.21769/BioProtoc.3629.

Vanoirbeek, Jeroen A. J., Manuela Rinaldi, Vanessa De Vooght, Steven Haenen, Sonja Bobic, Ghislaine Gayan-Ramirez, Peter H. M. Hoet, et al. 2010. “Noninvasive and Invasive Pulmonary Function in Mouse Models of Obstructive and Restrictive Respiratory Diseases.” *American Journal of Respiratory Cell and Molecular Biology* 42 (1): 96–104. https://doi.org/10.1165/rcmb.2008-0487OC

Vingren, Jakob L., William J. Kraemer, Nicholas A. Ratamess, Jeffrey M. Anderson, Jeff S. Volek, and Carl M. Maresh. 2010. “Testosterone Physiology in Resistance Exercise and Training: The up-Stream Regulatory Elements.” *Sports Medicine (Auckland, N.Z.)* 40 (12): 1037–53. https://doi.org/10.2165/11536910-000000000-00000.

Von Maltzahn, J., Jones, A. E., Parks, R. J., & Rudnicki, M. A. 2013. “Pax7 Is Critical for the Normal Function of Satellite Cells in Adult Skeletal Muscle.” *PNAS* 110 (41): 16474-16479-16474–79.

Wakefield, Brent, and Silvia Penuela. 2022. “Potential Implications of Exercise Training on Pannexin Expression and Function.” *Journal of Vascular Research*, November, 1–11. https://doi.org/10.1159/000527240.

Waldmann, Victor, Xavier Jouven, Kumar Narayanan, Olivier Piot, Sumeet S. Chugh, Christine M. Albert, and Eloi Marijon. 2020. “Association Between Atrial Fibrillation and Sudden Cardiac Death.” *Circulation Research* 127 (2): 301–9. https://doi.org/10.1161/CIRCRESAHA.120.316756.

Wang, Min-Jia, Bi-Ru Yang, Xin-Yu Jing, Yao-Zheng Wang, Lu Kang, Kai Ren, and Liang Kang. 2023. “P2Y1R and P2Y2R: Potential Molecular Triggers in Muscle Regeneration.” *Purinergic Signalling* 19 (1): 305–13. https://doi.org/10.1007/s11302-022-09885-z.

Wang, Yu Xin, Peter Feige, Caroline E. Brun, Bahareh Hekmatnejad, Nicolas A. Dumont, Jean-Marc Renaud, Sharlene Faulkes, Daniel E. Guindon, and Michael A. Rudnicki. 2019. “EGFR-Aurka Signaling Rescues Polarity and Regeneration Defects in Dystrophin-Deficient

Muscle Stem Cells by Increasing Asymmetric Divisions." *Cell Stem Cell* 24 (3): 419-432.e6. https://doi.org/10.1016/j.stem.2019.01.002.

Wen, Yefei, Pengpeng Bi, Weiyi Liu, Atsushi Asakura, Charles Keller, and Shihuan Kuang. 2012. "Constitutive Notch Activation Upregulates Pax7 and Promotes the Self-Renewal of Skeletal Muscle Satellite Cells." *Molecular and Cellular Biology* 32 (12): 2300–2311. https://doi.org/10.1128/MCB.06753-11.

Whyte-Fagundes, Paige, Stefan Kurtenbach, Christiane Zoidl, Valery I. Shestopalov, Peter L. Carlen, and Georg Zoidl. 2018. "A Potential Compensatory Role of Panx3 in the VNO of a Panx1 Knock Out Mouse Model." *Frontiers in Molecular Neuroscience* 11: 135. https://doi.org/10.3389/fnmol.2018.00135.

Wicki-Stordeur, Leigh E., Adrian D. Dzugalo, Rose M. Swansburg, Jocelyne M. Suits, and Leigh A. Swayne. 2012. "Pannexin 1 Regulates Postnatal Neural Stem and Progenitor Cell Proliferation." *Neural Development* 7 (1): 1–10. https://doi.org/10.1186/1749-8104-7-11.

Wicki-Stordeur, Leigh E., and Leigh Anne Swayne. 2013. "Panx1 Regulates Neural Stem and Progenitor Cell Behaviours Associated with Cytoskeletal Dynamics and Interacts with Multiple Cytoskeletal Elements." *Cell Communication and Signaling : CCS* 11 (August): 62. https://doi.org/10.1186/1478-811X-11-62.

Witcher, Phillip C., Chengyi Sun, and Douglas P. Millay. 2023. "Expression of Myomaker and Myomerger in Myofibers Causes Muscle Pathology." *Skeletal Muscle* 13 (1): 8. https://doi.org/10.1186/s13395-023-00317-z.

Xiang, Xiao, Huy-Dung Hoang, Victoria H. Gilchrist, Stéphanie Langlois, Tommy Alain, and Kyle N. Cowan. 2022. "Quercetin Induces Pannexin 1 Expression via an Alternative Transcript with a Translationally Active 5' Leader in Rhabdomyosarcoma." *Oncogenesis* 11 (1): 9. https://doi.org/10.1038/s41389-022-00384-9.

Xiang, Xiao, Stéphanie Langlois, Marie-Eve St-Pierre, Jessica F Barré, David Grynspan, Bibianna Purgina, and Kyle N Cowan. 2018. "Pannexin 1 Inhibits Rhabdomyosarcoma Progression through a Mechanism Independent of Its Canonical Channel Function." *Oncogenesis* 7 (11): 89–89. https://doi.org/10.1038/s41389-018-0100-4.

Xiang, Xiao, Stéphanie Langlois, Marie-Eve St-Pierre, Anna Blinder, Philippe Charron, Tyson E. Graber, Stephanie L. Fowler, et al. 2021. "Identification of Pannexin 1-Regulated Genes, Interactome, and Pathways in Rhabdomyosarcoma and Its Tumor Inhibitory Interaction with AHNAK." *Oncogene* 40 (10): 1868–83. https://doi.org/10.1038/s41388-020-01623-2.

Xu, Xiaoxue, Leigh E. Wicki-Stordeur, Juan C. Sanchez-Arias, Mei Liu, Maria S. Weaver, Catherine S. W. Choi, and Leigh A. Swayne. 2018. "Probenecid Disrupts a Novel Pannexin 1-Collapsin Response Mediator Protein 2 Interaction and Increases Microtubule Stability." *Frontiers in Cellular Neuroscience* 12: 124. https://doi.org/10.3389/fncel.2018.00124.

Yao, Shanshan, Zihao Chen, Yuanyuan Yu, Ning Zhang, Hewen Jiang, Ge Zhang, Zongkang Zhang, and Baoting Zhang. 2021. “Current Pharmacological Strategies for Duchenne Muscular Dystrophy.” *Frontiers in Cell and Developmental Biology* 9. https://www.frontiersin.org/articles/10.3389/fcell.2021.689533.

Yoshioka, Kiyoshi, Yasuo Kitajima, Narihiro Okazaki, Ko Chiba, Akihiko Yonekura, and Yusuke Ono. 2020. “A Modified Pre-Plating Method for High-Yield and High-Purity Muscle Stem Cell Isolation From Human/Mouse Skeletal Muscle Tissues.” *Frontiers in Cell and Developmental Biology* 8: 793. https://doi.org/10.3389/fcell.2020.00793.

Z, Kibar, Vogan KJ, J Groulx N, Ustice MJ, Underhill DA, and Gros P. 2001. . “. Ltap, a Mammalian Homolog of Drosophila Strabis- Mus/Van Gogh, Is Altered in the Mouse Neural Tube Mutant Loop-Tail.” *Nature Genetics*, 251-255-251–55.

Zammit, Peter S, Jon P Golding, Yosuke Nagata, Valérie Hudon, Terence A Partridge, and Jonathan R Beauchamp. 2004. “Muscle Satellite Cells Adopt Divergent Fates: A Mechanism for Self-Renewal?” *The Journal of Cell Biology* 166 (3): 347–57. https://doi.org/10.1083/jcb.200312007.

Zammit, Peter S., Frederic Relaix, Yosuke Nagata, Ana Pérez Ruiz, Charlotte A Collins, Terence A Partridge, and Jonathan R Beauchamp. 2006. “Pax7 and Myogenic Progression in Skeletal Muscle Satellite Cells.” *Journal of Cell Science* 119 (Pt 9): 1824–32. https://doi.org/10.1242/jcs.02908.

Appendix I: Additional Figures

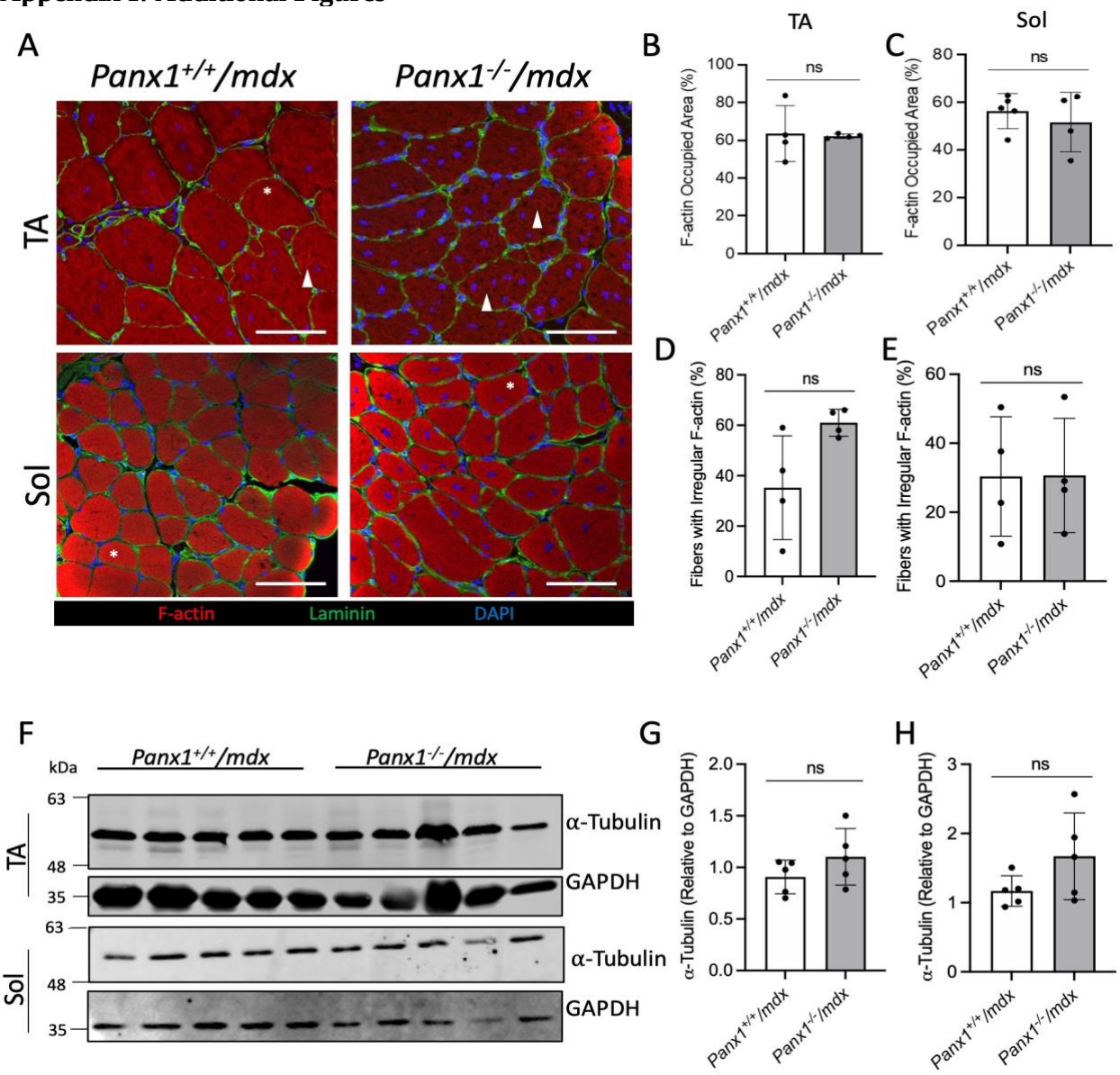

Appendix I Figure 1: Panx1$^{-/-}$/mdx mice do not lose cytoskeletal components.

A) Representative images of TA and Sol muscles of *Panx1$^{-/-}$/mdx* and *Panx1$^{+/+}$/mdx* mice were stained for Rhodamine phalloidin (red) a marker of F-actin, laminin (green), and DAPI (blue). Arrows indicate fibers displaying irregular F-actin staining while the * indicates fibers considered to have normal staining. Scale bar = 100 µm. The percentage of area covered by F-actin was calculated in the **B)** TA and **C)** Sol (n=4; unpaired two-tailed student's *t*-test). The percentage of irregular fibers were counted in the D) TA and E) Sol (n=4; unpaired two-tailed student's *t*-test). F) Representative western blots of α-tubulin and GAPDH in *Panx1$^{-/-}$/mdx* and *Panx1$^{+/+}$/mdx* TA and Sol muscles. Quantification of α-tubulin normalized to GAPDH in the **G)** TA and **H)** Sol of *Panx1$^{-/-}$/mdx* and *Panx1$^{+/+}$/mdx* mice (n=5; unpaired two-tailed student's *t*-test). ns, non-significant.

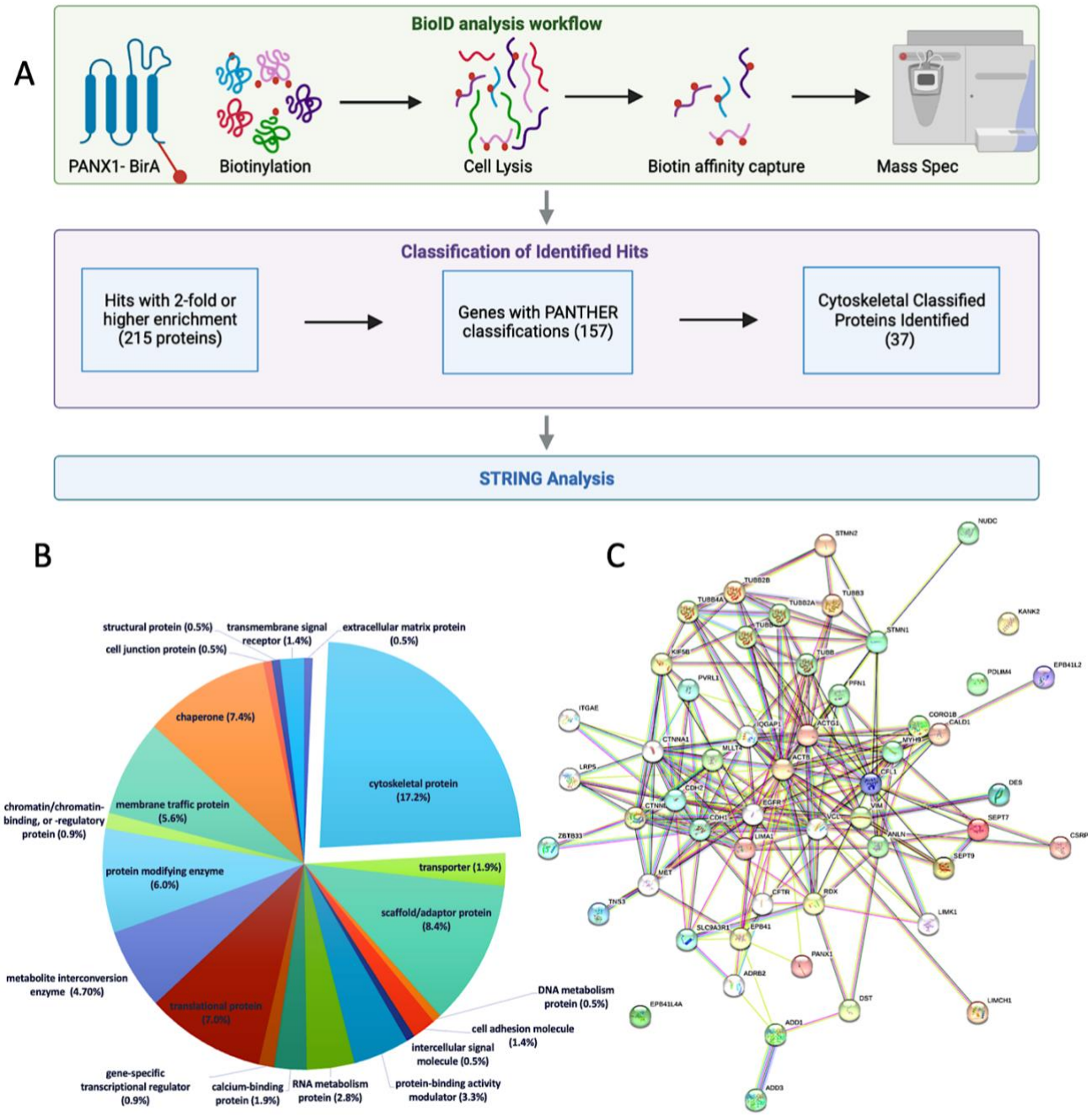

Appendix I Figure 2: PANX1 Cytoskeletal Interactors

A) Workflow of interactor analysis. Previously, rhabdomyosarcoma cell lines (RH18 and RH30) were transfected with a Panx1-BirA construct which biotinylated proteins withing a 10 nm radius of PANX1. Cells were then lysed, the biotinylated proteins selected for and identified via mass spectrometry and published on a public searchable database (Xiang et al. 2021). From this database, proteins with a 2-fold or higher enrichment were selected. From

the 215 proteins meeting this criterion, 157 were classified via PANTHER with 37 of the classified proteins attaining to cytoskeletal proteins and selected for STRING analysis. Figure created with BioRender. **B)** Pie chart displaying the classification of the 157 proteins that qualified with cytoskeletal proteins making up the largest (17.2%) fraction. **C)** STRING pathway analysis of PANX1, the 37 identified cytoskeletal hits from PANTHER and their primary and secondary predicted relations. For clarity, these hits have been summarized in Appendix Table 1.

Appendix Table 1 :Gene Ontology (GO) Panther Cytoskeletal Hits

Mapped ID	Gene Name / Symbol and Persistent ID	Panther Protein Class
MLLT4	Afadin AFDN PTN002470553	non-motor actin binding protein
RDX	Radixin RDX PTN002510854	actin or actin-binding cytoskeletal protein
PFN1	Profilin-1 PFN1 PTN002493405	non-motor actin binding protein
MYH9	Myosin-9 MYH9 PTN002490807	actin or actin-binding cytoskeletal protein
STMN2	Stathmin-2 STMN2 PTN002467994	non-motor microtubule binding protein
TNS3	Tensin-3 TNS3 PTN002487371	non-motor actin binding protein
CALD1	Caldesmon CALD1 PTN002498526	non-motor actin binding protein
TUBB2A	Tubulin beta-2A chain TUBB2A PTN002480623	tubulin
DST	Dystonin DST PTN000747957	intermediate filament binding protein
EPB41	Protein 4.1 EPB41 PTN002510833	non-motor actin binding protein
Sept7	Septin-7 SEPTIN7 PTN002498000	cytoskeletal protein

ADD3	Gamma-adducin ADD3 PTN002472865	non-motor actin binding protein
DES	Desmin DES PTN002509750	intermediate filament
VIM	Vimentin VIM PTN002509751	intermediate filament
LIMCH1	LIM and calponin homology domains-containing protein 1 LIMCH1 PTN002496213	actin or actin-binding cytoskeletal protein
ANLN	Anillin ANLN PTN002502315 orthologs	non-motor actin binding protein
EPB41L2	Band 4.1-like protein 2 EPB41L2 PTN002510838	non-motor actin binding protein
TUBB4A	Tubulin beta-4A chain TUBB4A PTN002480651	tubulin
KIF5B	Kinesin-1 heavy chain KIF5B PTN002516150	microtubule binding motor protein
ACTB	Actin, cytoplasmic 1 ACTB PTN002485092	actin and actin related protein
TUBB4B	Tubulin beta-4B chain TUBB4B PTN002480652	tubulin
CORO1B	Coronin-1B CORO1B PTN002474497	non-motor actin binding protein
TUBB2B	Tubulin beta-2B chain TUBB2B PTN002480622	tubulin

CTNND1	Catenin delta-1 CTNND1 PTN002470439	intermediate filament binding protein
NUDC	Nuclear migration protein nudC NUDC PTN002487680	microtubule or microtubule-binding cytoskeletal protein
EPB41L4A	Band 4.1-like protein 4A EPB41L4A PTN002510822	non-motor actin binding protein
PDLIM4	PDZ and LIM domain protein 4 PDLIM4 PTN002516891	actin or actin-binding cytoskeletal protein
STMN1	Stathmin STMN1 PTN002467997	non-motor microtubule binding protein
TUBB	Tubulin beta chain TUBB PTN002480643	tubulin
Sept9	Septin-9 SEPTIN9 PTN002498017	cytoskeletal protein Homo sapiens

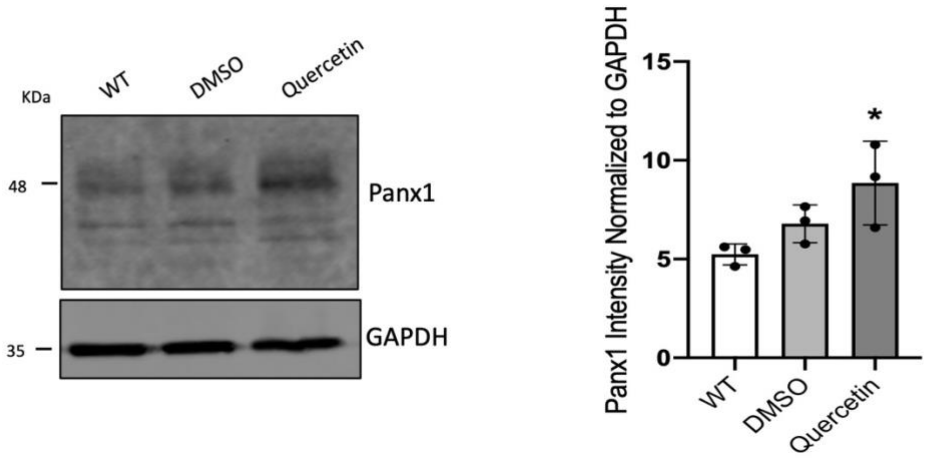

Appendix I Figure 3: Quercetin Increases Panx1 Levels in Murine Dystrophic Myoblasts.

Representative western blot of Panx1 and GAPDH after 48 hours of quercetin treatment (left). Quantification of Panx1 levels normalized to GAPDH (right) (n=3; one-way ANOVA, followed by Tukey's post hoc test). * $P \leq 0.05$ compared to WT. Everything else was non-significant.

Appendix II: Licences

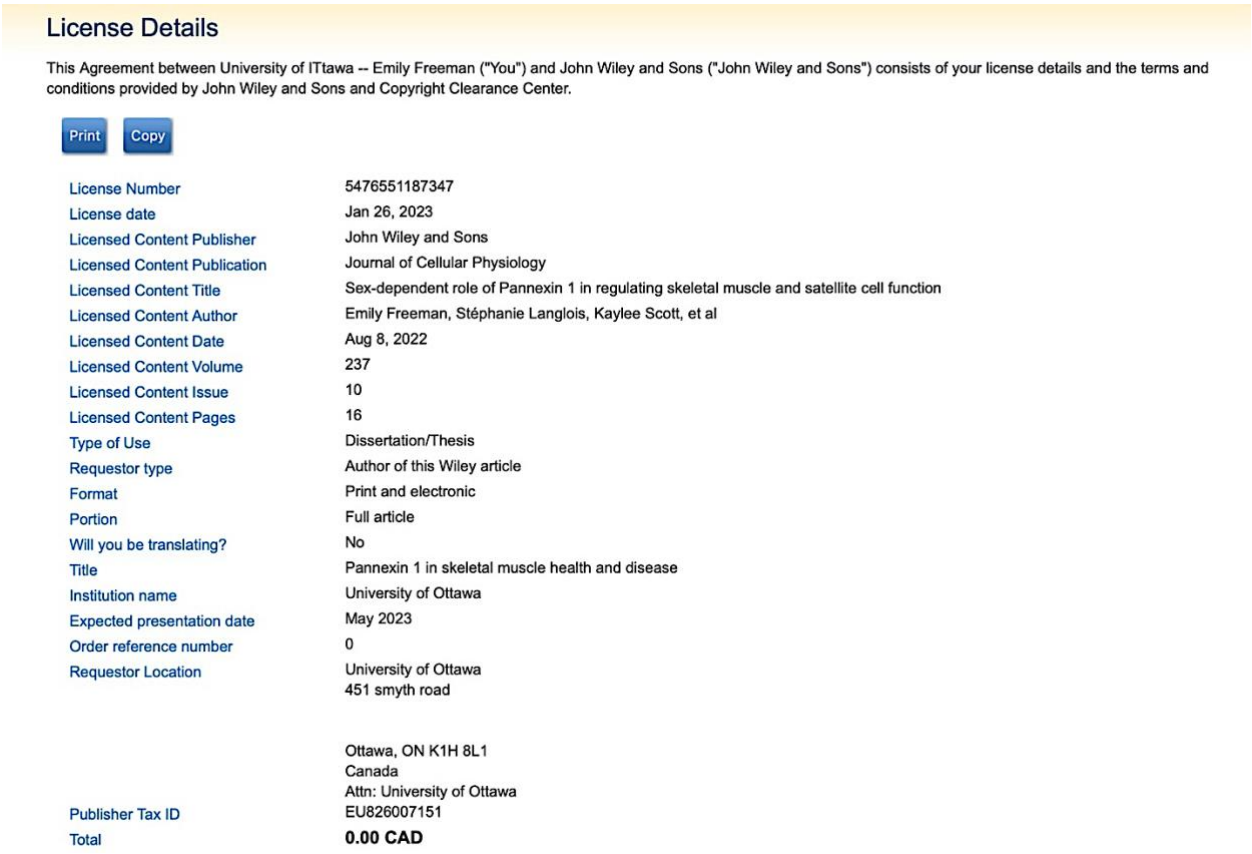

License Details

This Agreement between University of ITtawa -- Emily Freeman ("You") and John Wiley and Sons ("John Wiley and Sons") consists of your license details and the terms and conditions provided by John Wiley and Sons and Copyright Clearance Center.

Print Copy

License Number	5476551187347
License date	Jan 26, 2023
Licensed Content Publisher	John Wiley and Sons
Licensed Content Publication	Journal of Cellular Physiology
Licensed Content Title	Sex-dependent role of Pannexin 1 in regulating skeletal muscle and satellite cell function
Licensed Content Author	Emily Freeman, Stéphanie Langlois, Kaylee Scott, et al
Licensed Content Date	Aug 8, 2022
Licensed Content Volume	237
Licensed Content Issue	10
Licensed Content Pages	16
Type of Use	Dissertation/Thesis
Requestor type	Author of this Wiley article
Format	Print and electronic
Portion	Full article
Will you be translating?	No
Title	Pannexin 1 in skeletal muscle health and disease
Institution name	University of Ottawa
Expected presentation date	May 2023
Order reference number	0
Requestor Location	University of Ottawa 451 smyth road Ottawa, ON K1H 8L1 Canada Attn: University of Ottawa
Publisher Tax ID	EU826007151
Total	**0.00 CAD**

Figure 1: Copyright clearance. Data from chapter 3 has been published in the *Journal of Cellular Physiology*. This is the license to reproduce data and figures from this article for use in this thesis.